NTNU

Norwegian University of
Science and Technology

Large Time Step Methods for Hyperbolic Partial Differential Equations

Rolf Nygaard

NTNU

Norwegian University
of Science and Technology

Department of Energy
and Process Engineering

MASTER THESIS

for

Student Rolf Nygaard

Spring 2017

Large Time Step methods for hyperbolic partial differential equations
Metoder med høye tidsteg for hyperbolske partielle differensiallikninger

Background and objective

The project consists of numerical and theoretical studies of the explicit Large Time Step method originally developed by LeVeque in the 1980s, and currently being further developed by a research team involving the supervisors.

Although the approach so far has proved promising for a large class of simplified problems, challenges remain concerning robustness, in particular in the presence of source terms.

In this project, the student is expected to systematically investigate the *robustness* of the Large Time Step framework. The project is associated with the ongoing research project SIMCOFLOW at SINTEF Materials and Chemistry.

The following tasks are to be considered:

1. Review and select the relevant explicit Large Time Step discretizations for further investigation.
2. Implement the relevant Large Time Step schemes for hyperbolic PDEs.
3. Perform numerical simulations and investigate the robustness properties of the implemented schemes.
4. Evaluate potential applications of the method and give recommendations for further work and potential improvements.

-- " --

Within 14 days of receiving the written text on the master thesis, the candidate shall submit a research plan for his project to the department.

When the thesis is evaluated, emphasis is put on processing of the results, and that they are presented in tabular and/or graphic form in a clear manner, and that they are analyzed carefully.

The thesis should be formulated as a research report with summary both in English and Norwegian, conclusion, literature references, table of contents etc. During the preparation of the text, the candidate should make an effort to produce a well-structured and easily readable report. In order to ease the evaluation of the thesis, it is important that the cross-references are correct. In the making of the report, strong emphasis should be placed on both a thorough discussion of the results and an orderly presentation.

The candidate is requested to initiate and keep close contact with his/her academic supervisor(s) throughout the working period. The candidate must follow the rules and regulations of NTNU as well as passive directions given by the Department of Energy and Process Engineering.

Risk assessment of the candidate's work shall be carried out according to the department's procedures. The risk assessment must be documented and included as part of the final report. Events related to the candidate's work adversely affecting the health, safety or security, must be documented and included as part of the final report. If the documentation on risk assessment represents a large number of pages, the full version is to be submitted electronically to the supervisor and an excerpt is included in the report.

Pursuant to "Regulations concerning the supplementary provisions to the technology study program/Master of Science" at NTNU §20, the Department reserves the permission to utilize all the results and data for teaching and research purposes as well as in future publications.

The final report is to be submitted digitally in DAIM. An executive summary of the thesis including title, student's name, supervisor's name, year, department name, and NTNU's logo and name, shall be submitted to the department as a separate pdf file. Based on an agreement with the supervisor, the final report and other material and documents may be given to the supervisor in digital format.

☐ Work to be done in lab (Water power lab, Fluids engineering lab, Thermal engineering lab)
☐ Field work

Department of Energy and Process Engineering, 15. January 2017

Bernhard Müller
Academic Supervisor

Tore Flåtten
Research Advisor

Abstract

In this thesis we consider explicit finite volume methods that are not limited by the Courant-Friedrichs-Lewy (CFL) condition, referred to as large time step (LTS) methods. LeVeque proposed the first LTS method in the 1980's as an extension of the Godunov method. Since then, classic concepts in numerical analysis, such as total variation diminishing (TVD) schemes, modified equation and higher order schemes have been extended to LTS, as well as approximate Riemann solvers, such as the Roe scheme, the Lax-Friedrichs scheme and the HLL scheme.

At large time steps, LTS methods often yield entropy violating solutions, and oscillations appear due to interacting waves, especially for systems of equations. Because of this reduction in robustness, the maximum allowable time step is in practice limited for many LTS schemes.

We will look at LTS methods from a new angle, by introducing an *artificial flux function* framework. We show how the flux-difference splitting coefficients and numerical diffusion coefficient can be evaluated numerically from the artificial flux function, which gives us a convenient way of experimenting with new LTS schemes.

In his master's thesis, Solberg developed a class of LTS schemes, with an inherent mechanism for adding numerical diffusion. As an extension of this work, we develop a new three parameter LTS scheme, denoted LTS-HLLϕ, which is the main original contribution in this thesis. We propose special choices of parameters, which appears to give a good trade off between robustness and accuracy.

Numerical simulations are performed on the Burgers' equation and the Euler equations, assessing the robustness and accuracy of the new LTS-HLLϕ scheme, compared to more established LTS schemes.

Sammendrag

Denne avhandlingen omhandler metoder for høye tidssteg (LTS). Dette er eksplisitte numeriske metoder som ikke er begrenset av Courant-Friedrichs-Lewy (CFL) betingelsen. LeVeque innførte begrepet på 1980-tallet, da han utvidet Godunov-metoden for høye tidssteg. Senere har klassiske begreper som totalvariasjonsforminskende (TVD) skjema, modifisert likning og høyere ordens skjema blitt utvidet til LTS. Flere Riemann løsere har også blitt utvidet til LTS, blant annet Roe-, Lax-Friedrichs- og HLL-skjemaet.

Mange LTS-metoder gir entropi-reduserende og oscillerende løsninger når tidsstegene overstiger CFL-betingelsen. Disse fenomenene er spesielt fremtredende for ligningssystemer, fordi de ulike bølgene overkjører hverandre. I praksis gir disse fenomenene en begrensning for størrelsen på tidsstegene.

I denne avhandlingen ser vi på LTS-metoder fra en ny vinkel, når vi introduserer *kunstige fluksfunksjoner*. I dette rammeverket viser vi hvordan fluksdifferansesplittingskoeffisientene og den numeriske diffusjonskoeffisienten kan utrykkes numerisk for en gitt kunstig fluksfunksjon. Dette åpner for enkel eksperimentering med nye LTS-skjema i fremtiden.

Solberg utviklet en klasse av LTS-skjema i sin masteroppgave, som har en innebygd mekanisme for å justere numerisk diffusjon. Det viktigste originale bidraget i denne avhandlingen er utviklingen av det nye LTS-HLLϕ-skjemaet, som er basert på Solbergs skjema. Vi foreslår en metode for å velge parametere for LTS-HLLϕ-skjemaet som gir en god balanse mellom robusthet og nøyaktighet.

Vi gjennomfører numeriske simuleringer på Burgers' likning og Eulerlikningene, for å studere hvor robust og nøyaktig det nye LTS-HLLϕ-skjemaet er i forhold til mer etablerte LTS-skjema.

Preface

The figure on the cover of this thesis shows a simulation of the 2D Burgers' equation, where the seven peaks show the evolution from the initial data to the sixth time step. We see a Gauss curve moving to the left, forming a shock. Solutions were obtained using the Solberg* scheme on a $[100 \times 100]$ grid, with a maximum Courant number of CFL$= 10$.

This master's thesis is a continuation of my project work, concerning source term treatment in large time step methods. Hence, chapters 2 and 3 in this thesis are heavily based on content from the previously submitted report [17].

I would like to give a special thanks to my supervisors, Bernhard Müller and Tore Flåtten for excellent guidance and support throughout this whole process. I would also like to thank Marin Prebeg and Anders Solberg for fruitful discussions.

Contents

List of Figures

List of Tables

Chapter 1

Introduction

Hyperbolic partial differential equations (PDEs) are important models for many physical systems, such as, gas dynamics, meteorology, traffic modelling and geophysics to mention a few [14, 21, 27, 3]. In this thesis we consider a class of PDEs known as hyperbolic conservation laws

$$\mathbf{q}_t + \mathbf{f}(\mathbf{q})_x = \mathbf{0},$$

where $\mathbf{q}$ is the vector of conserved variables and $\mathbf{f}(\mathbf{q})$ is the flux function.

For scientific and engineering purposes, accurately solving problems of hyperbolic conservation laws, with minimal computational effort is highly valuable. In the past century, different numerical methods have been developed for solving hyperbolic conservation laws [15, 24]. Unfortunately, in most of these methods, there are trade-offs between accuracy, stability and computational effort.

Explicit methods are simple to evaluate and well suited for parallel computing. However, they often fall short compared to implicit methods, since explicit methods are typically limited by the Courant–Friedrichs–Lewy (CFL) condition [2]

$$\text{CFL} = \frac{\Delta t}{\Delta x} \max_p |\lambda^p| \le 1,$$

where CFL is the largest *Courant number* inherent to the problem, λ^p is the p-th *wave speed*, Δx is the length of one computational cell and Δt is the *time step*. The CFL condition is typically necessary for stability because most explicit methods cannot handle convecting conserved quantities more than one computational cell length during one time step.

Large time step (LTS) methods are explicit finite volume methods that are also stable for CFL> 1. We can relax the CFL condition to a less strict CFL-like condition,

$$\text{CFL} \le k.$$

by allowing the conserved quantity to convect for up to k computational cell lengths. When calculating the value of the conserved quantity in the next time step, we now need to consider a stencil of $(2k + 1)$ cells.

Most of the LTS methods studied so far, are not very robust for large time steps. Entropy violations and unphysical oscillations are typically more frequent at larger time steps, which in practice limit the maximum allowable time step for many LTS methods. Although diffusive LTS methods are often more robust against these errors, they are also less accurate. This motivates us to search for new LTS methods that are robust, without being unnecessarily diffusive.

This thesis on LTS methods is part of an ongoing research project, SIMCOFLOW, at SINTEF Materials and Chemistry. The ultimate goal of this project is to develop a highly efficient open source computer code for complex problems in multiphase flow.

1.1   Previous work

The first LTS methods were proposed by LeVeque in a series of papers in the 1980's [11, 12, 13], where he generalized the Godunov method for arbitrary Courant numbers. Although results were promising for scalar equations, LeVeque observed unphysical oscillations in the solutions for systems of equations. Harten later extended the entropy satisfying Harten scheme to LTS, and showed that this method is *total variation diminishing* (TVD) [7]. Harten also developed a procedure for creating large time step TVD schemes, that are second order accurate away from discontinuities.

More recently, Lindquist et al. expressed LeVeque's original LTS-Godunov method in closed form [16]. They defined a LTS extension of the Lax-Friedrichs scheme, and showed that the LTS-Roe scheme and the LTS-Lax-Friedrichs scheme are the least and most diffusive $(2k + 1)$-point TVD schemes, respectively. From these LTS schemes, they produced a hybrid scheme, that combines the sharp resolution of the LTS-Roe scheme with the robustness of the LTS-Lax-Friedrichs scheme. A random time stepping was also proposed for reducing entropy violations in the LTS-Roe scheme.

The same year, Prebeg et al. developed a LTS extension of the HLL scheme and the HLLC scheme [19]. Prebeg later showed that the LTS-HLL scheme with Einfeldt's choice of parameters [4], referred to as LTS-HLLE, yield entropy satisfying solutions for all Courant numbers [18].

In his master's thesis, Solberg proposed a new LTS scheme, with an inherent mechanism for adding numerical diffusion [23]. He use this method to smear out the oscillations that LeVeque reported in his original articles on LTS methods. Because of Solberg's promising results, a large portion of this thesis is devoted to investigating and further developing this scheme.

1.2   Outline of this thesis

In chapters 2 and 3, a review of hyperbolic conservation laws and explicit finite volume methods is given. This will give the reader the necessary tools and definitions to tackle the more advanced topics of large time step methods in chapter 4. In this chapter we

present the $(2k + 1)$-point flux-difference splitting framework, and study the numerical diffusion of a general flux-difference splitting scheme from a modified equation approach. In this framework, we briefly discuss the total variation diminishing condition, and present the LTS-Godunov method, the LTS-Roe scheme, the LTS-Lax-Friedrichs scheme and the LTS-HLL scheme.

In section 4.5, we look at LTS from a different perspective, when we introduce the artificial flux function framework. We find the artificial flux function of the LTS-Roe scheme and the LTS-HLL scheme, as well as a generalized form of Solberg's CD$\hat{k}$ scheme [23], denoted here as the Solberg scheme.

In chapter 5 we present a new three parameter LTS scheme, denoted as LTS-HLLϕ, based on the Solberg scheme and the LTS-HLL scheme. This new scheme is the main original contribution in this thesis. Using the concepts presented in the previous chapters, we derive the flux-difference splitting coefficients of the LTS-HLLϕ, and discuss how the three parameters affect the numerical diffusion of the scheme.

Numerical simulations for the inviscid Burgers' equation and the Euler equations are presented in chapter 6. Results obtained from the LTS-HLLϕ scheme are discussed and compared to results obtained from the LTS-Roe scheme. Finally, some concluding remarks and proposals for future work are found in chapter 7.

Chapter 2

Hyperbolic conservation laws

Physical phenomena in fluid dynamics, such as, transport of mass, momentum and energy are studied by considering the change of conserved quantities over a control volume Ω. A quantity, q^p, is conserved if the change of q^p inside Ω equals the net flux of q^p through the boundaries of the control volume, $\partial\Omega$. In general, the flux of one conserved quantity can depend on other conserved quantities. A system of m conserved quantities, is then governed by the *hyperbolic conservation law*,

$$\frac{\partial}{\partial t} \int_\Omega \mathbf{q}\mathrm{d}V + \int_{\partial\Omega} \mathbf{f}(\mathbf{q}) \cdot \mathbf{n}\mathrm{d}S = \mathbf{0}, \tag{2.1}$$

where $\mathbf{q}(x,t) = [q^1, \ldots, q^m]^T$ is the vector of conserved variables and $\mathbf{f}(\mathbf{q}) \cdot \mathbf{n}$ is the flux of $\mathbf{q}$ through $\partial\Omega$. We will refer to (2.1) as the *integral form*. Assuming that $\mathbf{q}$ is differentiable, we obtain the *differential form*

$$\frac{\partial\mathbf{q}}{\partial t} + \nabla \cdot \mathbf{f}(\mathbf{q}) = \mathbf{0}, \tag{2.2}$$

by applying the divergence theorem. In one space dimension, the differential form reduces to

$$\mathbf{q}_t + \mathbf{f}(\mathbf{q})_x = \mathbf{0}. \tag{2.3}$$

In the rest of this thesis we will only consider one-dimensional hyperbolic partial differential equations of the form (2.3). However, many of the concepts discussed in the thesis are extendable to multiple dimensions, e.g. through dimensional splitting [15].

2.1 Characteristic structure

Using the chain rule, we can rewrite (2.3) in the *quasi-linear form*

$$\mathbf{q}_t + \mathbf{J}(\mathbf{q})\mathbf{q}_x = \mathbf{0}, \tag{2.4}$$

where $\mathbf{J}(\mathbf{q}) = \frac{\partial \mathbf{f}}{\partial \mathbf{q}}(\mathbf{q})$ is the Jacobian matrix of the flux function $\mathbf{f}(\mathbf{q})$. A property of systems of hyperbolic partial differential equations is that the Jacobian matrix is diagonalizable with real eigenvalues [15]. We can therefore write $\mathbf{J}(\mathbf{q})$ on the from

$$\mathbf{J}(\mathbf{q}) = \mathbf{R}\Lambda\mathbf{R}^{-1}, \tag{2.5}$$

where $\mathbf{R} = \begin{pmatrix} \mathbf{r}^1, & \dots, & \mathbf{r}^m \end{pmatrix}$ is the matrix of right eigenvectors, where $\mathbf{r}^p$ is the p-th right eigenvector of $\mathbf{J}(\mathbf{q})$. The eigenvalue matrix, Λ, is defined as

$$\Lambda = \begin{pmatrix} \lambda^1 & 0 & \cdots & 0 \\ 0 & \lambda^2 & \cdots & 0 \\ \vdots & \vdots & \ddots & \vdots \\ 0 & 0 & \cdots & \lambda^m \end{pmatrix}, \tag{2.6}$$

where λ^p is the p-th eigenvalue of $\mathbf{J}$.

Pre-multiplying (2.4) by $\mathbf{R}^{-1}$ gives the *characteristic form*

$$\mathbf{w}_t + \Lambda\mathbf{w}_x = \mathbf{0}, \tag{2.7}$$

where $\mathbf{w} = [w^1, \dots, w^m]^T$ is the vector of *characteristic variables*, defined by

$$\partial\mathbf{w} = \mathbf{R}^{-1}\partial\mathbf{q}. \tag{2.8}$$

Because the rows in Λ only have one non-zero component, we have now transformed the system of m coupled equations into m uncoupled, scalar equations of the form

$$w_t^p + \lambda^p w_x^p = 0, \tag{2.9}$$

for all $p = 1, \dots, m$. We can use this transformation to apply theory developed for scalar equations on systems of equations. Note that for linear systems, we can use (2.8) to reconstruct $\mathbf{q}$ as the product of the matrix of right eigenvectors, $\mathbf{R}$ and the vector of characteristic variables, $\mathbf{w}$:

$$\mathbf{q} = \sum_{p=1}^m w^p \mathbf{r}^p. \tag{2.10}$$

2.2 Analytical solution

Let us consider a scalar conservation law on the quasi-linear form (2.4),

$$q_t + \lambda(q)q_x = 0, \tag{2.11}$$

where $\lambda(q) = \frac{\partial f}{\partial q}$. We define a *characteristic line*, $X(t)$, and note that

$$\frac{\mathrm{d}}{\mathrm{d}t}q(X(t), t) = q_t(X(t), t) + \frac{\mathrm{d}X(t)}{\mathrm{d}t}q_x(X(t), t). \tag{2.12}$$

We observe that the left hand side of (2.11) is equivalent to the right hand side of (2.12) if $\frac{\mathrm{d}X(t)}{\mathrm{d}t} = \lambda(q)$. Thus, on any characteristic line $X(t) = x + \lambda(q)t$, the value of q will remain constant because $\frac{\mathrm{d}}{\mathrm{d}t}q(X(t), t) = 0$. This means that for any given initial value $q(x, 0)$, the solution at time t is simply a translation in x-direction at speed $\lambda(q(x, 0))$, in other words,

$$q(x, t) = q(x - \lambda(q(x, 0))t, 0). \tag{2.13}$$

Figure 2.1: Analytical solution of the inviscid Burgers' equation for the initial data in (2.15). Left: The conserved quantity, q is convected in space from its initial state (solid line) until a shock is formed at $t = 1$ (dashed line). Right: The conserved quantity is constant along characteristic lines. When $t > 1$, some points are ambiguously defined.

2.3   Shock formation

Unfortunately, we cannot always use the analytical solution (2.13) for a general nonlinear conservation law, due to the phenomenon known as *shock formation*. We will illustrate this by an example.

Given the inviscid Burgers' equation

$$q_t + qq_x = 0, \tag{2.14}$$

and the initial data

$$q(x,0) = \begin{cases} 1 & \text{if } x < 0, \\ 1 - x & \text{if } 0 \le x \le 1, \\ 0 & \text{if } x > 1, \end{cases} \tag{2.15}$$

we can draw characteristic lines $X(t) = x + q(x,0)t$, and solve the problem using (2.13) as long as $t < 1$, as illustrated in figure 2.1. If we naively extend the characteristic lines beyond $t = 1$, we see that some points are defined by more than one characteristic line, thus the value of $q(x, t)$ is ambiguous in these points.

This happens whenever the solution form a discontinuity. We get an ambiguous result, because the differential equation (2.14) is no longer defined for discontinuous data. However, as we will see in the next section, we can find meaningful *weak solutions* for the ambiguous points. A good way of understanding weak solutions is by studying the *Riemann problem*.

2.4 The Riemann problem

A Riemann problem is an initial value problem consisting of a conservation law of the form (2.3) and initial data

$$\mathbf{q}(x, 0) = \begin{cases} \mathbf{q}_L & \text{if } x < 0 \\ \mathbf{q}_R & \text{if } x > 0. \end{cases} \tag{2.16}$$

where the vectors $\mathbf{q}_L$ and $\mathbf{q}_R$ are constant.

As illustrated in the previous section, using the inviscid Burgers' equation (2.14), differential equations are not defined when the initial data is discontinuous. In order to solve the Riemann problem at $x = 0$, we need to consider weak solutions of the conservation laws, that satisfies the corresponding integral equation.

An important weak solution is the shock solution. A shock is characterized by a discontinuity moving at speed s in space, without changing shape (see figure 2.2). We can find the speed of such a discontinuity by integrating (2.16) over a sufficiently large interval $\Omega = [-l, l]$. This gives

$$\frac{\partial}{\partial t} \int_{-l}^{l} \mathbf{q} \, \mathrm{d}x + \int_{-l}^{l} \frac{\partial}{\partial x} \mathbf{f}(\mathbf{q}) \, \mathrm{d}x = 0, \tag{2.17}$$

$$\frac{\mathrm{d}}{\mathrm{d}t} \left((l - x_{shock}) \mathbf{q}_R + (x_{shock} + l) \mathbf{q}_L \right) + \mathbf{f}(\mathbf{q}_R) - \mathbf{f}(\mathbf{q}_L) = 0, \tag{2.18}$$

where x_{shock} is the position of the discontinuity at any given time. Because $\frac{\mathrm{d}l}{\mathrm{d}t} = 0$, the expression simply reduces to

$$s(\mathbf{q}_R - \mathbf{q}_L) = \mathbf{f}(\mathbf{q}_R) - \mathbf{f}(\mathbf{q}_L), \tag{2.19}$$

where $s = \frac{\mathrm{d}x_{shock}}{\mathrm{d}t}$ is the speed of the discontinuity. In the scalar case, we can find this speed by simply dividing by $(q_R - q_L)$, which yields

$$s = \frac{f(q_R) - f(q_L)}{q_R - q_L}. \tag{2.20}$$

For a linear system of m equations, the Jacobian matrix is constant, and we can write (2.19) as

$$s(\mathbf{q}_R - \mathbf{q}_L) = \mathbf{J}(\mathbf{q}_R - \mathbf{q}_L), \tag{2.21}$$

which imply that the scalar s is an eigenvalue of $\mathbf{J}$. By writing $\mathbf{q}$ on the form (2.10) we can define *waves* as

$$\mathbf{q}_R - \mathbf{q}_L = \sum_{p=1}^{m} (w_R^p - w_L^p) \mathbf{r}^p$$

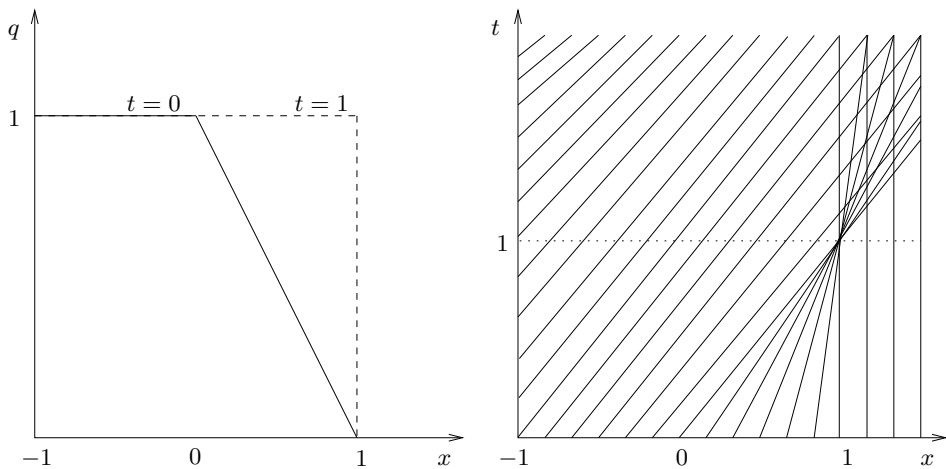$$= \sum_{p=1}^{m} \mathcal{W}^p, \tag{2.22}$$
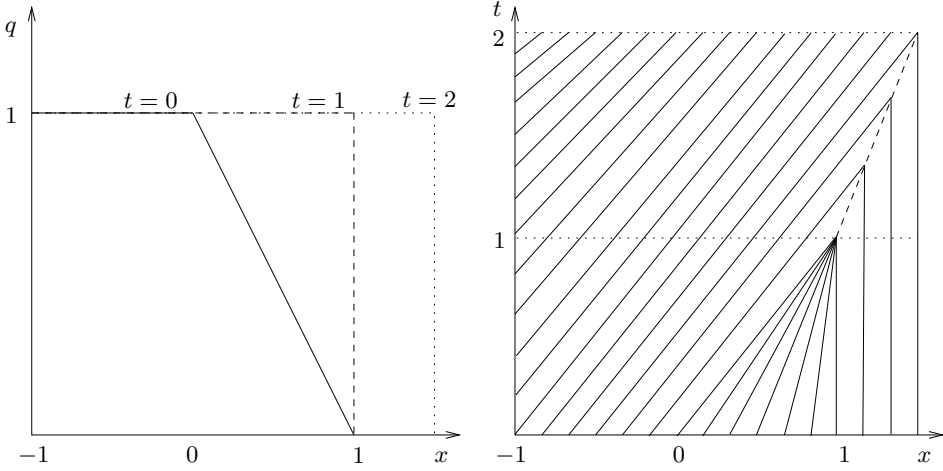
Figure 2.2: The shock solution of the inviscid Burgers' equation for the initial data in (2.15). Left: The conserved quantity, q is convected in space from its initial state (solid line) until a shock is formed at $t = 1$ (dashed line). The shock is simply translated in space (dotted line). Right: The conserved quantity is constant along characteristic lines. When $t > 1$, the shock follows the dashed characteristic line.

where $\mathcal{W}^p$ is the p-th wave. Using these definitions, we find that

$$
\begin{aligned}
\mathbf{J}(\mathbf{q}_R - \mathbf{q}_L) &= \mathbf{R}\boldsymbol{\Lambda}\mathbf{R}^{-1}\mathbf{R}(\mathbf{w}_R - \mathbf{w}_L) \\
&= \sum_{p=1}^{m} \lambda^p \mathcal{W}^p.
\end{aligned}
\tag{2.23}
$$

Hence, the discontinuity splits into m discontinuities, or waves $\mathcal{W}^p$, traveling at speeds λ^p.

Although the shock solution is a valid weak solution of the Riemann problem, it is not necessarily a unique solution. Since inviscid conservation laws often describe physical systems where some viscosity is present, we are interested in the unique solution of the corresponding viscous problem with diminishing viscosity. For a scalar conservation law, the *diminishing viscosity problem* is given by

$$
q_t + f(q)_x = \nu q_{xx},
\tag{2.24}
$$

where the viscosity coefficient $\nu \to 0$. Because solutions of (2.24) ensure non-decreasing entropy for the Euler equations, we will refer to them as *entropy satisfying solutions*. It can by shown that the shock solution is only entropy satisfying when

$$
f'(q_L) > s > f'(q_R),
\tag{2.25}
$$

where we assume the flux function $f(q)$ is either convex or concave, i.e. $f''(q) > 0$ or $f''(q) < 0$ respectively. This is known as the Lax entropy condition [10].
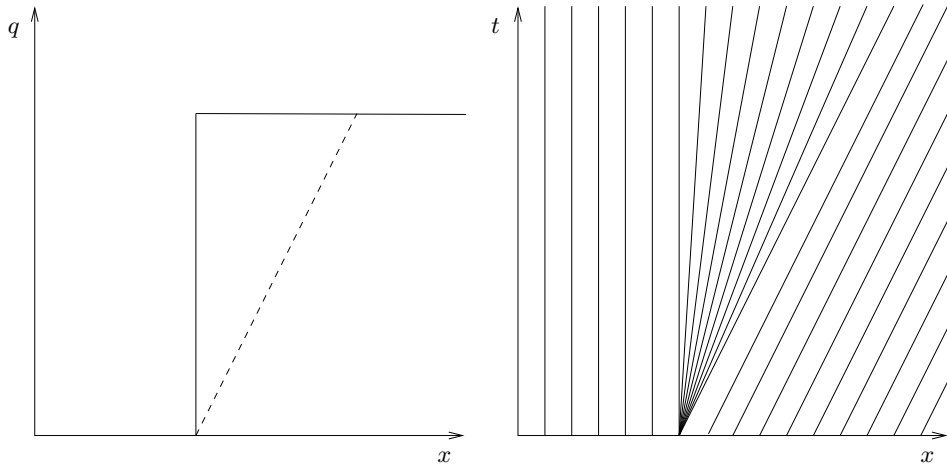
Figure 2.3: The rarefaction wave solution of a Riemann problem for the inviscid Burgers' equation. Left: The conserved quantity is experiencing rarefaction (dashed line). Right: The characteristic lines of a rarefaction wave spread into an expansion fan.

When the Lax entropy condition (2.25) is not satisfied, the entropy satisfying solution is a *rarefaction wave*. A rarefaction wave is, as the name suggests, a gradual reduction in the density of a conserved quantity, and is associated with expansion in gas dynamics. The characteristic lines of a rarefaction wave are separating from the discontinuity, forming an *expansion fan* in-between, as shown in figure 2.3.

For a system of m equations, the m new discontinuities can be either shocks waves, rarefaction waves or contact waves. The entropy satisfying solution can be decided by a more generalized version of the Lax entropy condition [15].

Chapter 3

Explicit finite volume methods

Finding an analytical solution of an initial value problem is often very hard, or even impossible. It is therefore desirable to find approximate numerical solutions of the problem. Before we can calculate numerical solutions, we need to convert the initial value problem into a discrete, arithmetic problem that can be solved by simple operations.

One popular method for discretizing conservation laws on the integral form (2.1), is to divide the domain into small finite control volumes. Given a one-dimensional control volume $\Omega = [x_L, x_R]$, we can integrate (2.1) in time over the interval $[t_n, t_{n+1}]$:

$$\int_{t_n}^{t_{n+1}} \int_{x_L}^{x_R} \mathbf{q}_t \mathrm{d}x \mathrm{d}t + \int_{t_n}^{t_{n+1}} \int_{x_L}^{x_R} \mathbf{f}(\mathbf{q})_x \mathrm{d}x \mathrm{d}t = 0. \tag{3.1}$$

By using the fundamental theorem of calculus and Fubini's theorem, we can write (3.1) as

$$\int_{x_L}^{x_R} [\mathbf{q}(x, t_{n+1}) - \mathbf{q}(x, t_n)] \mathrm{d}x + \int_{t_n}^{t_{n+1}} [\mathbf{f}(\mathbf{q}(x_R, t)) - \mathbf{f}(\mathbf{q}(x_L, t))] \mathrm{d}t = 0, \tag{3.2}$$

Let us now define average values for $\mathbf{q}$ and $\mathbf{f}$ as

$$\mathbf{Q}^n = \frac{1}{x_R - x_L} \int_{x_L}^{x_R} \mathbf{q}(x, t_n) \mathrm{d}x, \tag{3.3a}$$

$$\mathbf{F}_L = \frac{1}{t_{n+1} - t_n} \int_{t_n}^{t_{n+1}} \mathbf{f}(\mathbf{q}(x_L, t)) \mathrm{d}t, \tag{3.3b}$$

respectively. By using the new definitions in (3.3), we can write (3.2) as

$$\mathbf{Q}^{n+1} = \mathbf{Q}^n - \frac{t_{n+1} - t_n}{x_R - x_L} (\mathbf{F}_R - \mathbf{F}_L). \tag{3.4}$$

This expression is valid for any domain, or control volume. In the finite volume method (FVM), we divide the x-axis into smaller subdomains, $\Omega_j = [x_{j-1/2}, x_{j+1/2}]$, where
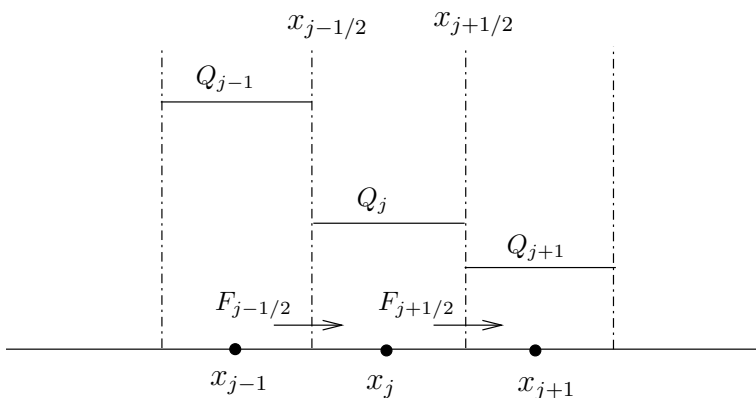
Figure 3.1: Computational grid in the finite volume method.

$x_{j\pm 1/2}$ are the faces of the *computational cell* j, as illustrated in figure 3.1. We associate every computational cell with the average value of the cell, defined in (3.3). For each cell j we have

$$\mathbf{Q}_j^{n+1} = \mathbf{Q}_j^n - \frac{\Delta t}{\Delta x}(\mathbf{F}_{j+1/2} - \mathbf{F}_{j-1/2}). \tag{3.5}$$

where the grid size $\Delta x = x_{j+1/2} - x_{j-1/2}$ is assumed to be uniform. Equation (3.5) implies that the change in $\mathbf{Q}_j$ during one time step is equal to the net flux entering the computational cell from the neighbouring cells during the time step.

We now need a way of approximating the fluxes at the interfaces. *Explicit finite volume methods* only use values from the previous time step to approximate the fluxes, which implies that we can calculate $\mathbf{Q_j^{n+1}}$ explicitly. Many of the classic explicit schemes only consider the neighbouring cells in the previous time step, which means that the *numerical flux function*,

$$\mathbf{F}_{j-1/2}^n = \mathbf{F}(\mathbf{Q}_{j-1}^n, \mathbf{Q}_j^n), \tag{3.6}$$

only depends on the two computational cells that are sharing the interface at $x_{j-1/2}$. We will refer to such schemes as *3-point schemes*, because $\mathbf{Q}_j^{n+1}$ depends on the values in three computational cells.

3.1   The flux-difference splitting formulation

Looking at figure 3.1, the value of $\mathbf{Q}$ is piecewise constant function, with discontinuities at the interfaces between cells. Because of these discontinuities, we need to solve a Riemann problem on every interface. We can think of the discontinuities as waves entering the cell from the interfaces. This wave description of the finite volume method (3.5) will be referred to as the *flux-difference splitting* formulation. By using the definition of waves

(2.22), (3.5) becomes

$$\mathbf{Q}_j^{n+1} = \mathbf{Q}_j^n - \frac{\Delta t}{\Delta x} \sum_{p=1}^m \left((\lambda_{j-1/2}^p)^+ \mathcal{W}_{j-1/2}^p + (\lambda_{j+1/2}^p)^- \mathcal{W}_{j+1/2}^p \right) \qquad (3.7)$$

where $(\lambda_{j-1/2}^p)^+ = \max(\lambda_{j-1/2}^p, 0)$ and $(\lambda_{j+1/2}^p)^- = \min(\lambda_{j+1/2}^p, 0)$. For scalar conservation laws, we will write this as

$$Q_j^{n+1} = Q_j^n - \left(C_{j-1/2}^+ \Delta_{j-1/2} + C_{j+1/2}^- \Delta_{j+1/2} \right), \qquad (3.8)$$

where we have introduced the shorthand

$$\Delta_{j-1/2} = Q_j - Q_{j-1}, \qquad (3.9a)$$

$$C_{j\mp 1/2}^\pm = \frac{\Delta t}{\Delta x} \lambda_{j\mp 1/2}^\pm. \qquad (3.9b)$$

We can think of the coefficients $C^\pm$ as a measure of how far a wave will travel during one time step. If $C_{j-1/2}^+ = 1$ this means that the wave from the left interface will travel all the way to the right interface, and $C_{j+1/2}^- = -1$ means the wave from the right interface will travel all the way to the left interface during one time step.

3.2 The Godunov method

As discussed in the previous section, we need to solve Riemann problems on every cell interface in explicit finite volume methods. In 1959, Godunov proposed solving these Riemann problems exactly [5], and this method has been named after him. For scalar equations, the exact unique entropy satisfying solution of the local Riemann problem at the interface $x_{j-1/2}$ is obtained using the numerical flux function

$$\tilde{F}_{j-1/2} = \begin{cases} \min\limits_{q \in [Q_{j-1}, Q_j]} f(q) & \text{if } Q_{j-1} < Q_j, \\ \max\limits_{q \in [Q_j, Q_{j-1}]} f(q) & \text{if } Q_{j-1} > Q_j, \end{cases} \qquad (3.10)$$

In the Godunov method, we use this *exact* numerical flux function in (3.4). Although we can now solve any scalar conservation law, the Godunov method is not always the most practical method, since we need to solve an optimization problem in order to find $\tilde{F}_{j-1/2}$. If this cannot be done analytically, we need to use some iterative method (like Newton's method), which can be very costly. For non-linear systems, the Godunov method is even more complex and computationally costly.

3.3 Approximate Riemann solvers

It is often too computationally costly to solve the Riemann problems at the interfaces exactly, and *approximate Riemann solvers* are therefore often more expedient. Some relevant approximate schemes are presented below.

3.3.1 The Roe scheme

In the Roe scheme [20], the Riemann problems on each cell interface are linearized. At interface $x_{j-1/2}$, the true Riemann problem is approximated by

$$\mathbf{q}_t + \widehat{\mathbf{J}}_{j-1/2}\mathbf{q}_x = \mathbf{0} \tag{3.11}$$

$$\mathbf{q}(x,0) = \begin{cases} \mathbf{Q}_{j-1} & \text{if } x < x_{j-1/2} \\ \mathbf{Q}_j & \text{if } x > x_{j-1/2} \end{cases} \tag{3.12}$$

where $\widehat{\mathbf{J}}$ is a constant matrix known as the *Roe matrix*. In order for the linearized problem to be consistent with the true Riemann problem, the Roe matrix must have the following properties:

Property 1. *The linearized problem is hyperbolic, hence, $\widehat{\mathbf{J}}_{j-1/2}$ has real eigenvalues and linearly independent eigenvectors.*

Property 2. *When $\mathbf{Q}_j = \mathbf{Q}_{j-1} = \mathbf{Q}$, the Roe matrix is consistent with the exact Jacobian matrix in the sense,*

$$\widehat{\mathbf{J}}_{j-1/2}(\mathbf{Q},\mathbf{Q}) = \mathbf{J}(\mathbf{Q}). \tag{3.13}$$

Property 3. *The Roe matrix is conservative in the sense that,*

$$\widehat{\mathbf{J}}_{j-1/2}(\mathbf{Q}_j - \mathbf{Q}_{j-1}) = \mathbf{f}(\mathbf{Q}_j) - \mathbf{f}(\mathbf{Q}_{j-1}). \tag{3.14}$$

From property 1, we know that the Roe matrix can be written in the form

$$\widehat{\mathbf{J}}_{j-1/2} = \widehat{\mathbf{R}}_{j-1/2}\widehat{\mathbf{\Lambda}}_{j-1/2}\widehat{\mathbf{R}}_{j-1/2}^{-1}, \tag{3.15}$$

where $\widehat{\mathbf{\Lambda}}_{j-1/2}$ is a matrix with the *Roe speeds*, $\hat{\lambda}^p_{j-1/2}$, in the diagonal. Using (2.23), we can write (3.14) as a sum of waves

$$\widehat{\mathbf{J}}_{j-1/2}(\mathbf{Q}_j - \mathbf{Q}_{j-1}) = \sum_{p=1}^{m} \hat{\lambda}^p_{j-1/2}\mathcal{W}^p_{j-1/2}, \tag{3.16}$$

giving the following flux-difference splitting coefficients for the Roe scheme:

$$(\lambda^p_{j-1/2})^{\pm} = \pm \max(0, \pm\hat{\lambda}^p_{j-1/2}), \tag{3.17}$$

or for a scalar equation

$$C^{\pm}_{j-1/2} = \pm \max(0, \pm\hat{c}_{j-1/2}), \tag{3.18}$$

where we have introduced the shorthand

$$\hat{c} = \frac{\Delta t}{\Delta x}\hat{\lambda}. \tag{3.19}$$
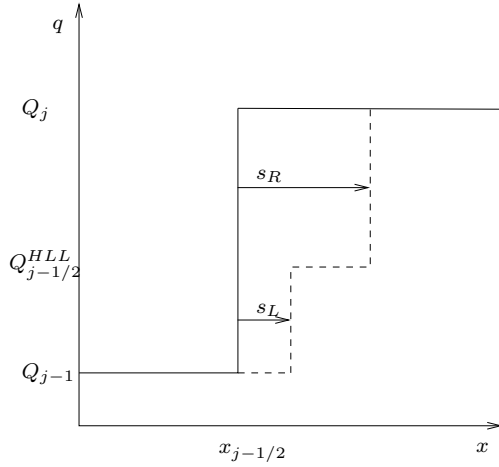
Figure 3.2: Illustration of the HLL scheme. The discontinuity is split into two discontinuities, traveling at speeds s_L and s_R.

3.3.2 The HLL scheme

Harten, Lax and van Leer [8] proposed approximating the solution of the Riemann problems at the interfaces as

$$\mathbf{Q}(x,t) = \begin{cases} \mathbf{Q}_{j-1} & \text{if } \zeta \leq s_L, \\ \mathbf{Q}_{j-1/2}^{HLL} & \text{if } s_L \leq \zeta \leq s_R, \\ \mathbf{Q}_j & \text{if } \zeta \geq s_R. \end{cases} \tag{3.20}$$

where

$$\zeta = \frac{x - x_{j-1/2}}{t - t_0} \tag{3.21}$$

which means that the discontinuity split into two waves, moving at speeds s_L and s_R, i.e.

$$s(\mathbf{Q}_j - \mathbf{Q}_{j-1}) = s_R(\mathbf{Q}_j - \mathbf{Q}_{j-1/2}^{HLL}) + s_L(\mathbf{Q}_{j-1/2}^{HLL} - \mathbf{Q}_{j-1}). \tag{3.22}$$

This is illustrated in figure 3.2. For now, let us assume s_L and s_R to be known. We then need to choose $\mathbf{Q}_{j-1/2}^{HLL}$ in such a way that (3.20) is a weak solution of the hyperbolic conservation law. Given the domain $[x_L, x_R]$, we can integrate (2.1) in the time interval $[t_n, t_n + \Delta t]$,

$$\int_{x_L}^{x_R} \mathbf{q}(x, t_n + \Delta t) \mathrm{d}x = \int_{x_L}^{x_R} \mathbf{q}(x, t_n) \mathrm{d}x - \int_{t_n}^{t_n + \Delta t} [\mathbf{f}(x_R, t) - \mathbf{f}(x_L, t)] \mathrm{d}t. \tag{3.23}$$

If $x_L \leq s_L \Delta t + x_{j-1/2}$ and $x_R \geq s_R \Delta t + x_{j-1/2}$, we can evaluate the integrals on the right hand side using the cell averages (3.3),

$$\int_{x_L}^{x_R} \mathbf{q}(x, t_n + \Delta t) \mathrm{d}x = x_R \mathbf{Q}_j - x_L \mathbf{Q}_{j-1} - \Delta t (\mathbf{F}_j - \mathbf{F}_{j-1}). \tag{3.24}$$

By using the desired solution in (3.20), $\int_{x_L}^{x_R} \mathbf{q}(x, t_n + \Delta t)\mathrm{d}x$ can be split into three integrals,

$$\int_{x_L}^{x_R} \mathbf{q}(x, t_n + \Delta t)\mathrm{d}x = \int_{x_L}^{s_L \Delta t} \mathbf{Q}_{j-1}\mathrm{d}x + \int_{s_L \Delta t}^{s_R \Delta t} \mathbf{Q}_{j-1/2}^{HLL}\mathrm{d}x + \int_{s_R \Delta t}^{x_R} \mathbf{Q}_j \mathrm{d}x. \quad (3.25)$$

Comparing this to (3.24), we can show that

$$\mathbf{Q}_{j-1/2}^{HLL} = \frac{s_R \mathbf{Q}_j - s_L \mathbf{Q}_{j-1} + \mathbf{F}_{j-1} - \mathbf{F}_j}{s_R - s_L}. \quad (3.26)$$

For a linear system, we can insert this into (3.22) and use the wave definition in (2.23). We then get

$$s(\mathbf{Q}_j - \mathbf{Q}_{j-1}) = \sum_{p=1}^{m} \left(\frac{\lambda_{j-1/2}^p - s_L}{s_R - s_L} s_R + \frac{s_R - \lambda_{j-1/2}^p}{s_R - s_L} s_L \right) \mathcal{W}_{j-1/2}^p, \quad (3.27)$$

which we can also apply to non-linear systems through Roe averaging, described in section 3.3.1. We see that the flux-difference splitting coefficients of the HLL scheme are given by

$$(\lambda_{j-1/2}^p)^{\pm} = \pm \frac{\hat{\lambda}_{j-1/2}^p - s_L}{s_R - s_L} \max(\pm s_R, 0) \pm \frac{s_R - \hat{\lambda}_{j-1/2}^p}{s_R - s_L} \max(\pm s_L, 0), \quad (3.28)$$

which for scalar conservation laws can be written as

$$C_{j-1/2}^{\pm} = \pm \frac{\hat{c}_{j-1/2} - c_L}{c_R - c_L} \max(\pm c_R, 0) \pm \frac{c_R - \hat{c}_{j-1/2}}{c_R - c_L} \max(\pm c_L, 0), \quad (3.29)$$

using the shorthand

$$c_R = \frac{\Delta t}{\Delta x} s_R, \quad (3.30)$$

$$c_L = \frac{\Delta t}{\Delta x} s_L. \quad (3.31)$$

The HLLE scheme

So far we have not discussed how we choose s_L and s_R. Einfeldt [4] proposed using

$$s_{L,j-1/2} = \min(\lambda^1(\mathbf{Q}_{j-1}), \hat{\lambda}^1(\hat{\mathbf{Q}}_{j-1/2})), \quad (3.32a)$$
$$s_{R,j-1/2} = \max(\hat{\lambda}^m(\hat{\mathbf{Q}}_{j-1/2}), \lambda^m(\mathbf{Q}_j)). \quad (3.32b)$$

which ensures that $\hat{\lambda}^p(\hat{\mathbf{Q}}_{j-1/2}) \in [s_L, s_R], \forall p$. Einfeldt's choice also has Lax entropy conditions (2.25) built in, so that the scheme reduces to the Roe scheme for the 1st and m-th wave when the entropy satisfying solution is a shock. We will refer to the HLL scheme with Einfeldt's choice of parameters as the HLLE scheme.
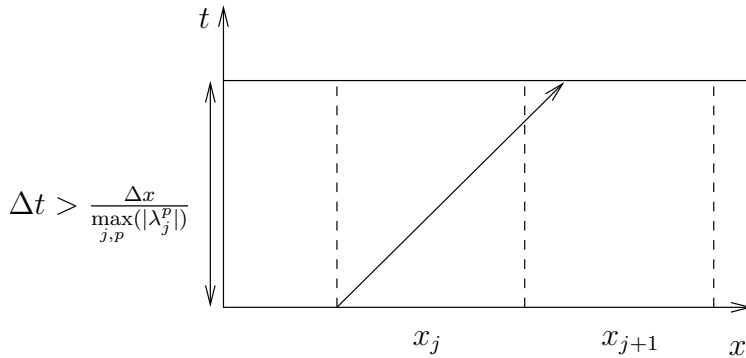
$$\Delta t > \frac{\Delta x}{\max_{j,p}(|\lambda_j^p|)}$$

Figure 3.3: Illustration of characteristic lines when CFL> 1.

3.4 The CFL condition

For simple explicit 3-point schemes, the maximal allowed time step is limited by the Courant-Friedrichs-Lewy (CFL) condition [2]:

$$\text{CFL} = \frac{\Delta t}{\Delta x} \max_{j,p}|\lambda_j^p| \leq 1, \tag{3.33}$$

where CFL is the greatest *Courant number* inherent to the problem. To get a more intuitive understanding of the CFL condition, let us consider a scalar equation where $\lambda_{j-1/2} > \frac{\Delta x}{\Delta t}$. In this case, the Roe scheme will give $C_{j-1/2}^+ > 1$, meaning that the wave from the left interface of cell j should travel through the entire cell, and start entering cell $j + 1$, as illustrated in figure 3.3. However, in a 3-point scheme, this is not taken into account when we perform calculations for cell $j + 1$.

Because of the CFL condition we are often forced to use small time steps, which is computationally costly. Since $\Delta t \propto \Delta x$, we must use even smaller time steps when we refine the grid.

Large time step methods

Large time step methods (LTS) are explicit finite volume methods that are not limited by the CFL condition. In this chapter we show how the flux-difference splitting formulation (section 3.1) can be expanded to allow for higher time steps, and generalize the approximate Riemann solvers to LTS. For the sake of simple explanation, we only consider scalar equations in this chapter. However, we can extend the LTS schemes to non-linear systems through Roe linearization, described in section 3.3.1.

4.1   Large time step methods

If a wave is allowed to travel further than one cell length during one time step, this implies the numerical flux function must depend on a wider stencil of cells

$$F_{j-1/2} = F(Q_{j-k}, \dots, Q_{j-1+k}). \tag{4.1}$$

When $k = 1$, we have a 3-point scheme that is limited by the CFL condition. In general, a $(2k + 1)$-point scheme is limited by a relaxed CFL-like condition

$$\text{CFL} = \frac{\Delta t}{\Delta x} \max_j |\lambda_j| \leq k, \tag{4.2}$$

where $\lambda = \frac{\mathrm{d}f}{\mathrm{d}q}$. In flux-difference splitting formulation, the change in the conserved quantity is now a sum of all the waves passing through or ending up inside the cell. In total, a cell can be affected by up to k waves from the left, and k waves from the right. The large time step extension of the flux-difference splitting formulation (3.7) is therefore

$$Q_j^{n+1} = Q_j^n - \sum_{i=0}^{k-1} \left(C_{j-1/2-i}^{i+} \Delta_{j-1/2-i} + C_{j+1/2+i}^{i-} \Delta_{j+1/2+i} \right), \tag{4.3}$$

where the coefficient $C_{j-1/2-i}^{i+}$ describes how far the wave from interface $x_{j-1/2-i}$ has traveled into cell j. Note that for 3-point schemes (4.3) reduces to (3.7) where $C_{j\mp1/2}^{0\pm} = C_{j\mp1/2}^{\pm}$.

4.2 Modified equation and numerical diffusion

Because a numerical solution is often based on approximated fluxes and projected onto a finite number of cells, it will generally not satisfy the hyperbolic conservation law exactly. If this is the case, we can find *modified equations* that the numerical solution satisfies more accurately than the original conservation law.

Bore showed that a $(2k+1)$-point explicit finite volume method on the form (4.3), gives a second order accurate approximation to the modified equation [1],

$$q_t + f(q)_x = \frac{\Delta x^2}{2\Delta t}\left[\left(\sum_{i=0}^{N-1}(2i+1)(C^{i+}-C^{i-})-C^2\right)q_x\right]_x, \qquad (4.4)$$

where $C = \frac{\Delta t}{\Delta x}f'(q)$ is the *local Courant number*. We can also write the modified equation in terms of a modified flux function $f(q) - g(q)$, where

$$g(q) = \frac{\Delta x^2}{2\Delta t}\sigma(C)q_x, \qquad (4.5)$$

and $\sigma(C)$ is the numerical diffusion coefficient

$$\sigma(C) = \sum_{i=0}^{N-1}(2i+1)(C^{i+}-C^{i-})-C^2. \qquad (4.6)$$

We will refer to the error term on the right hand side of (4.4) as the *numerical diffusion* of a scheme, because it is proportional to q_{xx} for linear equations. A numerical method is then a second order approximation of a viscous partial differential equation, where the *numerical viscosity* coefficient is $\nu_{num} = \frac{2\Delta t}{\Delta x^2}\sigma(C)$. For more detailed derivations of the modified equation (4.4), we refer to [1].

4.3 The total variation diminishing condition

The CFL condition is not sufficient to ensure stability for a general non-linear conservation law. In 1983, Harten [6] introduced the stricter *total variation diminishing* (TVD) condition,

$$\text{TV}^{n+1} \le \text{TV}^n, \qquad (4.7)$$

where TV is the *total variation* given by

$$\text{TV}^n = \sum_j |Q_j^n - Q_{j-1}^n|. \qquad (4.8)$$

The TVD condition is a strong stability condition, that guarantees that a scheme will converge to a weak solutions [10]. Harten showed that a 3-point scheme is unconditionally TVD if and only if

$$C_{j-1/2}^+ - C_{j-1/2}^- \le 1. \qquad (4.9)$$

This was later generalized for $(2k + 1)$-point schemes by Jameson and Lax [9]. A $(2k + 1)$-point scheme is TVD if

$$C_{j-1/2}^{(i+1)+} - C_{j-1/2}^{i+} \leq 0, \quad \forall i \geq 0, \tag{4.10a}$$

$$C_{j-1/2}^{0+} - C_{j-1/2}^{0-} \leq 1, \tag{4.10b}$$

$$C_{j-1/2}^{(i+1)-} - C_{j-1/2}^{i-} \geq 0, \quad \forall i \geq 0. \tag{4.10c}$$

for all j.

4.4 Some large time step methods

When a LTS scheme reduces to a known 3-point scheme for $k = 1$, and they share many characteristics, we say that the LTS scheme is a LTS extension of the 3-point scheme. A few LTS extension are given in the next sections.

4.4.1 The LTS-Godunov method

The LTS-Godunov method, which is characterized by solving every Riemann problem exactly, was the first LTS-method used by LeVeque in [13]. A closed form formulation of the method was derived by Solberg in his project work [22], and later published in [16]. The flux-difference splitting coefficients for the LTS-Godunov method are given by

$$
\begin{aligned}
[C^{i+}\Delta]_{j-1/2} = Q_j \\
+ \mathcal{M}_{j-1/2}\left(\frac{\Delta t}{\Delta x}f(q) - (i+1)q\right) - \mathcal{M}_{j-1/2}\left(\frac{\Delta t}{\Delta x}f(q) - iq\right),
\end{aligned}
\tag{4.11a}
$$

$$
\begin{aligned}
[C^{i-}\Delta]_{j-1/2} = Q_j \\
+ \mathcal{M}_{j-1/2}\left(\frac{\Delta t}{\Delta x}f(q) + iq\right) - \mathcal{M}_{j-1/2}\left(\frac{\Delta t}{\Delta x}f(q) + (i+1)q\right),
\end{aligned}
\tag{4.11b}
$$

where the operator $\mathcal{M}$ is defined as

$$
\mathcal{M}_{j-1/2}(f(q)) = \begin{cases} \min\limits_{q \in [Q_{j-1}, Q_j]} f(q) & \text{if} \quad Q_{j-1} < Q_j, \\ \max\limits_{q \in [Q_j, Q_{j-1}]} f(q) & \text{if} \quad Q_{j-1} \geq Q_j. \end{cases}
\tag{4.12}
$$

4.4.2 The LTS-Roe scheme

The Roe scheme treats the Riemann problem at every cell interface as a linearized Riemann problem, and waves are convected unchanged at Roe speed. If a positive wave from the interface at $x_{j-1/2}$ passes through cell $j + i$, this cell is fully affected by the wave, hence $C_{j-1/2}^{i+} = 1$. If the wave ends up inside cell $j + i$, the cell is only partially affected, and we get $0 < C_{j-1/2}^{i+} = \hat{c}_{j-1/2} - i < 1$. We can perform the same analysis for negative waves, giving the flux-difference splitting coefficients of the LTS-Roe scheme,

$$C^{i+} = \begin{cases} 1 & \text{if } i \leq \hat{c} - 1 \\ \hat{c} - i & \text{if } \hat{c} - 1 < i < \hat{c} \\ 0 & \text{if } i \geq \hat{c} \end{cases} \tag{4.13a}$$

$$C^{i-} = \begin{cases} -1 & \text{if } i \leq -\hat{c} - 1 \\ \hat{c} + i & \text{if } -\hat{c} - 1 < i < -\hat{c} \\ 0 & \text{if } i \geq -\hat{c} \end{cases} \tag{4.13b}$$

which we can write more compactly as

$$C^{i\pm} = \pm \max(0, \min(\pm\hat{c} - i, 1)). \tag{4.14}$$

If we insert (4.14) into the expression for the numerical diffusion coefficient (4.6), we can show that

$$\sigma_{Roe}(\hat{c}) = \alpha(1 - \alpha), \tag{4.15}$$

where $\alpha = \lceil |\hat{c}| \rceil - |\hat{c}|$. Note that $\sigma_{Roe}(\hat{c}) = 0$ when $\hat{c} \in \mathbb{Z}$. Lindquist et al. [16] showed that the LTS-Roe scheme is the least diffusive LTS scheme that satisfies the TVD conditions (4.10).

Note that the 3-point LTS-Roe scheme reduces to the original Roe scheme (3.18),

$$\begin{aligned} C^{0\pm} &= C^{\pm} \\ &= \pm \max(0, \pm\hat{c}). \end{aligned} \tag{4.16}$$

4.4.3 The LTS-Lax-Friedrichs scheme

The most diffusive LTS scheme that satisfies the TVD conditions (4.10), is obtained when $C_{j-1/2}^{\pm i} = C_{j-1/2}^{\pm(i+1)}$ for all i and j. The LTS-Lax-Friedrichs scheme given in flux-difference splitting formulation as

$$C^{i\pm} = \frac{1}{2k}(\hat{c} \pm k), \tag{4.17}$$

is the only consistent scheme that satisfies this condition [16]. Here, we differentiate between the local LTS-Lax-Friedrichs scheme, where $k = \lceil |\hat{c}| \rceil$, and the global LTS-Lax-Friedrichs scheme, where $k = \lceil CFL \rceil$.

When we insert (4.17) into the expression for the numerical diffusion coefficient (4.6), we get that

$$\sigma_{LF}(\hat{c}) = k^2 - \hat{c}^2. \tag{4.18}$$

4.4.4 The LTS-HLL scheme

The HLL scheme is characterized as a scheme that splits discontinuities into two shock waves. A LTS extension of the HLL scheme was recently developed by Prebeg et al. [19]. The flux-difference splitting coefficients of this scheme are given by:

$$C^{i\pm} = \pm\frac{\hat{c} - c_L}{c_R - c_L} \max\left(0, \min(\pm c_R - i, 1)\right) \pm \frac{c_R - \hat{c}}{c_R - c_L} \max\left(0, \min(\pm c_L - i, 1)\right).$$

$$(4.19)$$

Note how similar this expression is to the corresponding expression for LTS-Roe scheme (4.14). In the limit when $c_L \to \hat{c}$ and $c_R \to \hat{c}$ the LTS-HLL scheme reduce to the LTS-Roe scheme.

If we insert (4.19) into the general expression for the numerical diffusion coefficient in (4.6), Prebeg showed in [18] that

$$\sigma_{HLL}(\hat{c}) = (c_R - \hat{c})(\hat{c} - c_L) + \frac{\hat{c} - c_L}{c_R - c_L}\alpha_R(1 - \alpha_R) + \frac{c_R - \hat{c}}{c_R - c_L}\alpha_L(1 - \alpha_L), \quad (4.20)$$

where $\alpha_L = \lceil|c_L|\rceil - |c_L|$ and $\alpha_R = \lceil|c_R|\rceil - |c_R|$.

4.5 Artificial flux functions

Another way of defining an approximate Riemann solver is by finding an approximate equation on the form,

$$q_t + \bar{f}(q; q_L; q_R)_x = 0, \qquad (4.21)$$

that, when solved exactly by the Godunov method, yields the same solution as if we solve the exact problem using the approximate Riemann solver. We will refer to $\bar{f}(q; q_L; q_R)$ as the *artificial flux function*.

4.5.1 The artificial flux framework

In order to find schemes that are consistent to the exact problem, $\bar{f}(q; q_L; q_R)$ must have the following properties:

Property 1. *The artificial flux function is Lipschitz continuous.*

Property 2. *The artificial flux function is consistent with the true flux function in the sense*

$$\bar{f}(q_L; q_L; q_R) = f(q_L), \qquad (4.22a)$$
$$\bar{f}(q_R; q_L; q_R) = f(q_R). \qquad (4.22b)$$

Property 3. *The artificial flux function is conservative when,*

$$\int_{q_L}^{q_R} \bar{f}'(q; q_L; q_R)dq = f(q_R) - f(q_L). \qquad (4.23)$$

In the next sections, we will mostly express the artificial flux function, $\bar{f}(q; q_L; q_R)$, in terms of a *relative flux functions* $\mathcal{F}(\theta)$ defined by the relationship

$$\bar{f}(\theta(q; q_L; q_R)) = f_L + \frac{\Delta x}{\Delta t}\mathcal{F}(\theta)\Delta, \qquad (4.24)$$

where

$$\theta = \frac{q - q_L}{q_R - q_L}, \tag{4.25}$$

and $\Delta = q_R - q_L$. This formulation is practical, because an artificial flux function $\bar{f}(q; q_L; q_R)$ always satisfies property 2 and property 3 as long as

$$\mathcal{F}(0) = 0, \tag{4.26a}$$
$$\mathcal{F}(1) = \hat{c}. \tag{4.26b}$$

Note that for any relative flux functions, the chain rule gives

$$\bar{f}'(q; q_L; q_R) = \frac{\Delta x}{\Delta t} \mathcal{F}'(\theta), \tag{4.27}$$

thus, the function $\mathcal{F}'(\theta)$ is a *non-dimensional wave speed*, whose size determine the number of cells a wave will travel in one time step.

4.5.2 Some relative flux functions

In (4.24) we defined the relative flux function $\mathcal{F}(\theta)$. In this section we look at some special relative flux functions and show how these relate to known approximate Riemann solvers.

The Roe scheme

If we choose $\mathcal{F}(\theta)$ to be linear,

$$\mathcal{F}(\theta) = a_0 + a_1 \theta, \tag{4.28}$$

there is only one choice that satisfies (4.26), namely $a_0 = 0$ and $a_1 = \hat{c}$. This corresponds to the artificial flux function

$$\bar{f}(q; q_L; q_R) = \hat{\lambda} q, \tag{4.29}$$

which is the same linearization as in the Roe scheme. The Roe scheme has a constant non-dimensional wave speed, as illustrated in 4.1.

The HLL scheme

Another interesting choice of $\mathcal{F}$ is a continuous function consisting of two piecewise linear functions

$$\mathcal{F}(\theta) = \begin{cases} c_L \theta & \text{if } \theta \leq \theta^* \\ c_L \theta^* + c_R(\theta - \theta^*) & \text{if } \theta > \theta^* \end{cases} \tag{4.30}$$
$$= c_L \theta + (c_R - c_L) \max(0, \theta - \theta^*),$$

where c_L and c_R are the slopes of the two linear functions and θ^* is the point of intersection. When enforcing the consistency condition (4.26) we get that
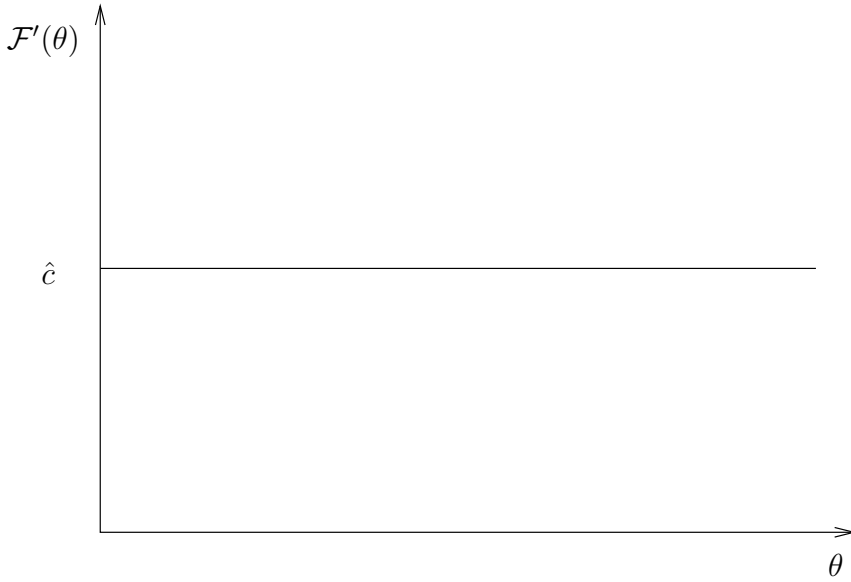
Figure 4.1: The non-dimensional wave speed of the Roe scheme

$$\theta^* = \frac{c_R - \hat{c}}{c_R - c_L}.$$ (4.31)

which corresponds to Q^{HLL} in (3.26) since

$$\begin{aligned} q^* &= q_L + (q_R - q_L)\theta^* \\ &= \frac{s_R q_R - s_L q_L + f(q_L) - f(q_R)}{s_R - s_L}. \end{aligned}$$ (4.32)

The non-dimensional wave speed of the HLL schemes consist of two piecewise constant values,

$$\mathcal{F}'(\theta) = c_L + (c_R - c_L)H(\theta - \theta^*),$$ (4.33)

where $H(x)$ is the Heaviside function. This is illustrated in figure 4.2.

The Solberg scheme

Solberg [23] proposed a LTS scheme in his master's thesis, which he denoted the Constant-Diffusion-$\hat{k}$ (CD$\hat{k}$) scheme. We will now express a similar scheme in artificial flux formulation, denoted here as the Solberg scheme.

Let the relative flux function $\mathcal{F}(\theta)$ be a second order polynomial,

$$\mathcal{F}(\theta) = a_0 + a_1\theta + a_2\theta^2.$$ (4.34)
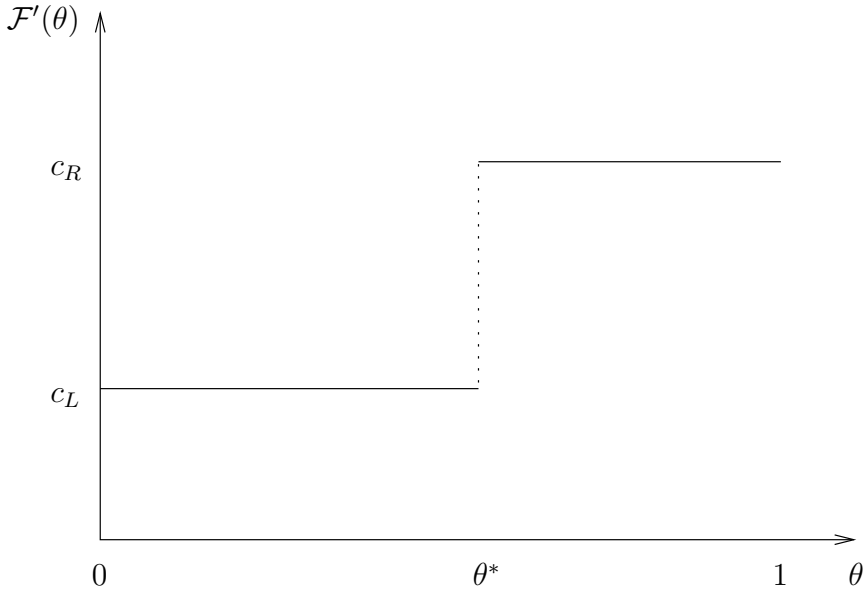
Figure 4.2: The non-dimensional wave speed of the HLL scheme

When enforcing the consistency conditions (4.26), we find that $a_0 = 0$, $a_1 = \hat{c} - a_2$ and $a_2 = \hat{k}$, where $\hat{k}$ is a free parameter. With these restrictions, we get a one parameter scheme

$$\mathcal{F}(\theta) = (\hat{c} - \hat{k})\theta + \hat{k}\theta^2, \tag{4.35}$$

with the non-dimensional wave speed

$$\mathcal{F}'(\theta) = \hat{c} - \hat{k} + 2\hat{k}\theta, \tag{4.36}$$

which is illustrated in figure 4.3. If we denote the lowest and highest non-dimensional wave speed in the Solberg scheme as

$$\mathcal{F}'(0) = c_L \tag{4.37a}$$
$$= \hat{c} - \hat{k},$$

$$\mathcal{F}'(1) = c_R \tag{4.37b}$$
$$= \hat{c} + \hat{k},$$

we can think of the Solberg scheme as a HLL-type scheme, but where the non-dimensional wave speed changes linearly between c_L and c_R in stead of through a discontinuity.

Note that $\hat{k}$ can be any positive number, while Solberg's original CD$\hat{k}$ scheme was restricted by $\hat{k} \in \mathbb{Z}$. We will discuss the Solberg scheme further in section 5.4.2.
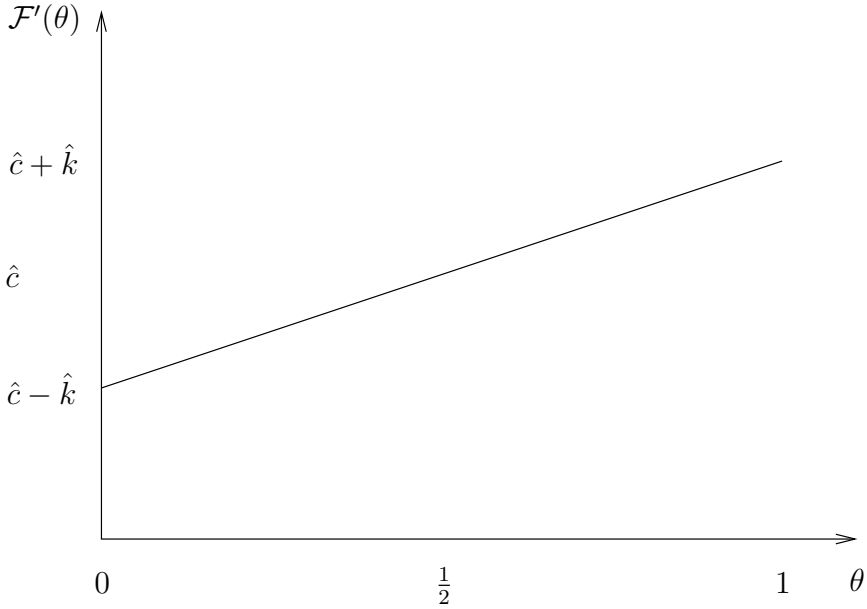
Figure 4.3: The non-dimensional wave speed of the Solberg scheme

4.5.3 The Godunov method for relative flux functions

We can find the flux-difference splitting coefficients for any scheme defined by a relative flux function, by replacing the true flux function in the Godunov method (4.11) by an artificial flux function on the form (4.24). This yields

$$[C^{i+}\Delta] = \Delta + \mathcal{M}\Big((\mathcal{F}(\theta) - (i+1)\theta)\,\Delta\Big) - \mathcal{M}\Big((\mathcal{F}(\theta) - i\theta)\Delta\Big), \quad (4.38a)$$

$$[C^{i-}\Delta] = \mathcal{M}\Big((\mathcal{F}(\theta) + i\theta)\Delta\Big) - \mathcal{M}\Big((\mathcal{F}(\theta) + (i+1)\theta)\Delta\Big). \quad (4.38b)$$

Since the terms inside the operator $\mathcal{M}$ are multiplied by Δ, we can simplify the operator $\mathcal{M}$ as

$$\mathcal{M}(z(\theta)\Delta) = \begin{cases} \min\limits_{\theta\in[0,1]}(z(\theta)|\Delta|) & \text{if } \Delta > 0, \\ \max\limits_{\theta\in[0,1]}(z(\theta)(-|\Delta|)) & \text{if } \Delta < 0. \end{cases} \quad (4.39)$$
$$= \min\limits_{\theta\in[0,1]}(z(\theta))\Delta,$$

where $z(\theta)$ is an arbitrary function.

Using this simplification, we can divide by Δ in (4.38) to obtain

$$C^{i+} = 1 + \min\limits_{\theta\in[0,1]}\Big((\mathcal{F}(\theta) - (i+1)\theta)\Big) - \min\limits_{\theta\in[0,1]}\Big((\mathcal{F}(\theta) - i\theta)\Big), \quad (4.40a)$$

$$C^{i-} = \min\limits_{\theta\in[0,1]}\Big((\mathcal{F}(\theta) + i\theta)\Big) - \min\limits_{\theta\in[0,1]}\Big((\mathcal{F}(\theta) + (i+1)\theta)\Big). \quad (4.40b)$$

4.5.4 Similarity solutions

A similarity solution can be written as

$$q(x, t) = \tilde{q}(\zeta) \qquad (4.41)$$

where

$$\zeta = \frac{x - x_0}{t - t_0}. \qquad (4.42)$$

If the similarity solution satisfies a scalar conservation law, we get that

$$f'(\tilde{q})\tilde{q}'(\zeta) = \zeta\tilde{q}'(\zeta), \qquad (4.43)$$

which for $\tilde{q}'(\zeta) \neq 0$ reduces to

$$f'(\tilde{q}) = \zeta. \qquad (4.44)$$

Hence, if the derivative of an artificial flux function $\bar{f}'(q)$ is an injective function, we can write the similarity solution in terms of ζ,

$$\tilde{q}(\zeta) = (\bar{f}')^{-1}(\zeta). \qquad (4.45)$$

A new three parameter LTS scheme

As mentioned in section 4.5.2, the Solberg scheme can be thought of as a HLL-type scheme, where the non-dimensional wave speeds, c_L and c_R, are connected by a straight line in stead of by a discontinuity. Can we make a similar scheme that take in arbitrary c_L and c_R?

Starting from the non-dimensional wave speed of the HLL scheme, we can connect c_L and c_R by a linear function in the interval $\theta \in [\theta^* - \phi, \theta^* + \phi]$,

$$\mathcal{F}'(\theta) = \begin{cases} c_L & \text{if } \theta \leq \theta^* - \phi, \\ a_1 + a_2\theta & \text{if } \theta^* - \phi < \theta < \theta^* + \phi, \\ c_R & \text{if } \theta \geq \theta^* + \phi, \end{cases} \tag{5.1}$$

where c_L, c_R and ϕ are free parameters. We have illustrated this function in figure 5.1. There is only one choice of a_1 and a_2 that makes $\mathcal{F}'(\theta)$ continuous, that is

$$\mathcal{F}'(\theta) = \begin{cases} c_L & \text{if } \theta \leq \theta^* - \phi, \\ \frac{c_R+c_L}{2} + \frac{c_R-c_L}{2\phi}(\theta - \theta^*) & \text{if } \theta^* - \phi < \theta < \theta^* + \phi, \\ c_R & \text{if } \theta \geq \theta^* + \phi, \end{cases} \tag{5.2}$$

where we have inserted $a_1 = \frac{c_R+c_L}{2} - \frac{c_R-c_L}{2\phi}\theta^*$ and $a_2 = \frac{c_R-c_L}{2\phi}$. By integrating (5.2) we get that the relative flux function is given by

$$\mathcal{F}(\theta) = \begin{cases} c_L\theta & \text{if } \theta \leq \theta^* - \phi, \\ \left(\frac{c_R+c_L}{2} - \frac{c_R-c_L}{2\phi}\theta^*\right)\theta + \frac{c_R-c_L}{4\phi}\theta^2 & \text{if } \theta^* - \phi < \theta < \theta^* + \phi, \\ c_L\theta^* + c_R(\theta - \theta^*) & \text{if } \theta \geq \theta^* - \phi. \end{cases} \tag{5.3}$$

To ensure that the scheme is consistent, we enforce the conditions in (4.26), which yields

$$\theta^* = \frac{c_R - \hat{c}}{c_R - c_L}. \tag{5.4}$$
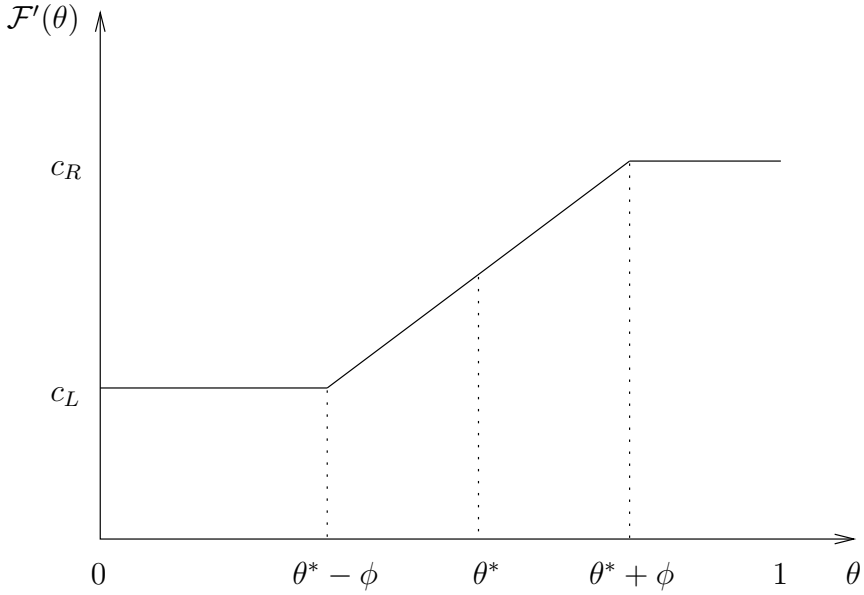
Figure 5.1: The non-dimensional wave speed of the LTS-HLLϕ scheme

We have now created a new three parameter LTS scheme, based on the LTS-HLL scheme and the Solberg scheme, which we will denote as the LTS-HLLϕ scheme.

5.1 Similarity solution

Since the non-dimensional wave speeds of the LTS-HLLϕ scheme (5.2) is one-to-one for $\theta \in (\theta^* - \phi, \theta^* + \phi)$, we can express the scheme as a similarity solution in this interval by using (4.45). The similarity solution of the LTS-HLLϕ scheme is then

$$\tilde{q}(\zeta) = \begin{cases} q_L & \text{if } \zeta \leq s_L, \\ 2\phi\frac{q_R - q_L}{s_R - s_L}\left(\zeta - \frac{s_R + s_L}{2}\right) + q^{HLL} & \text{if } s_L < \zeta < s_R, \\ q_R & \text{if } \zeta \geq s_R, \end{cases} \tag{5.5}$$

which we can also express in one line as

$$\begin{aligned} \widetilde{q}(\zeta) = q_L + H\left(\zeta - s_L\right)\left(2\phi\frac{q_R - q_L}{s_R - s_L}\left(\zeta - \frac{s_R + s_L}{2}\right) + q^{HLL} - q_L\right) \\ - H\left(\zeta - s_R\right)\left(2\phi\frac{q_R - q_L}{s_R - s_L}\left(\zeta - \frac{s_R + s_L}{2}\right) + q^{HLL} - q_R\right) \end{aligned} \tag{5.6}$$

using the Heaviside function $H(x)$.

5.2 The flux-difference splitting coefficients

The flux-difference splitting coefficients of the LTS-HLLϕ scheme can be written as

$$
\begin{aligned}
C^{i\pm} = \pm &\left[\frac{c_R - \hat{c}}{c_R - c_L} \right.\\
&\left. + \phi \frac{-(c_R + c_L) \pm 2i \pm \max\left(0, \min(\pm c_L - i, 1)\right)}{c_R - c_L} \right] \max(0, \min(\pm c_L - i, 1))\\
\pm &\left[\frac{\hat{c} - c_L}{c_R - c_L} \right.\\
&\left. - \phi \frac{-(c_R + c_L) \pm 2i \pm \max\left(0, \min(\pm c_R - i, 1)\right)}{c_R - c_L} \right] \max(0, \min(\pm c_R - i, 1)).
\end{aligned}
\tag{5.7}
$$

Proof. The LTS-HLLϕ Riemann solver can be written as

$$
\begin{aligned}
\widetilde{Q}(\zeta) = Q_{j-1} &+ H\left(\zeta - s_L\right) \left(2\phi \frac{Q_j - Q_{j-1}}{s_R - s_L} \left(\zeta - \frac{s_R + s_L}{2} \right) + Q^{HLL} - Q_{j-1} \right)\\
&- H\left(\zeta - s_L\right) \left(2\phi \frac{Q_j - Q_{j-1}}{s_R - s_L} \left(\zeta - \frac{s_R + s_L}{2} \right) + Q^{HLL} - Q_j \right)
\end{aligned}
\tag{5.8}
$$

which is equivalent to

$$
\begin{aligned}
\widetilde{Q}(\zeta) = Q_{j-1} &+ \frac{H\left(\zeta - s_L\right)}{s_R - s_L} \left(2\phi \left(\zeta - \frac{s_R + s_L}{2} \right) + s_R - \hat{\lambda} \right) (Q_j - Q_{j-1})\\
&- \frac{H\left(\zeta - s_L\right)}{s_R - s_L} \left(2\phi \left(\zeta - \frac{s_R + s_L}{2} \right) + s_L - \hat{\lambda} \right) (Q_j - Q_{j-1})
\end{aligned}
\tag{5.9}
$$

From [16], we know that for $i \leq 0$ we have

$$
\int_{(i-1)\frac{\Delta x}{\Delta t}}^{i\frac{\Delta x}{\Delta t}} \widetilde{Q}(\zeta) d\zeta = \frac{\Delta x}{\Delta t} Q_{j-1} - \frac{\Delta x}{\Delta t} C^{(-i)-} \left(Q_j - Q_{j-1} \right).
\tag{5.10}
$$

Using the identities,

$$
\int H\left(x - a\right) dx = \max(x - a, 0),
\tag{5.11a}
$$

$$
\int x H\left(x - a\right) dx = \frac{1}{2}\max(x - a, 0)^2 + a \max(x - a, 0),
\tag{5.11b}
$$

$$
\max(x, 0) - \max(x - a, 0) = \max\left(0, \min(x, a)\right),
\tag{5.11c}
$$

$$
\max(x, 0)^2 - \max(x - a, 0)^2 = \left[-2x - \max\left(0, \min(x, a)\right)\right] \max\left(0, \min(x, a)\right),
\tag{5.11d}
$$

we can solve the integral in (5.10), and get that

$$C^{i-} = -\left[\frac{c_R - \hat{c}}{c_R - c_L}\right.$$
$$\left. + \phi\frac{-(c_R + c_L) - 2i - \max\left(0, \min(-c_L - i, 1)\right)}{c_R - c_L}\right] \max\left(0, \min(-c_L - i, 1)\right)$$
$$-\left[\frac{\hat{c} - c_L}{c_R - c_L}\right.$$
$$\left. - \phi\frac{-(c_R + c_L) - 2i - \max\left(0, \min(-c_R - i, 1)\right)}{c_R - c_L}\right] \max\left(0, \min(-c_R - i, 1)\right).$$

$$(5.12)$$

Using the same procedure, we can find a similar expression for C^{i+}.

□

By inserting the coefficients (5.7) into the TVD conditions (4.10), we can show that the LTS-HLLϕ scheme is TVD if

$$0 \le \phi \le \min(\theta^*, 1 - \theta^*). \tag{5.13}$$

5.3 Numerical diffusion coefficient

We can calculate the numerical diffusion of the LTS-HLLϕ scheme by inserting the flux-difference splitting coefficients (5.7) into the expression for the numerical diffusion coefficient (4.6). For the 3-point LTS-HLLϕ scheme, this yields

$$\sigma_{HLL\phi}(\hat{c}) = \sigma_{HLL}(\hat{c}) - \frac{\phi}{c_R - c_L}\left(c_R|c_L| - |c_R|c_L\right), \tag{5.14}$$

where $\sigma_{HLL}(\hat{c})$ is given in (4.20). Note that the numerical diffusion is identical to the numerical diffusion of the LTS-HLL scheme when c_R and c_L have equal signs. If c_R and c_L have different signs, the numerical diffusion decreases proportionally to ϕ, because $c_R|c_L| - |c_R|c_L > 0$. We can therefore conclude that for a 3-point scheme $\sigma_{HLL\phi} \le \sigma_{HLL}$.

5.4 Parameter study

In this section, we show how other LTS schemes can be written as special cases of the LTS-HLLϕ scheme, by selecting appropriate parameters. We also discuss which parameters give the most robust scheme. A summary of the different LTS schemes, and the corresponding parameters are listed in table 5.1.

5.4.1 Ceiling schemes

We define a ceiling scheme as a LTS-HLLϕ scheme with parameters $c_R = k$ and $c_L = -k$, where $k = \lceil|\hat{c}|\rceil$. For a ceiling scheme, the flux-difference splitting coefficients simply reduce to

$$C^{i\pm} = \frac{1}{2k}\left[\hat{c} \pm k \mp \phi(2i+1)\right], \quad \forall i < k. \tag{5.15}$$

Inserting this into (4.6), we find that the numerical diffusion of a ceiling scheme is

$$\sigma_{HLL\phi} = k^2 - \hat{c}^2 - \frac{\phi}{3}(4k^2 - 1). \tag{5.16}$$

Lax-Friedrichs

By inspecting the flux difference coefficients (5.15), we see that the local LTS-Lax-Friedrichs scheme is the ceiling scheme with parameter $\phi = 0$.

Lax-Wendroff

An interesting 3-point scheme is the Lax-Wendroff scheme. It is interesting because it is the only second order 3-point scheme, and the least diffusive scheme that is linearly stable.

We can define the Lax-Wendroff scheme as a 3-point ceiling scheme, by finding a ϕ that gives $\sigma(\hat{c}) = 0$. From (5.16), we see that the diffusion is zero when,

$$\phi = 1 - \hat{c}^2. \tag{5.17}$$

The flux-difference splitting coefficients in (5.15) reduce in this case to,

$$C^{\pm} = \frac{1}{2}(\hat{c} \pm \hat{c}^2), \tag{5.18}$$

which are identical to the coefficients of the Lax-Wendroff scheme [15].

We can generalize this procedure for a $(2k+1)$-point ceiling scheme, and find a LTS extension of the Lax-Wendroff scheme. The $(2k+1)$-point ceiling scheme that gives zero numerical diffusion has the parameter

$$\phi = 3\frac{k^2 - \hat{c}^2}{4k^2 - 1}, \tag{5.19}$$

which gives the following flux-difference splitting coefficients for the LTS-Lax-Wendroff scheme

$$C^{\pm i} = \frac{1}{2k}\left[\hat{c} \pm k \mp 3\frac{k^2 - \hat{c}^2}{4k^2 - 1}(2i+1)\right], \quad \forall i < k. \tag{5.20}$$

Not all schemes are ceiling schemes

By choosing different ϕ, we can create ceiling schemes with arbitrary numerical diffusion. However, more than one scheme can give the same numerical diffusion. For instance, if we choose

$$\phi = 3\frac{k - \hat{c}}{2k + 1}, \tag{5.21}$$

we get a scheme with the same numerical diffusion as the LTS-Roe scheme. But if we insert this parameter into (5.15), we do not get the same flux-difference splitting coefficients as for the LTS-Roe scheme, unless $k = 1$. Noting this, we emphasize that (5.20) is not a unique LTS extension of the Lax-Wendroff scheme.

5.4.2 The Solbergφ scheme

Solberg [23] proposed a class of schemes, denoted $CD\hat{k} - \phi$, that in the LTS-HLLϕ framework correspond to choosing $c_L = \hat{c} - \hat{k}$ and $c_R = \hat{c} + \hat{k}$, where $\hat{k} \in \mathbb{Z}$, but where ϕ is a free parameter. With this choice of parameters, Solberg showed that the numerical diffusion coefficient reduces to

$$\sigma_{\text{Solberg}\phi} = (1 - 2\phi)\left(\frac{4\hat{k}^2 - 1}{6} + \alpha - \alpha^2\right) + \frac{2\hat{k}^2 + 1}{6}. \qquad (5.22)$$

Note that Solberg used a slightly different parameter, namely, $\phi_{\text{Solberg}} = \frac{\phi}{\hat{k}}$. The parameter $\hat{k}$ refers to the necessary extension of the computational stencil $(2(\lceil|\hat{c}|\rceil + \hat{k}) + 1)$.

We can generalize this scheme for all $\hat{k} > 0$, since the scheme is simply a special case of the LTS-HLLϕ scheme. The computational stencil is then $(2\lceil|\hat{c}| + \hat{k}\rceil + 1)$. We will refer to this generalization of the $CD\hat{k} - \phi$ scheme as the Solbergϕ scheme. The flux-difference splitting coefficients of the Solbergϕ scheme is

$$
\begin{aligned}
C^{i\pm} = &\pm \frac{1}{2}\left[\max\left(0, \min(\pm(\hat{c} - \hat{k}) - i, 1)\right) + \max\left(0, \min(\pm(\hat{c} + \hat{k}) - i, 1)\right)\right] \\
&\pm \frac{\phi}{\hat{k}}\left[-\hat{c} \pm i \pm \frac{1}{2}\max\left(0, \min(\pm(\hat{c} - \hat{k}) - i, 1)\right)\right]\max\left(0, \min(\pm(\hat{c} - \hat{k}) - i, 1)\right) \\
&\mp \frac{\phi}{\hat{k}}\left[-\hat{c} \pm i \pm \frac{1}{2}\max\left(0, \min(\pm(\hat{c} + \hat{k}) - i, 1)\right)\right]\max\left(0, \min(\pm(\hat{c} + \hat{k}) - i, 1)\right).
\end{aligned}
$$
$$(5.23)$$

From the condition in (5.13), we can show that the Solbergϕ scheme is TVD when $\phi \in [0, \frac{1}{2}]$.

In figure 5.2, we have performed a numerical study of the numerical diffusion coefficient of the Solbergϕ scheme. The figure suggests that numerical diffusion increases with increasing $\hat{k}$, and that the scheme is identical to the LTS-Roe scheme when $\hat{k} \to 0$. Increasing ϕ towards $\phi = \frac{1}{2}$, we note that numerical diffusion decreases and is less dependent on Courant number.

The optimal choice of parameters remains an open problem. Adding numerical diffusion removes oscillations, but it also reduces the accuracy. Solberg suggested using $\hat{k} \propto \text{CFL}$, as oscillations are increasingly problematic at higher Courant numbers. However, we have no a priori knowledge of the appropriate proportionality constant of a given Riemann problem.

Here, we suggest that the necessary numerical diffusion is also related to the *strength* of the discontinuity. We take this into account by defining the parameter $\hat{k}$ in terms of the difference between the highest and lowest wave velocity in the Riemann problem. For the Riemann problem located at $x_{j-1/2}$, we define

$$C_{\max,j-1/2} = \frac{\Delta t}{\Delta x}\max(\lambda^m(\mathbf{Q}_{j-1}), \hat{\lambda}^m_{j-1/2}, \lambda^m(\mathbf{Q}_j)), \qquad (5.24a)$$

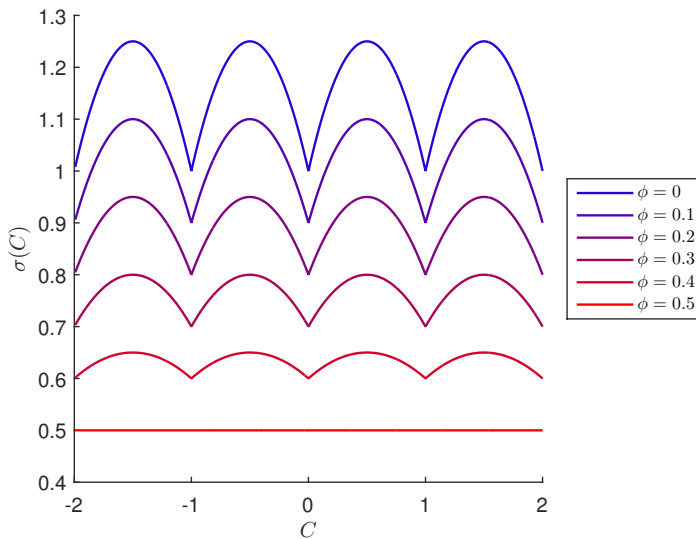$$C_{\min,j-1/2} = \frac{\Delta t}{\Delta x}\min(\lambda^1(\mathbf{Q}_{j-1}), \hat{\lambda}^1_{j-1/2}, \lambda^1(\mathbf{Q}_j)), \qquad (5.24b)$$

$$\hat{k}^*_{j-1/2} = \sqrt{C_{\max,j-1/2} - C_{\min,j-1/2}}. \qquad (5.24c)$$
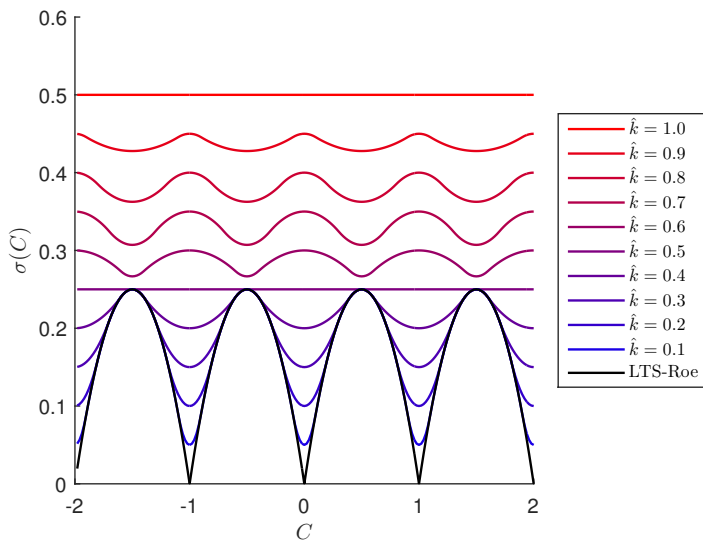
(a) Constant $\phi = \frac{1}{2}$.

(b) Constant $\hat{k} = 1$.

Figure 5.2: The numerical diffusion coefficient of the Solberg scheme as a function of Courant number.

LTS scheme	ϕ	c_L	c_R
LTS-Roe	–	$\hat{c}$	$\hat{c}$
LTS-Lax-Friedrichs	0	$-k$	k
LTS-Lax-Wendroff	$3\frac{k^2-\hat{c}^2}{4k^2-1}$	$-k$	k
Solberg	$\frac{1}{2}$	$\hat{c}-\hat{k}$	$\hat{c}+\hat{k}$
Solberg*	$\frac{1}{2}$	$\hat{c}-\hat{k}^*$	$\hat{c}+\hat{k}^*$
Solbergϕ	–	$\hat{c}-\hat{k}$	$\hat{c}+\hat{k}$
LTS-HLLE	0	E	E
LTS-HLLEϕ^*	ϕ^*	E	E

Table 5.1: Different LTS schemes expressed as special cases of the LTS-HLLϕ scheme. A dash indicates that the variable is free. E refers to Einfeldt's choice, defined in (3.32).

The Solbergϕ scheme with the parameters $\hat{k} = \hat{k}^*$ and $\phi = \frac{1}{2}$ will be referred to as the Solberg* scheme. By choosing these parameters, we are effectively adding numerical diffusion proportionally to Courant number, since $\sigma \sim \hat{k}^2$ from (5.22), and dependence on α is minimal.

5.4.3   The LTS-HLLEϕ^* scheme

In general, we can choose c_L, c_R and ϕ arbitrarily. A simple way to apply the scheme to a system of equations is to use Einfeldt's choice (3.32) of s_L and s_R, to select c_L and c_R. When $\phi = 0$, this reduces to the LTS-HLLE scheme. A well known shortcoming of the HLLE scheme, is that it is very diffusive on the contact wave of the Euler equations [25]. In order to reduce this problem, we suggest choosing the highest possible value of ϕ that satisfies the TVD conditions:

$$\phi^* = \min(\theta^*, 1 - \theta^*), \tag{5.25}$$

since the analysis in figure 5.2b suggests that high values of ϕ give low numerical diffusion.

Chapter 6

Numerical simulations

In this section we perform numerical simulations on the inviscid Burgers' equation and the Euler equations for different LTS schemes.

In the scalar tests, we check if the different schemes give accurate and entropy satisfying solutions.

We will run six tests for the Euler equations; Toro's five tests and the Woodward-Colella blast-wave problem [24, 26]. The tests are run at different Courant numbers, for the LTS-Roe scheme, the LTS-HLLEϕ^* scheme and the Solberg* scheme. The purpose of these tests is to check the robustness of the new schemes in different scenarios.

In all the figures 6.1 to 6.34, the solutions are compared against reference solutions (dashed line) obtained from a refined grid ($N = 10000$) at $CFL = 0.99$. For the transonic rarefaction test and Toro's test 2, the reference solution is calculated using a second order accurate HLLE scheme, while a second order accurate Roe scheme was used for the other reference solutions. All numerical simulations in this thesis are calculated using adaptive time stepping. Most of the tests are presented in a similar fashion in [1], and we refer to this publication for comparisons.

6.1 The inviscid Burgers' equation

We recall from (2.14) that the inviscid Burgers' equation is given by

$$q_t + \left(\frac{1}{2} q^2 \right)_x = 0, \tag{6.1}$$

which has the Roe averaged characteristic speed of

$$\hat{\lambda} = \frac{1}{2}(q_R + q_L). \tag{6.2}$$

Although the Burgers' equation is simple, certain initial value problems can cause problems. In this section we will study the initial data in table 6.1.

Test case	q_L	q_M	q_R	x_1	x_2
1. Transonic rarefaction	-1	-	1	0.5	0.5
2. Square pulse	0	1	0	0.3	0.6
3. Double shock	1	0.5	0	0.1	0.2

Table 6.1: Summary of test cases for the Burgers' equation

6.1.1 Transonic rarefaction

From the Lax entropy condition (2.25), we can show that a rarefaction wave is the correct entropy satisfying solution for this initial data. The rarefaction wave is transonic, because the characteristic speed changes sign across the discontinuity. Since $q_L = -q_R$, the Roe speed is zero at $x = 0.5$. The solution from the LTS-Roe scheme is therefore simply a stationary shock, regardless of CFL-number or grid resolution, because the LTS-Roe scheme has no numerical diffusion when $\hat{c} = 0$. We see this solution in figures 6.1a and 6.1b.

The solution in figure 6.1d is obtained during a single time step, using the LTS-HLLE scheme. We see that this method splits the discontinuity into two shocks moving at different speeds. Since the solution in figure 6.1c is obtained using four time steps, the final solution consists of 16 shocks, that combined resemble a rarefaction wave.

In figure 6.1f we obtain the exact solution, because the parabolic artificial flux function in the LTS-HLLEϕ^* scheme mimics the true flux function of the Burger's equation. Some errors are introduced because of averaging when using multiple time steps, as we can see from figure 6.1e.

The global Lax-Friedrichs scheme also successfully solves the transonic rarefaction, but with very low accuracy due to high numerical diffusion, as we see from figures 6.2a and 6.2b. A better option is therefore the Solberg* scheme, which solves the rarefaction wave, but accurately after a few time steps, according to figures 6.2c and 6.2d. Note that solving the problem using the Solberg scheme with parameter $\hat{k} = (\hat{k}^*)^2$ yields the same solution as when we use the LTS-HLLEϕ^* scheme (see figures 6.2e and 6.2f).

6.1.2 Square Pulse

The solution of the square pulse test case consists of a rarefaction wave starting at $x_1 = 0.3$m, and a shock wave starting at $x_2 = 0.6$m. Since we expect different solutions for the two discontinuities, it is a good test for confirming that the Lax entropy condition (2.25) is satisfied.

We know that the LTS-Roe scheme gives the shock solution for all discontinuities, unless some diffusion is present. When the local Courant number is an integer, we have zero diffusion, and can never produce an entropy satisfying solution, regardless of grid resolution, as we can see from figures 6.3a and 6.3b.

The LTS-HLLE and LTS-HLLEϕ^* scheme successfully distinguish the shock wave and the rarefaction wave, with only small errors. These errors appear to diminish after grid refinement, which suggests that the schemes yield entropy satisfying solutions (see figures 6.3c to 6.3f).

The local LTS-Lax-Friedrichs scheme is also entropy violating, as we can see from figures 6.2b and 6.4a. The Solberg* scheme and the Solberg scheme with parameter $\hat{k} = (\hat{k}^*)^2$ yields similar, entropy satisfying solutions, as we can see from figures 6.4c to 6.2f. Note that the Solberg scheme with $\hat{k} = (\hat{k}^*)^2$ gives the same solution as LTS-HLLEϕ^* for the rarefaction wave, but adds some additional diffusion on the shock wave.

6.1.3 Double shock

This initial data consists of two shock waves traveling at different speeds. The first wave, starting at $x_1 = 0.1$m is traveling at speed $s_1 = 0.75$m/s, while the second wave, starting at $x_2 = 0.2$m, is traveling at speed $s_2 = 0.25$m/s. Thus, we expect these two shocks to merge at $x_3 = 0.25$m at $t = 0.2$s.

However, if we choose $\Delta t > \Delta t_{crit} = 0.2$s, we cannot capture the shocks merging, and the first wave will simply overtake the second wave. Something even more interesting happens if $\Delta t = 2\Delta t_{crit} = 0.4$s. At this time step, the first and second wave has exactly the same relative distance as initially, thus the initial condition is simply transported. In figure 6.5 we show the solutions at $t = 0.4$s, $t = 0.8$s and $t = 1.2$s, using $\Delta t = 0.4$s.

From figure 6.5a, we see that the LTS-Roe scheme simply translates the discontinuity, because of the phenomenon described in the previous paragraph. In fact, the same phenomenon can also be observed for the LTS-HLLE scheme and the LTS-HLLEϕ^* scheme, because all of these methods solve shocks with zero diffusion when the Courant number is integer.

If we add some numerical diffusion, we can gradually merge the shocks. In the Solberg scheme, we can add an arbitrary amount of diffusion. We see from figure 6.5 that the shock waves merge after fewer time steps when we increase $\hat{k}$, at the cost of smearing out the solutions.
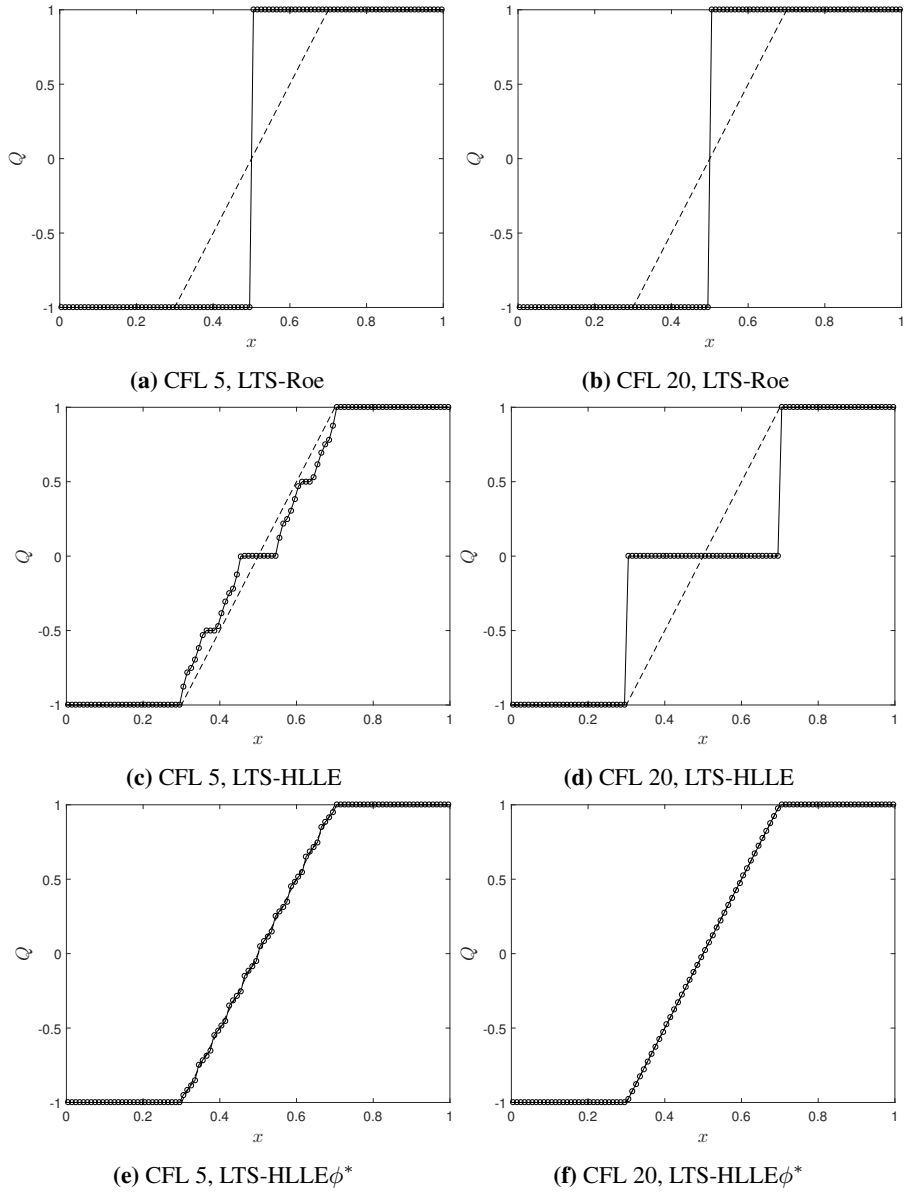
(a) CFL 5, LTS-Roe

(b) CFL 20, LTS-Roe

(c) CFL 5, LTS-HLLE

(d) CFL 20, LTS-HLLE

(e) CFL 5, LTS-HLLEϕ^*

(f) CFL 20, LTS-HLLEϕ^*

Figure 6.1: Transonic rarefaction. $t = 0.2$, $N = 100$

(a) CFL 5, global LTS-Lax-Friedrichs

(b) CFL 20, global LTS-Lax-Friedrichs

(c) CFL 5, Solberg*

(d) CFL 20, Solberg*

(e) CFL 5, Solberg, $\hat{k} = (\hat{k}^*)^2$

(f) CFL 20, Solberg, $\hat{k} = (\hat{k}^*)^2$
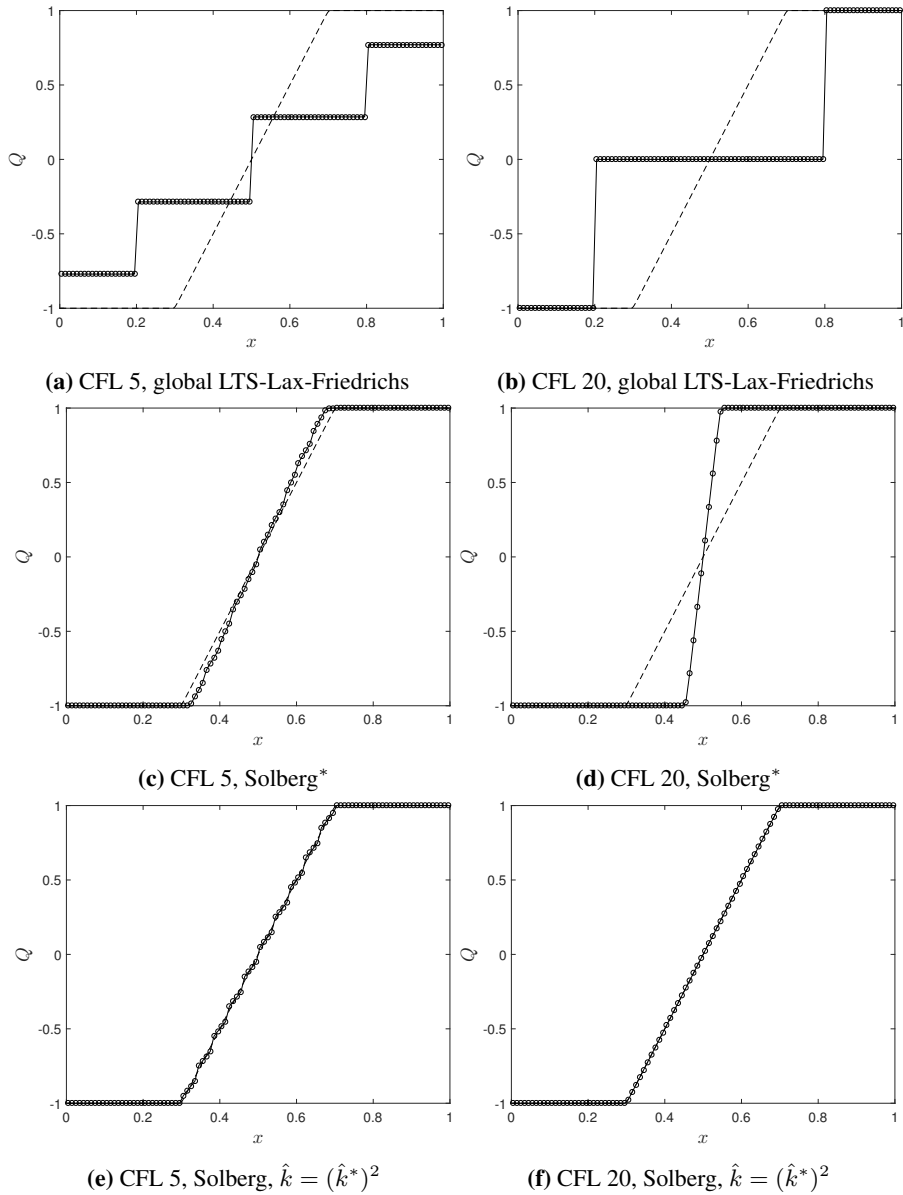
Figure 6.2: Transonic rarefaction. $t = 0.2$, $N = 100$

(a) $N = 100$, LTS-Roe

(b) $N = 1000$, LTS-Roe

(c) $N = 100$, LTS-HLLE

(d) $N = 1000$, LTS-HLLE

(e) $N = 100$, LTS-HLLEϕ^*

(f) $N = 1000$, LTS-HLLEϕ^*
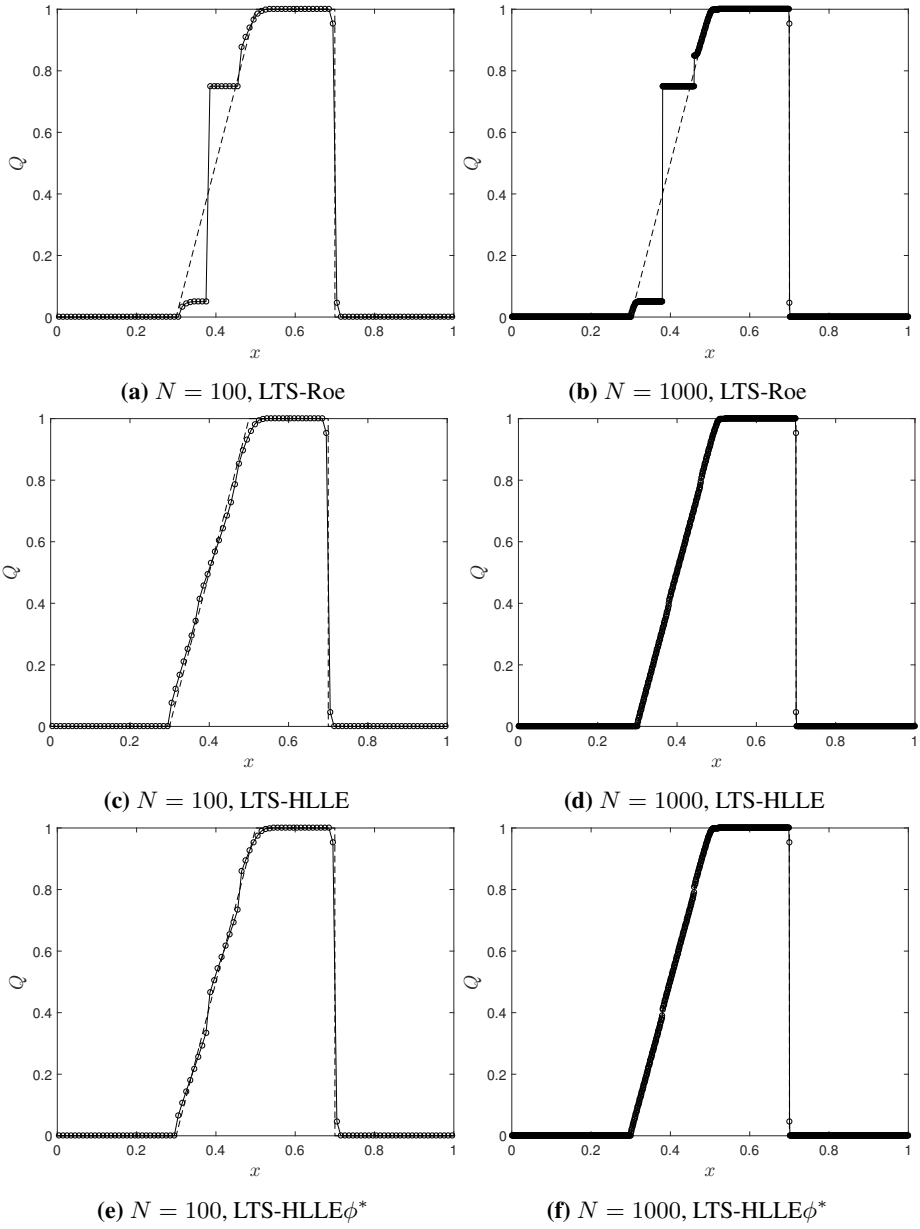
Figure 6.3: Square pulse. Solution at $t = 0.2$s obtained at CFL= 2.5.

(a) N=100, local LTS-Lax-Friedrichs

(b) N=1000, local LTS-Lax-Friedrichs

(c) N=100, Solberg*

(d) N=1000, Solberg*

(e) N=100, Solberg, $\hat{k} = (\hat{k}^*)^2$

(f) N=1000, Solberg, $\hat{k} = (\hat{k}^*)^2$
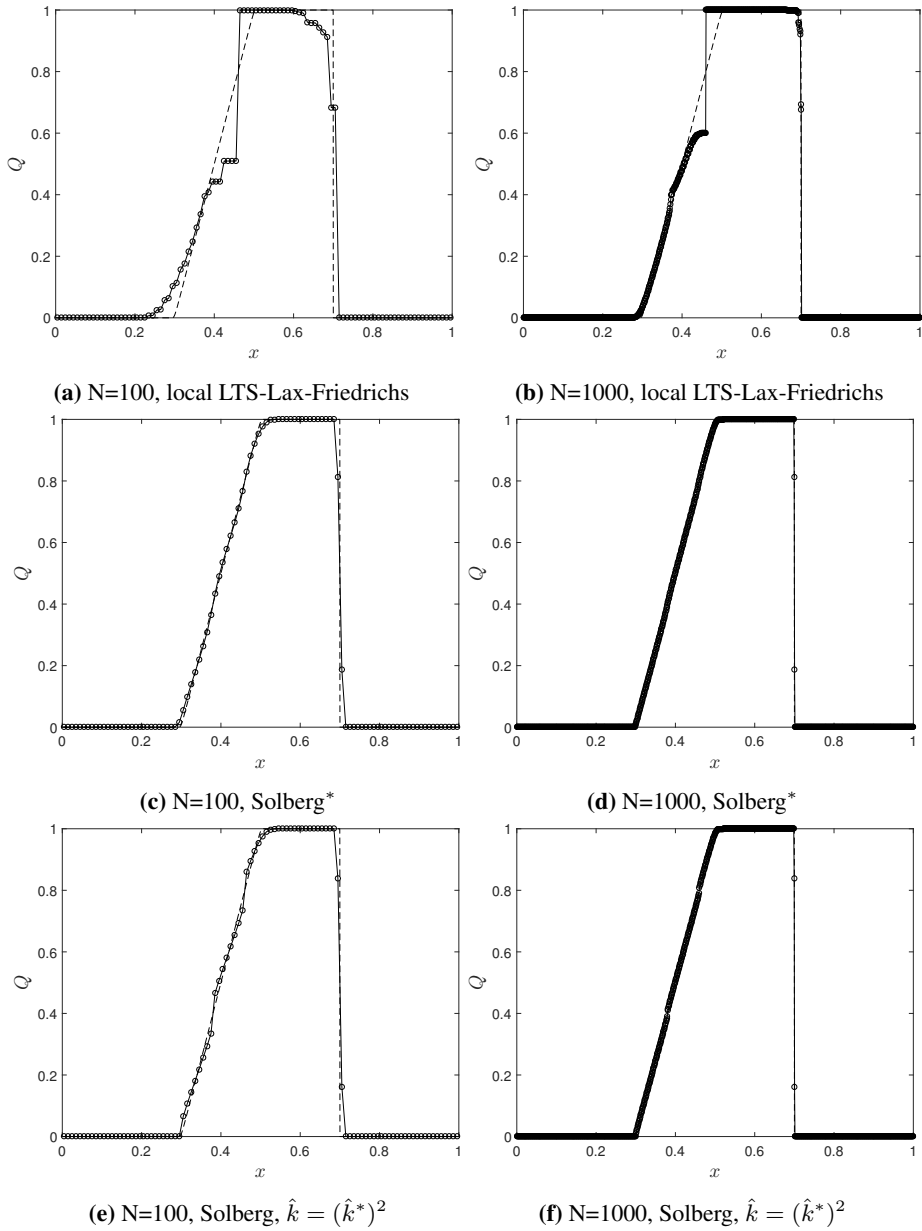
Figure 6.4: Square pulse. Solution at $t = 0.2$s obtained at CFL= 2.5.

(a) LTS-Roe

(b) Solberg, $\hat{k} = 0.5$

(c) Solberg, $\hat{k} = 1$

(d) Solberg, $\hat{k} = 2$

(e) Solberg*

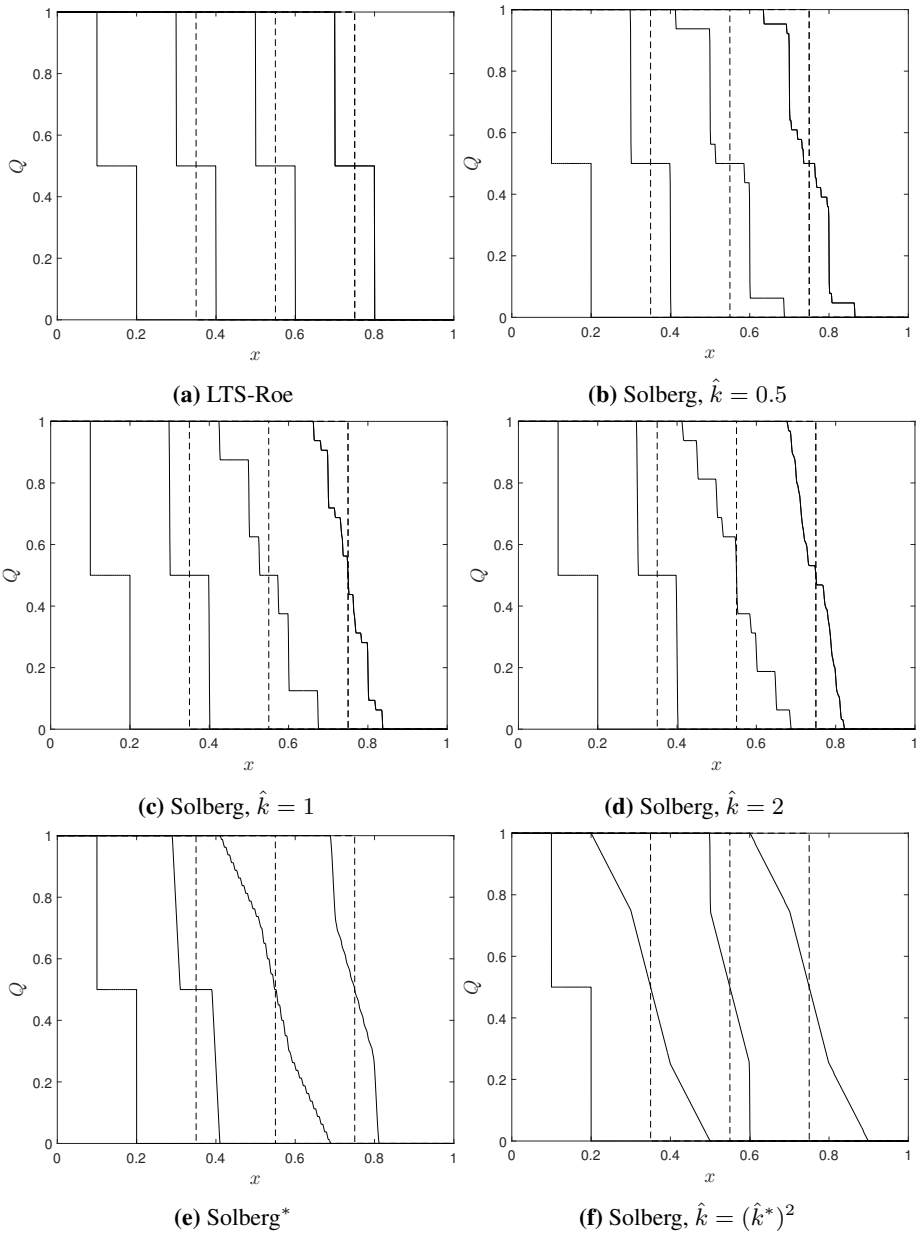**(f)** Solberg, $\hat{k} = (\hat{k}^*)^2$

Figure 6.5: Double shock. $N = 1000$, CFL$= 400$, $\rightarrow \Delta t = 0.4$s

6.2 The Euler equations

The Euler equations is a nonlinear system of hyperbolic conservation laws, and is a common model for gas dynamics. In differential form, the system is given by

$$\begin{pmatrix} \rho \\ \rho u \\ E \end{pmatrix}_t + \begin{pmatrix} \rho u \\ \rho u^2 + p \\ (E + p)u \end{pmatrix}_x = \begin{pmatrix} 0 \\ 0 \\ 0 \end{pmatrix}, \tag{6.3}$$

where ρ is the density, u is the velocity, E is the energy density and p is the pressure of a fluid. If we assume ideal gas, we can use the ideal gas law

$$p = (\gamma - 1) \left(E - \frac{1}{2}\rho u^2 \right), \tag{6.4}$$

where the ratio of specific heats, γ is a fluid property. For air $\gamma = 1.4$, which will be used in this section. For further details on eigenstructure and Roe speeds of the Euler equations, we refer to chapter 14 in [15].

Five tests for the Euler equations were proposed by Toro in [24]. The initial data of these test cases are given in primitive variables in table 6.2. We will also consider the Woodward-Colella blast-wave problem [26], which is presented in section 6.2.6.

Test	ρ_L	u_L	p_L	ρ_R	u_R	p_R	x_0	t
1	1.0	0.75	1.0	0.125	0.0	0.1	0.3	0.2
2	1.0	-2.0	0.4	1.0	2.0	0.4	0.5	0.15
3	1.0	0.0	1000	1.0	0.0	0.01	0.5	0.012
4	5.9992	19.5975	460.894	5.9992	-6.19633	46.095	0.5	0.035
5	1.0	-19.5975	1000	1.0	-19.59745	0.01	0.8	0.012

Table 6.2: Summary of Toro's tests for the Euler equations

These test cases are common benchmark tests for assessing robustness, accuracy and computational cost of a numerical method. We will test the performance of the LTS-HLLEϕ^* scheme and the Solberg* scheme, and compared to the LTS-Roe scheme.

6.2.1 Toro's test 1

The solution of this test case consists of a right shock wave, a right contact wave and a left sonic rarefaction. Because the rarefaction wave is sonic, this particular test case is useful for testing if the numerical scheme is entropy satisfying. The results of this test are shown in figures 6.6 to 6.11.

Recall that the Roe scheme has no numerical diffusion when the characteristic speed is zero, and will therefore yield entropy violations in the rarefaction wave. Note however that for CFL= 4, the LTS-Roe scheme yields a pretty accurate solution, with only a small entropy violation and very sharp shock and contact waves. When we increase the CFL-number further, oscillations start to appear.

The LTS-HLLEϕ^* scheme yields entropy satisfying solutions, with pretty high accuracy up to CFL= 8. At very high CFL-numbers we get some oscillations, but they are less severe than the ones obtained from the LTS-Roe scheme. The scheme is quite diffusive on the contact wave, but solves shocks as sharp as the LTS-Roe scheme.

As expected, the Solberg* scheme is more diffusive at shocks, compared to the other schemes. However, the solutions appear to be entropy satisfying and almost smooth for all the tested Courant numbers.

6.2.2 Toro's test 2

In test case 2, we have two symmetric rarefaction waves moving away from each other, with a trivial contact wave between. In the centre, between the rarefaction waves, the pressure is near vacuum. This test is therefore good for checking a scheme's positivity preserving properties. The results of this test are shown in figures 6.12 to 6.15.

Both the LTS-Roe scheme and the LTS-HLLEϕ^* scheme failed to produce a solution for this test case, because negative values of ρ or p enter the intermediate calculations, and yield complex values of $\mathbf{Q}$.

However, the LTS-HLLE scheme yield relatively accurate results for this near-vacuum test, as previously reported by [18]. This can suggest that the LTS-HLLE scheme is more robust than the LTS-HLLEϕ^* scheme in cases with very low pressure.

The Solberg* scheme suffered from the same problem as the LTS-Roe scheme and the LTS-HLLEϕ^* scheme with our usual parameter. However, the method is stable for sufficiently high values of $\hat{k}$ as shown in figures 6.14 and 6.15. Although these solutions are nice and smooth, we get very low accuracy for CFL> 1.

6.2.3 Toro's test 3

This test case consists of a left rarefaction wave, a right contact wave and a right rarefaction. The high pressure difference in the Riemann problem gives rise to strong waves. The results of this test are shown in figures 6.16 to 6.21.

As in test 1, we see that the LTS-Roe scheme yields an entropy violating solution at the rarefaction wave, but this time it is because the local Courant number is integer, not because it is zero. The solutions at higher Courant numbers are quite accurate for the shock and rarefaction wave, but contain strong oscillations in between. The LTS-HLLEϕ^* yields entropy satisfying solutions, that are oscillatory at very high Courant numbers.

The Solberg* scheme also gives some oscillations at very high Courant numbers, but the solution is still quite smooth and accurate compared to the other schemes. We could remove the oscillations completely, by adding even more numerical diffusion, but this would also reduce the accuracy.

6.2.4 Toro's test 4

In this test case, all the characteristic speeds are positive, and the solution consists of two shocks moving to the right, with a contact wave in between. The results of this test are displayed in figures 6.22 to 6.27.

Both the LTS-Roe scheme and the LTS-HLLEϕ^* scheme yield severe oscillations at high Courant numbers, while the Solberg* scheme performs well, with only small oscillations at very high Courant numbers. The LTS-Roe scheme gives the sharpest resolution on the contact discontinuity.

6.2.5   Toro's test 5

Test 5 consist of a right moving shock wave, a stationary contact wave and a left moving rarefaction wave. The results of this test are displayed in figures 6.28 to 6.33.

As in previous tests, both the LTS-Roe scheme and the LTS-HLLEϕ^* scheme yield solutions containing strong oscillations. LTS-Roe give the sharpest resolution for the contact wave, but suffer from entropy violations on the rarefaction wave. The Solberg* scheme yields nice and smooth solutions, with only minor oscillations at very high Courant numbers.

Note that the LTS-Roe scheme lost positivity for CFL= 16, and is therefore calculated at CFL= 15.8 in figure 6.29.

6.2.6   Woodward-Colella blast-wave problem

As a last test, we will consider the Woodward-Colella blast-wave problem [26]. The initial data for this test is given by the pressure distribution

$$p(x,0) = \begin{cases} 1000 & \text{if } x < 0.1 \\ 0.01 & \text{if } 0.1 < x < 0.9 \ , \\ 100 & \text{if } x > 0.9 \end{cases} \tag{6.5}$$

and uniform density and velocity of $\rho(x,0) = 1.0$ and $u(x,0) = 0$ respectively. The solution is evaluated at $t = 0.038$s with reflective boundary conditions. The main purpose of this test is to evaluate how well the schemes can handle colliding waves, and more complex problems.

We will also use this test to illustrate how we can increase the accuracy of the scheme, by adjusting the scheme to be second order accurate away from discontinuities. Here we use the modified flux and limiting approach by Harten [7]. We refer to [1] for more details.

The density solution is shown in figure 6.34, for the first and second order LTS-Roe, LTS-HLLEϕ^* and Solberg* schemes.

For the first order schemes, we observe that we have increased accuracy at CFL= 5, compared to CFL= 1. We see that the Solberg* scheme is the most diffusive scheme, while the LTS-Roe scheme is the sharpest.

We observe that the second order accurate schemes resembles the reference solution much more accurately than the first order schemes. Here, we also observe that higher Courant numbers yield sharper solutions, and that the LTS-Roe scheme and the Solberg* scheme are the least and most diffusive schemes.
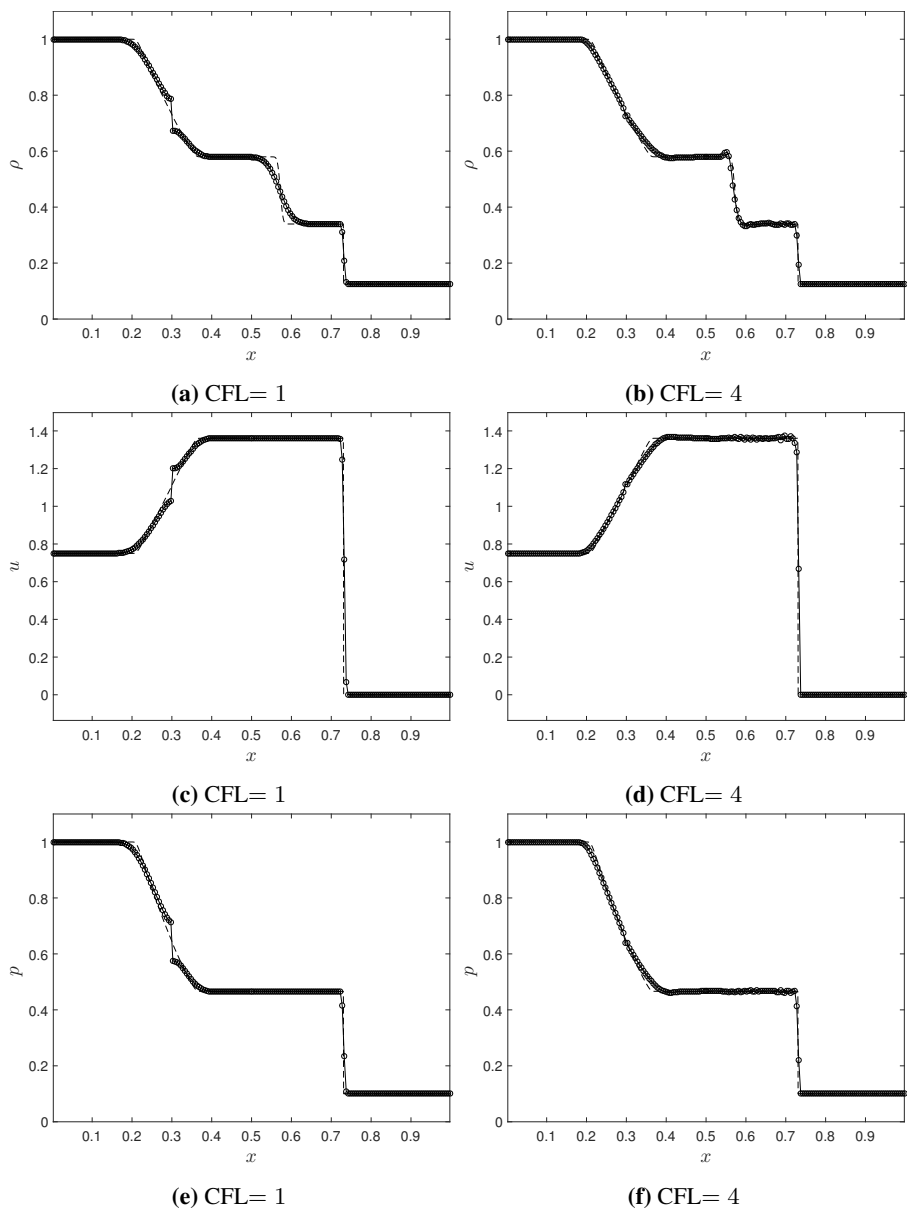
(a) CFL= 1

(b) CFL= 4

(c) CFL= 1

(d) CFL= 4

(e) CFL= 1

(f) CFL= 4

Figure 6.6: Numerical solutions of Toro's test 1 using LTS-Roe with $N = 200$.

(a) CFL= 8

(b) CFL= 16

(c) CFL= 8

(d) CFL= 16

(e) CFL= 8

(f) CFL= 16
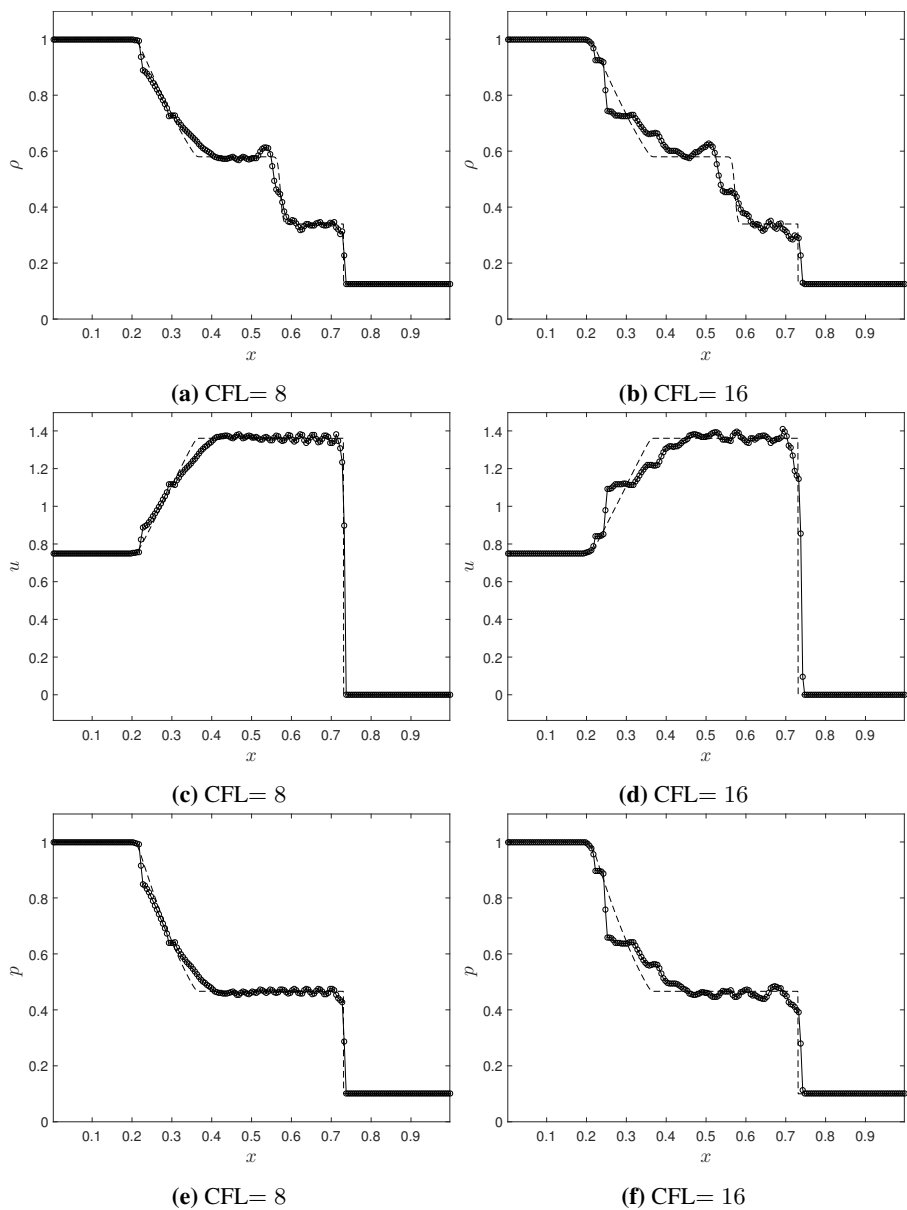
Figure 6.7: Numerical solutions of Toro's test 1 using LTS-Roe with $N = 200$.

(a) CFL$= 1$

(b) CFL$= 4$

(c) CFL$= 1$

(d) CFL$= 4$

(e) CFL$= 1$

(f) CFL$= 4$
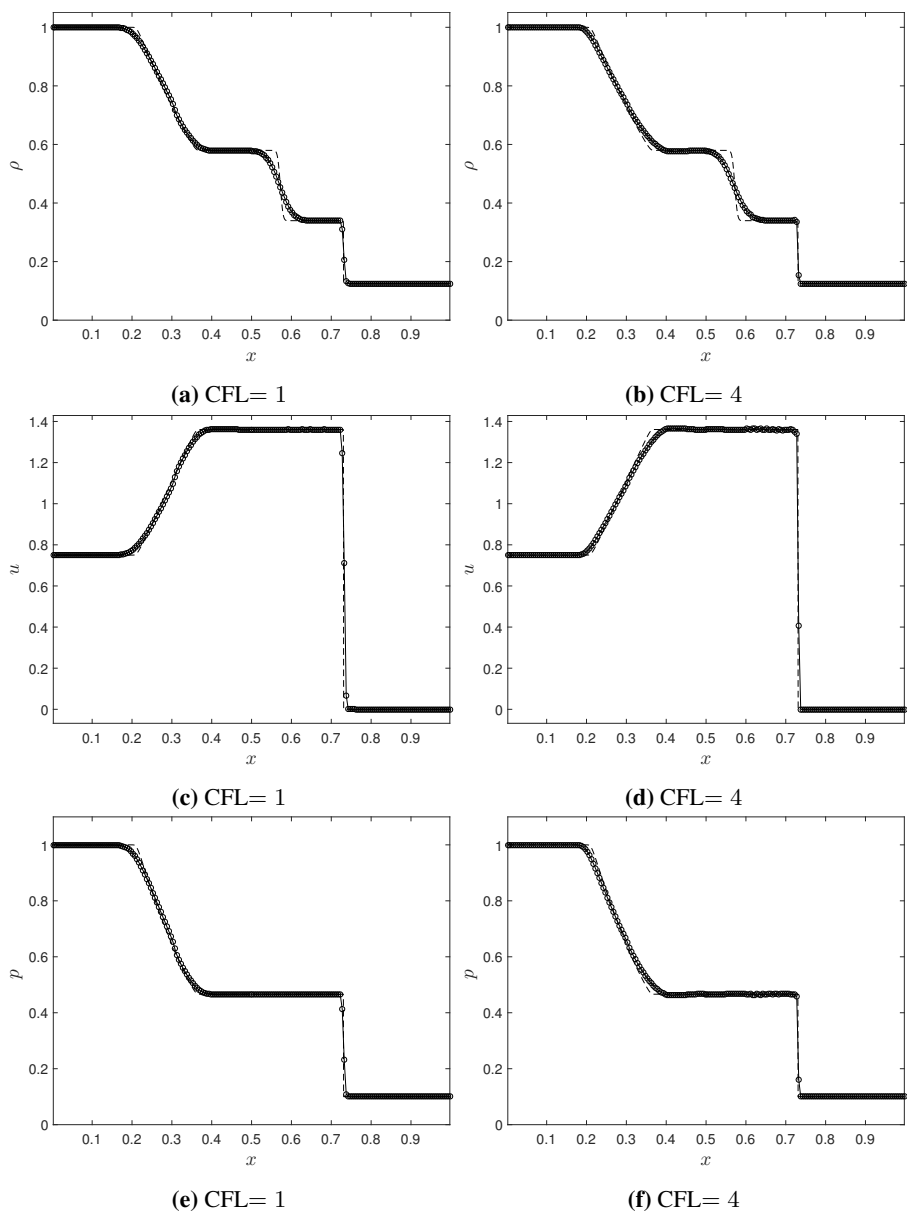
Figure 6.8: Numerical solutions of Toro's test 1 using LTS-HLLEϕ^* with $N = 200$.

(a) CFL= 8

(b) CFL= 16

(c) CFL= 8

(d) CFL= 16

(e) CFL= 8

(f) CFL= 16
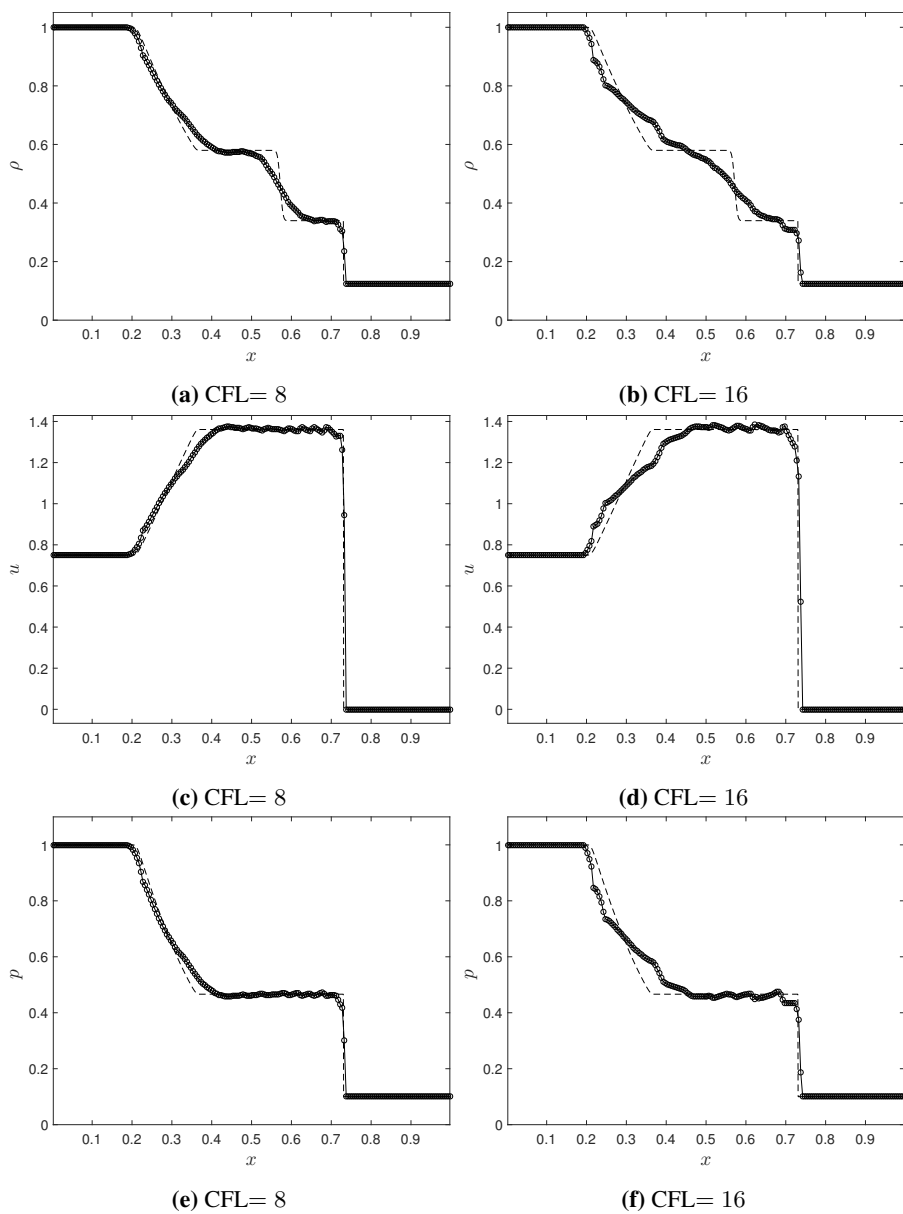
Figure 6.9: Numerical solutions of Toro's test 1 using LTS-HLLEϕ^* with $N = 200$.

(a) CFL= 1   **(b)** CFL= 4

(c) CFL= 1   **(d)** CFL= 4

(e) CFL= 1   **(f)** CFL= 4
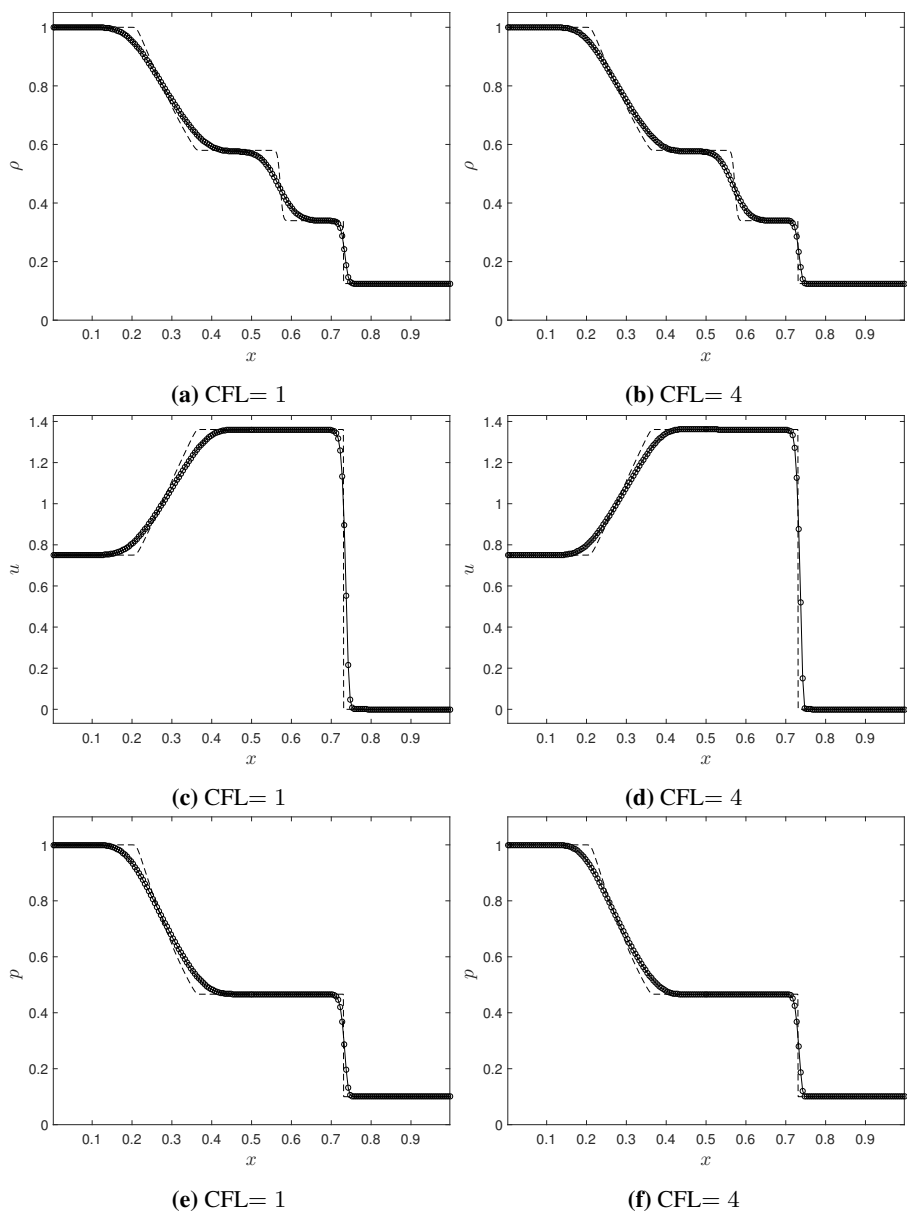
Figure 6.10: Numerical solutions of Toro's test 1 using Solberg* with $N = 200$.

(a) CFL= 8

(b) CFL= 16

(c) CFL= 8

(d) CFL= 16

(e) CFL= 8

(f) CFL= 16
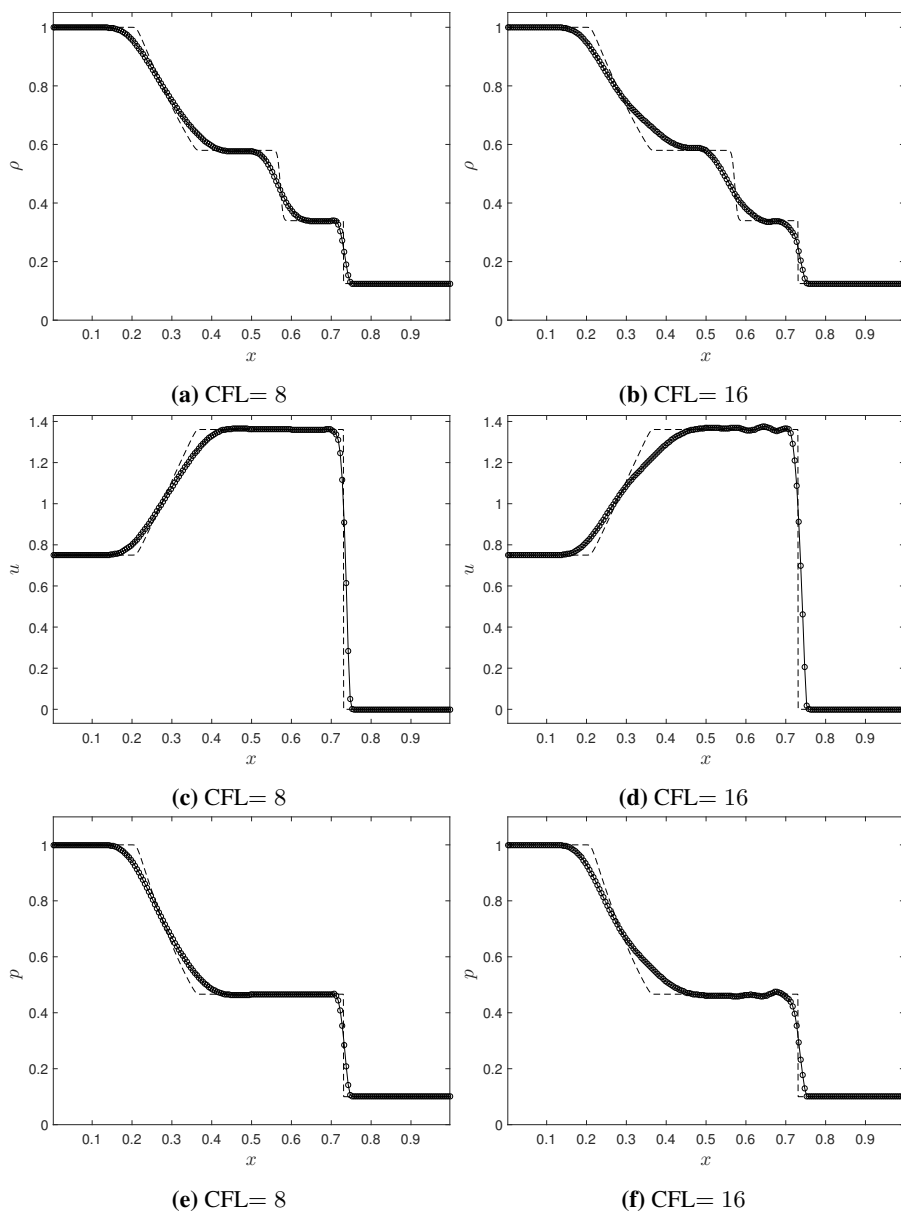
Figure 6.11: Numerical solutions of Toro's test 1 using Solberg* with $N = 200$.
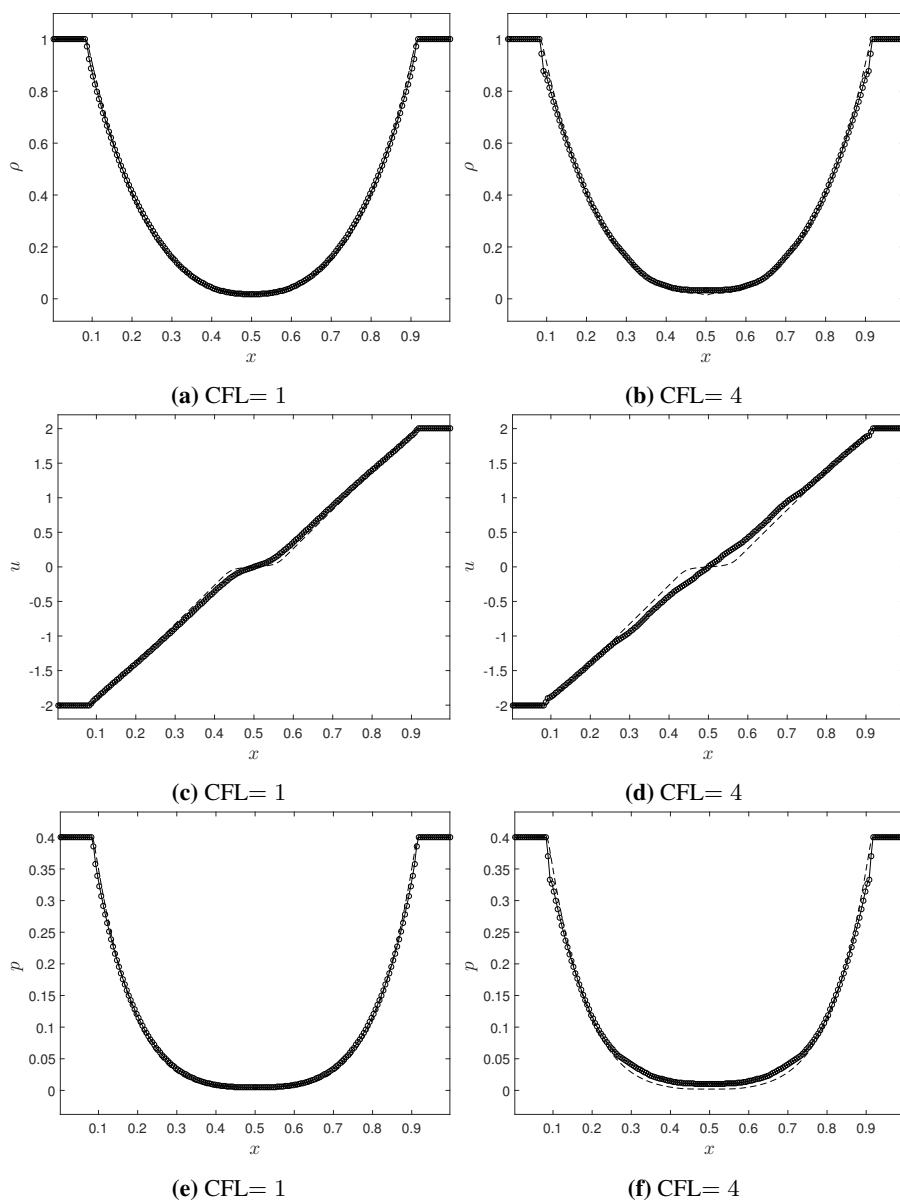
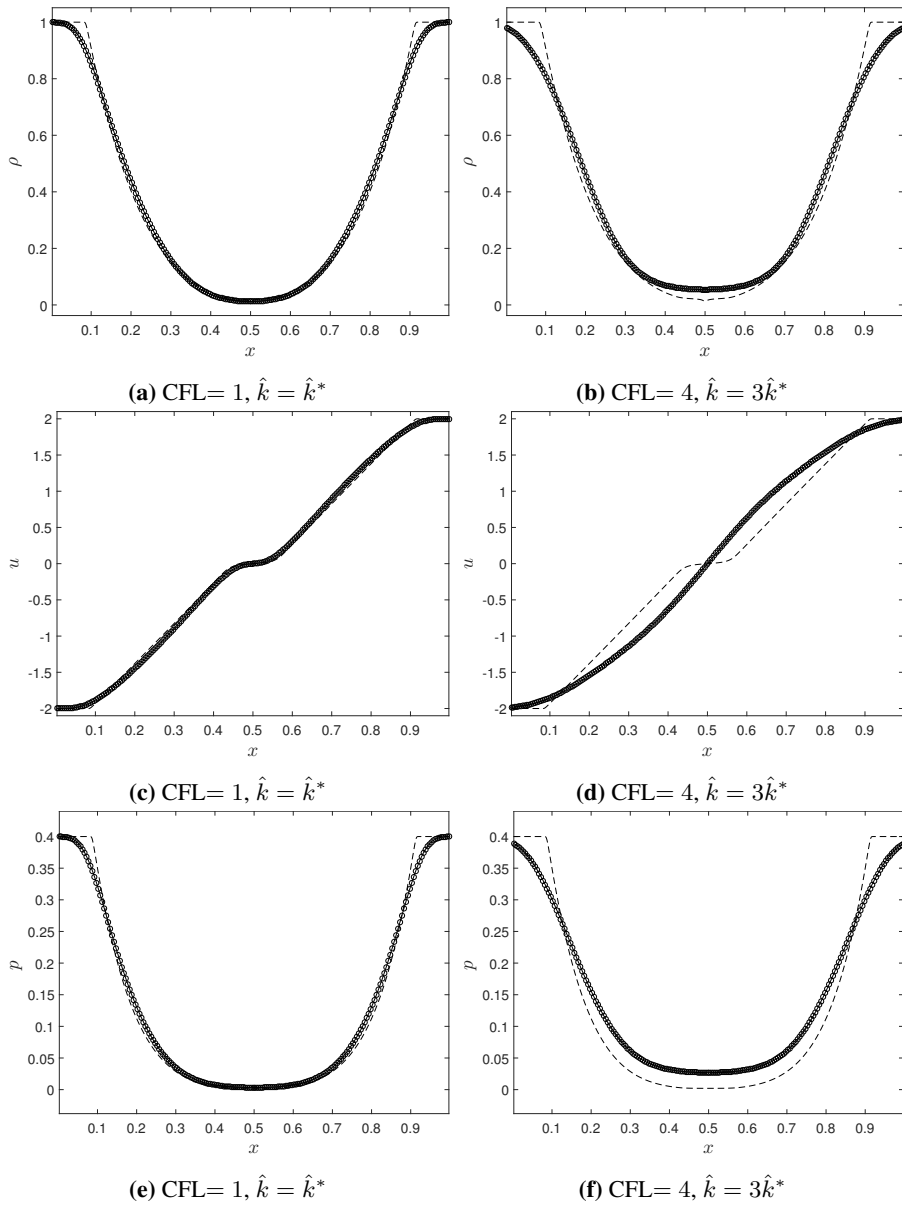**Figure 6.12:** Numerical solutions of Toro's test 2 using LTS-HLLE with $N = 200$.
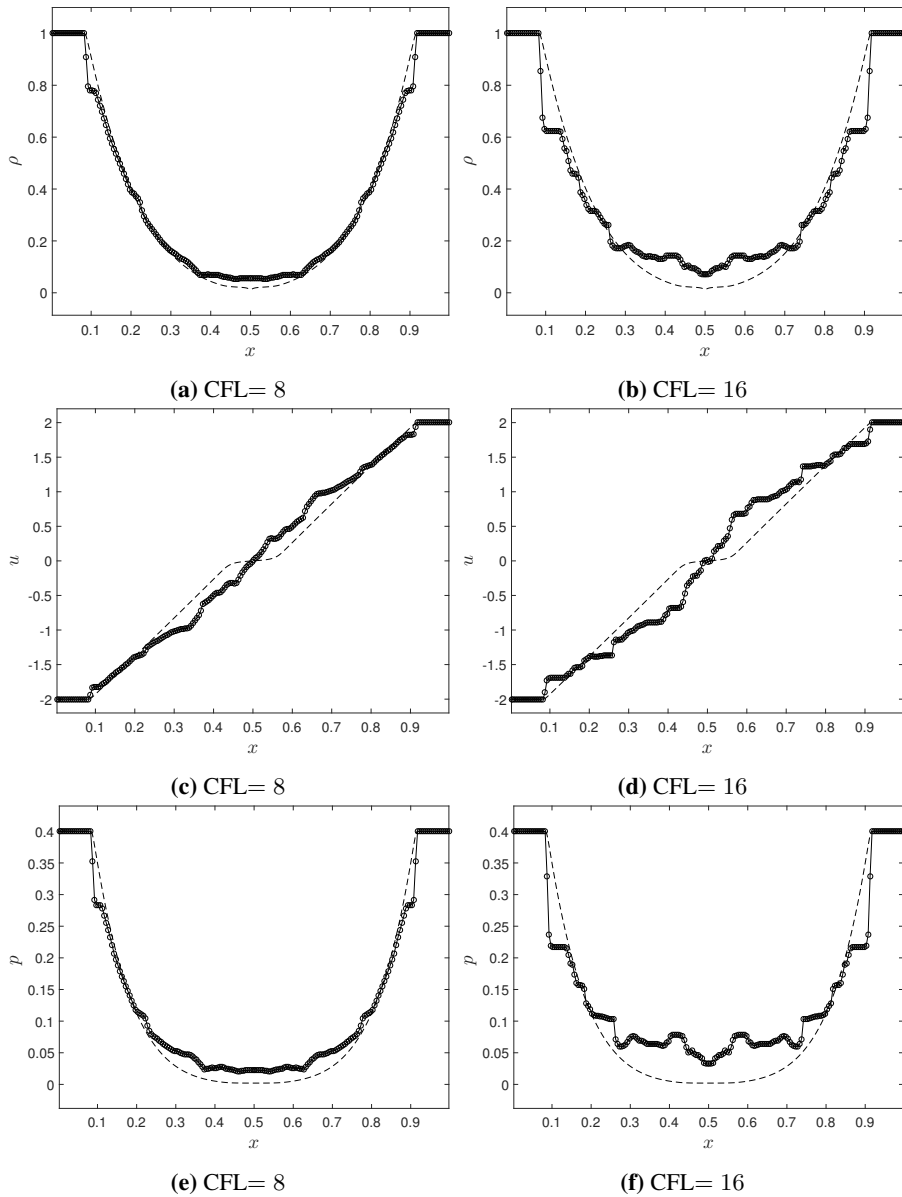
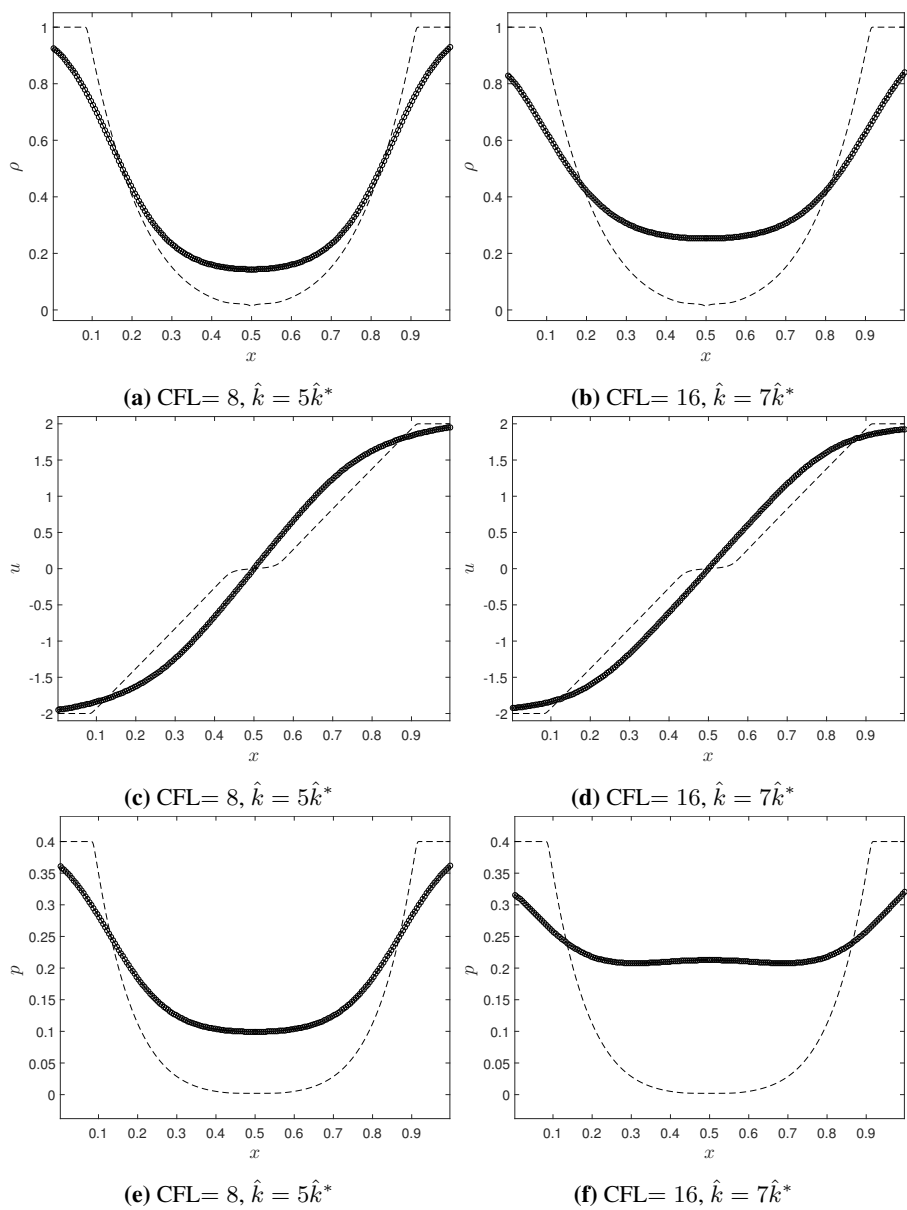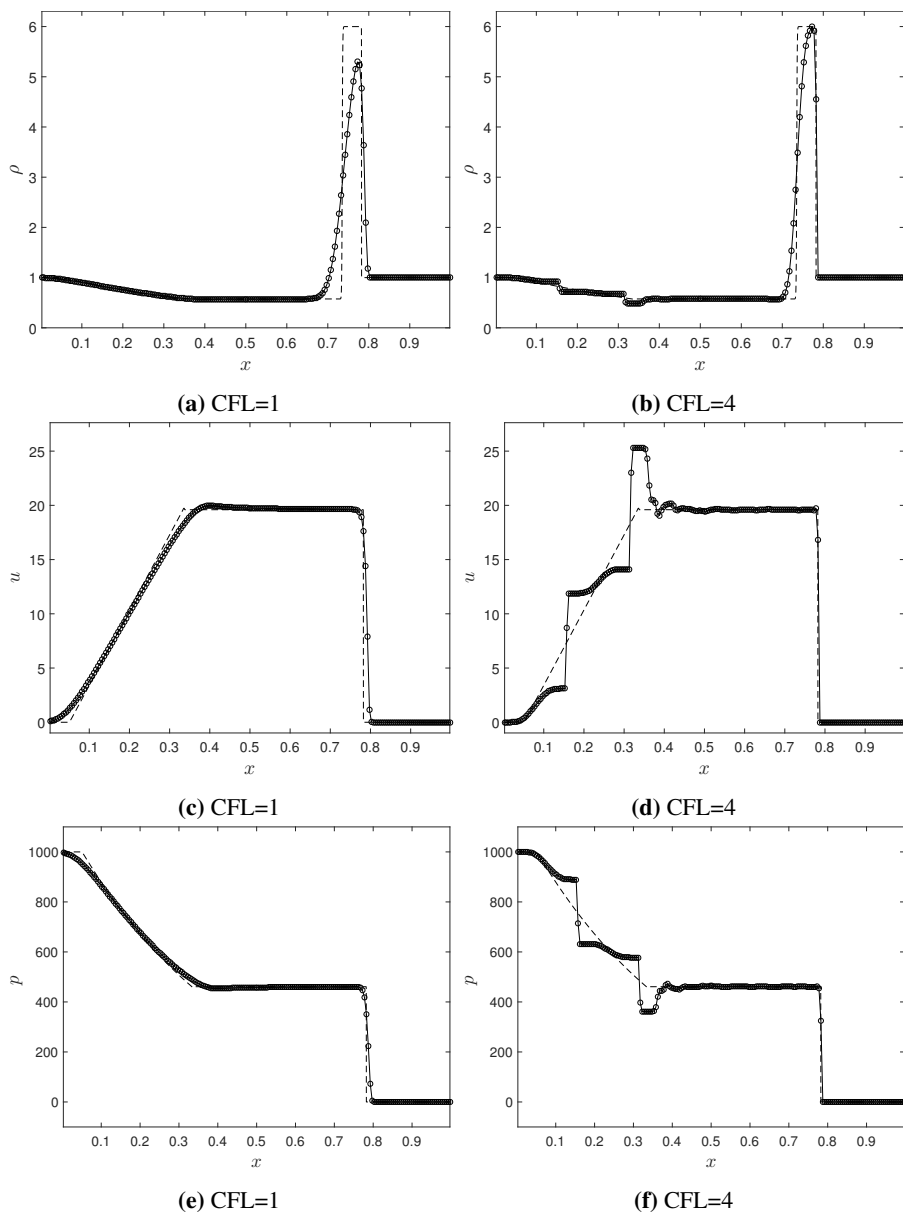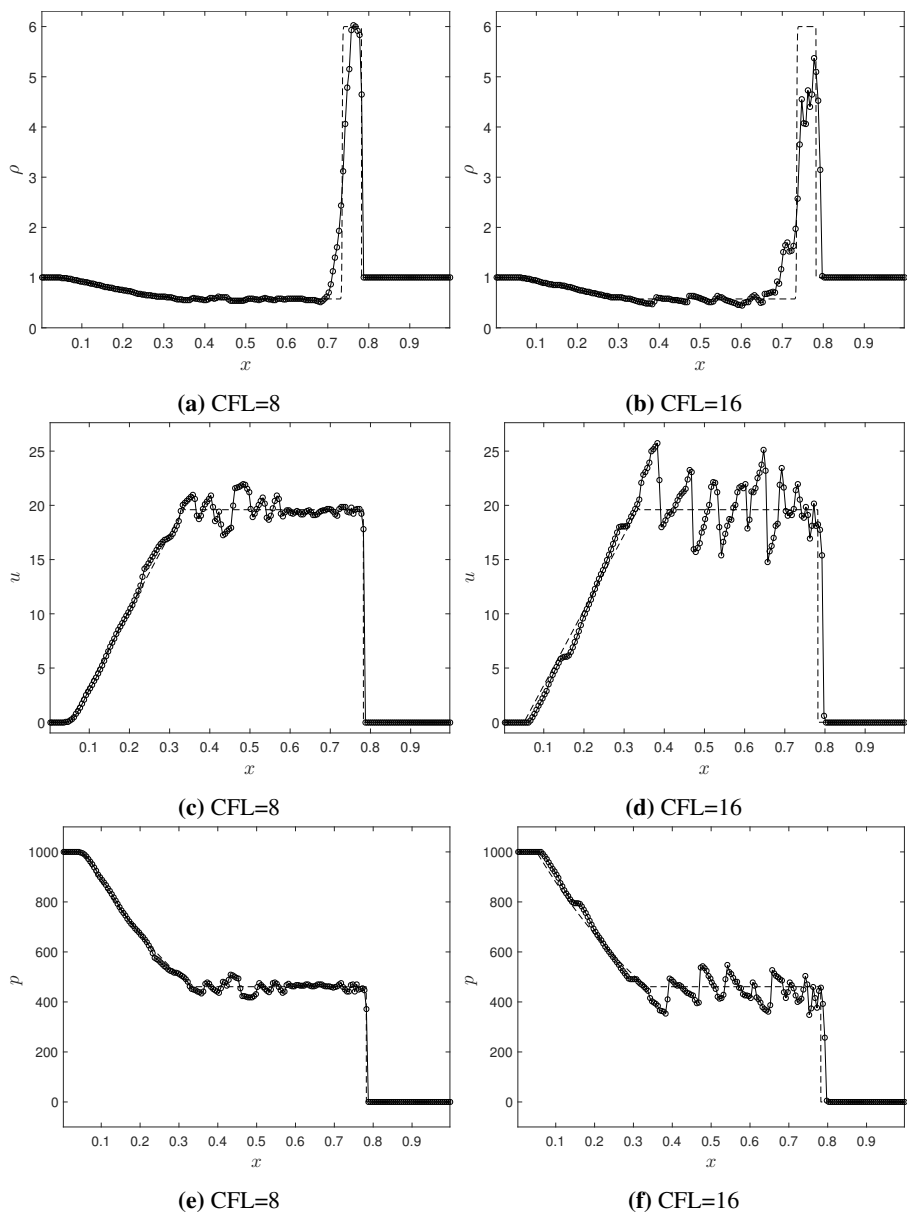**Figure 6.13:** Numerical solutions of Toro's test 2 using LTS-HLLE with $N = 200$.

(a) CFL= 1, $\hat{k} = \hat{k}^*$

(b) CFL= 4, $\hat{k} = 3\hat{k}^*$

(c) CFL= 1, $\hat{k} = \hat{k}^*$

(d) CFL= 4, $\hat{k} = 3\hat{k}^*$

(e) CFL= 1, $\hat{k} = \hat{k}^*$

(f) CFL= 4, $\hat{k} = 3\hat{k}^*$

Figure 6.14: Numerical solutions of Toro's test 2 using the Solberg scheme with $N = 200$.

(a) CFL= 8, $\hat{k} = 5\hat{k}^*$

(b) CFL= 16, $\hat{k} = 7\hat{k}^*$

(c) CFL= 8, $\hat{k} = 5\hat{k}^*$

(d) CFL= 16, $\hat{k} = 7\hat{k}^*$

(e) CFL= 8, $\hat{k} = 5\hat{k}^*$

(f) CFL= 16, $\hat{k} = 7\hat{k}^*$

Figure 6.15: Numerical solutions of Toro's test 2 using the Solberg scheme with $N = 200$.

(a) CFL=1   **(b)** CFL=4

(c) CFL=1   **(d)** CFL=4

(e) CFL=1   **(f)** CFL=4

Figure 6.16: Numerical solutions of Toro's test 3 using LTS-Roe with $N = 200$.

(a) CFL=8

(b) CFL=16

(c) CFL=8

(d) CFL=16

(e) CFL=8

(f) CFL=16

Figure 6.17: Numerical solutions of Toro's test 3 using LTS-Roe with $N = 200$.

(a) CFL= 1

(b) CFL= 4

(c) CFL= 1

(d) CFL= 4

(e) CFL= 1

(f) CFL= 4
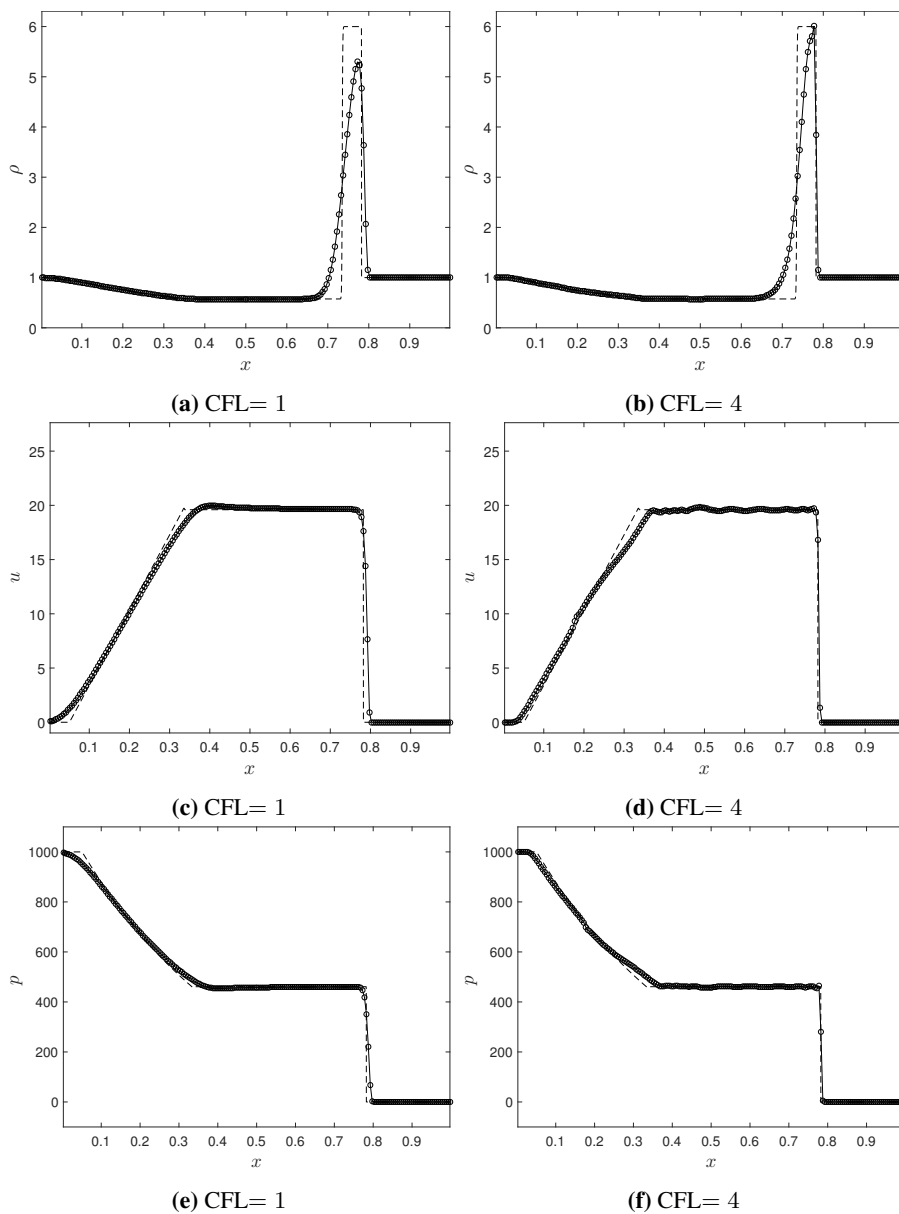
Figure 6.18: Numerical solutions of Toro's test 3 using LTS-HLLEϕ^* with $N = 200$.

(a) CFL= 8

(b) CFL= 16

(c) CFL= 8

(d) CFL= 16

(e) CFL= 8

(f) CFL= 16
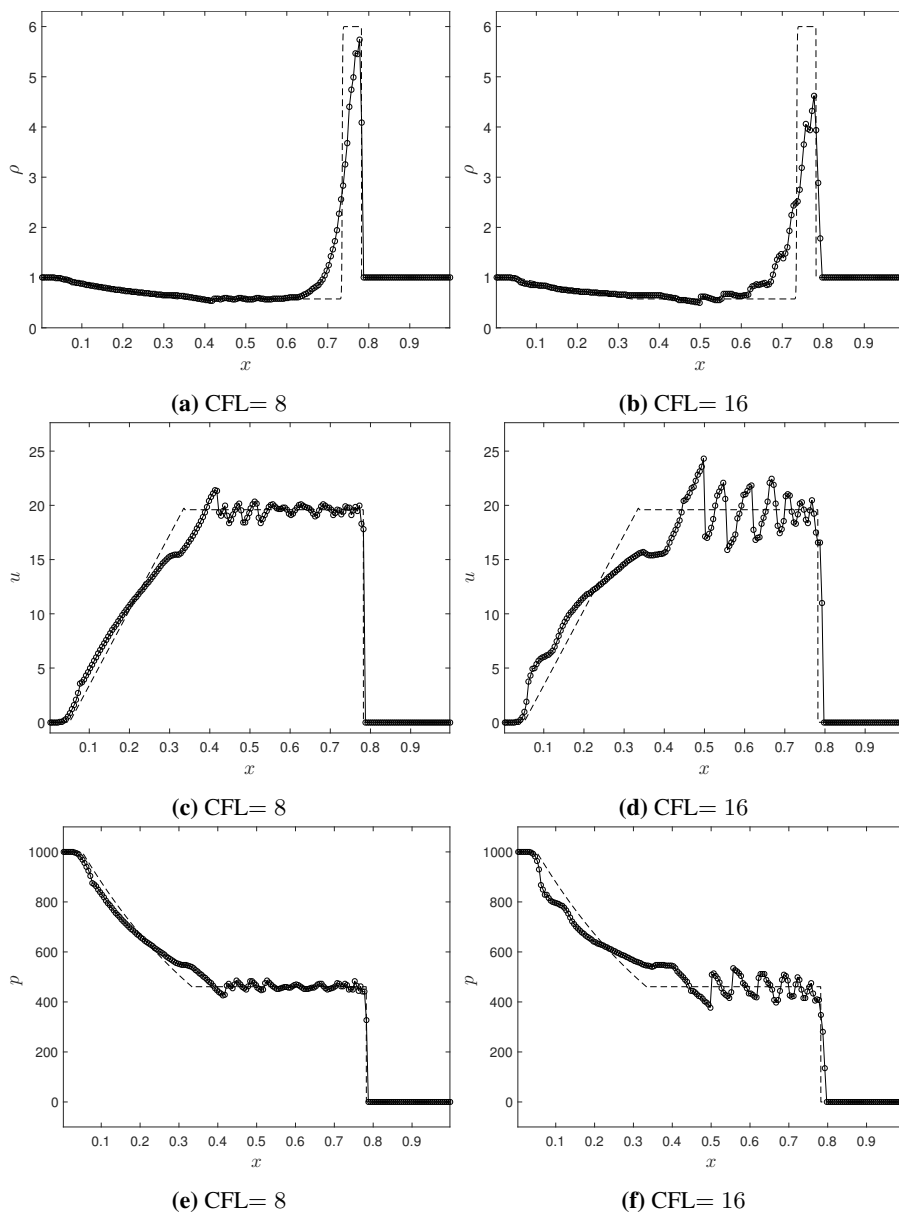
Figure 6.19: Numerical solutions of Toro's test 3 using LTS-HLLEϕ^* with $N = 200$.

(a) CFL=1

(b) CFL=4

(c) CFL=1

(d) CFL=4

(e) CFL=1

(f) CFL=4
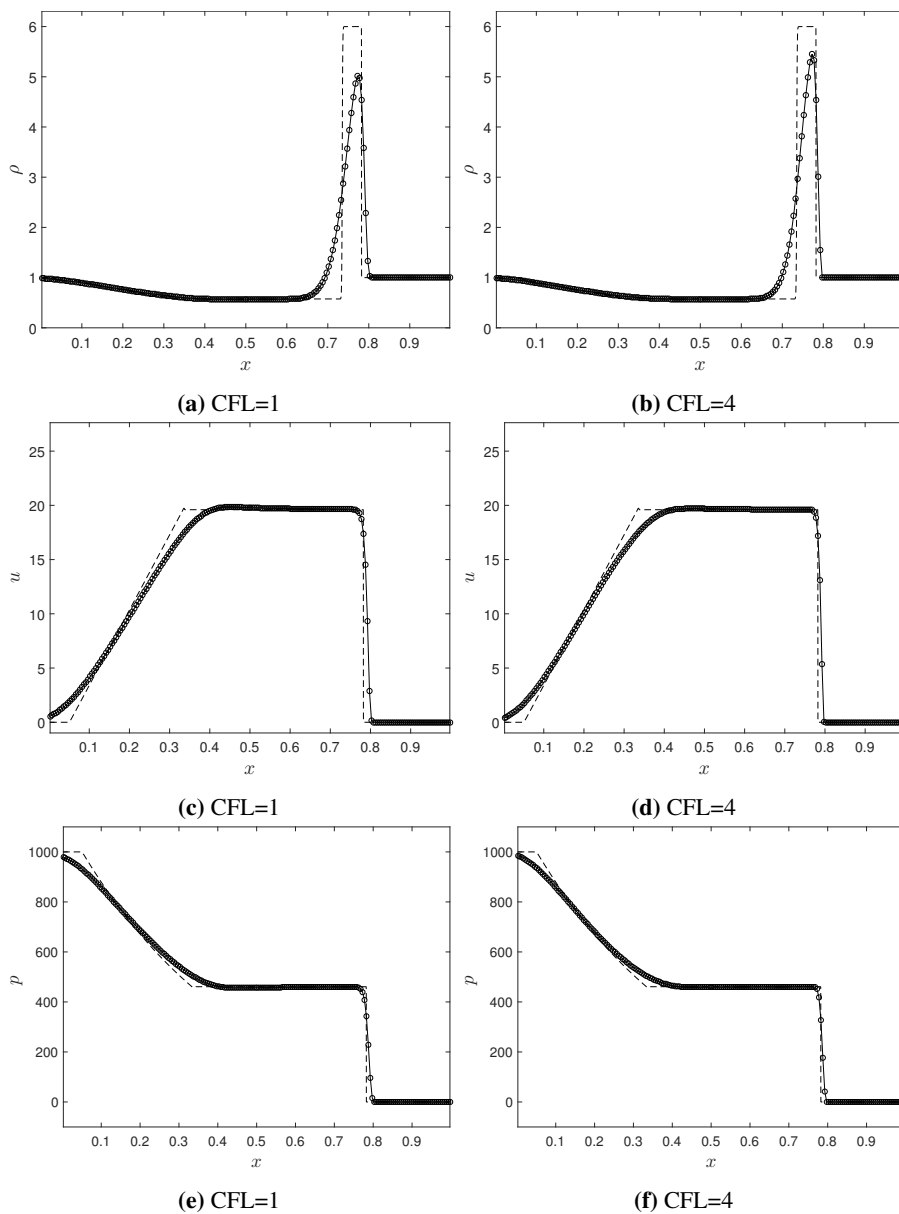
Figure 6.20: Numerical solutions of Toro's test 3 using Solberg* with $N = 200$.

(a) CFL=8

(b) CFL=16

(c) CFL=8

(d) CFL=16

(e) CFL=8

(f) CFL=16
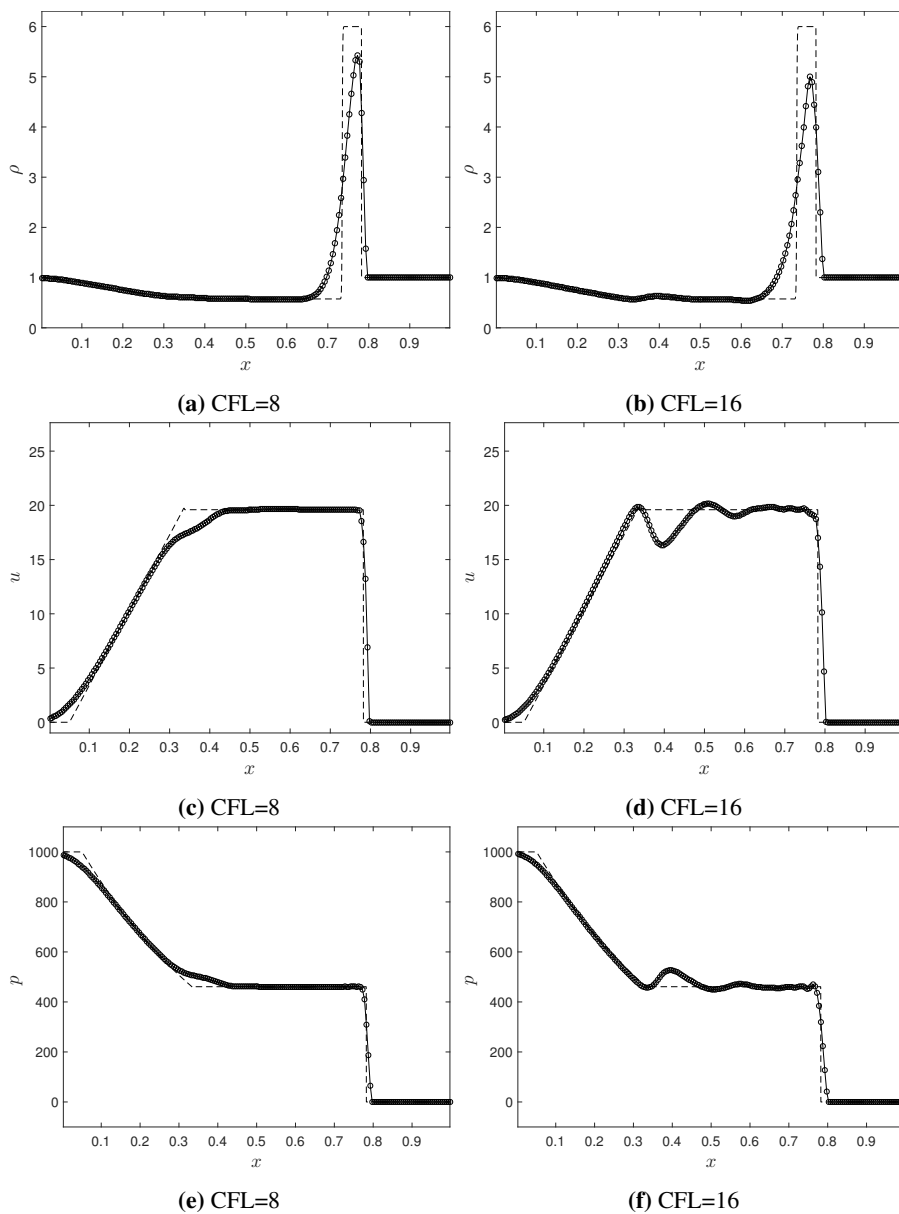
Figure 6.21: Numerical solutions of Toro's test 3 using Solberg* with $N = 200$.

(a) CFL=1

(b) CFL=4

(c) CFL=1

(d) CFL=4

(e) CFL=1

(f) CFL=4
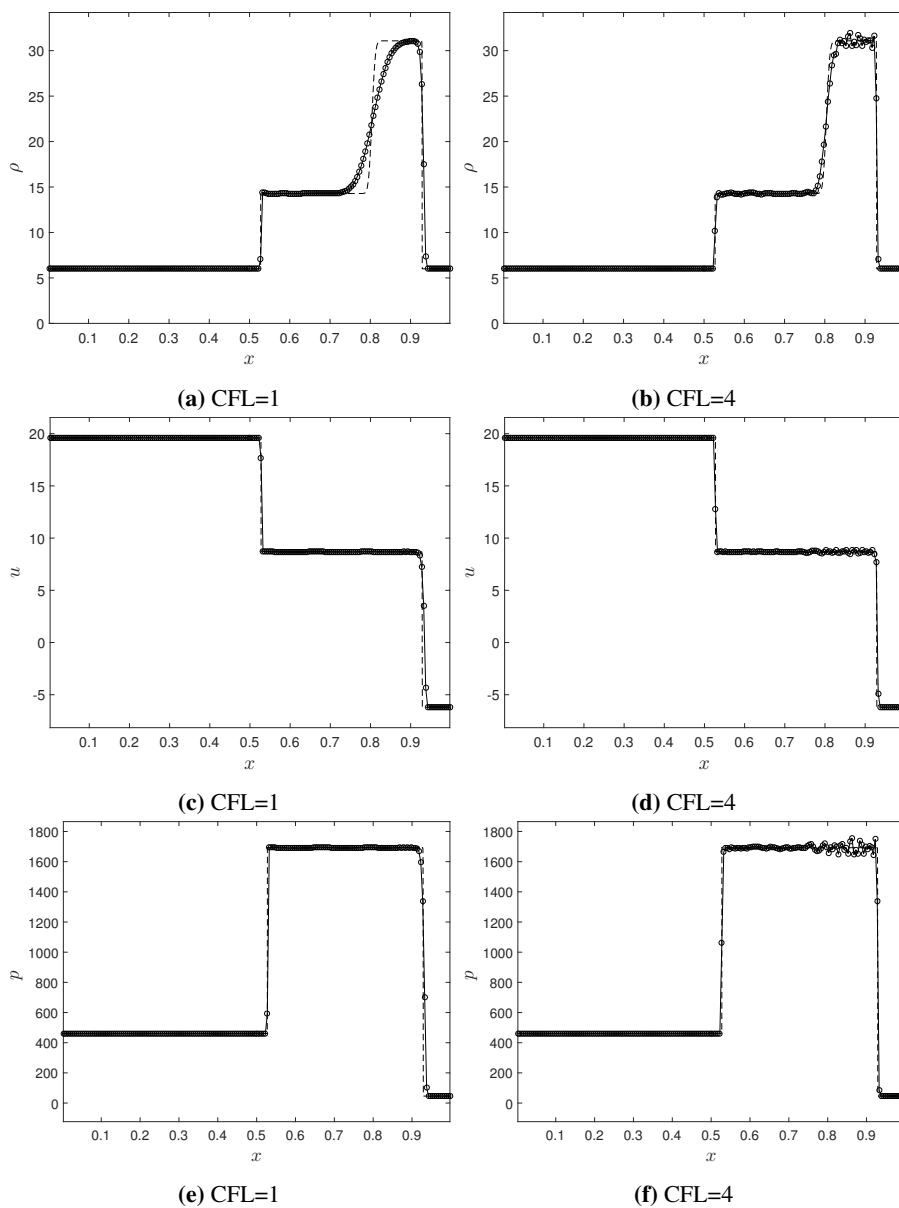
Figure 6.22: Numerical solutions of Toro's test 4 using LTS-Roe with $N = 200$.

(a) CFL=8

(b) CFL=16

(c) CFL=8

(d) CFL=16

(e) CFL=8

(f) CFL=16
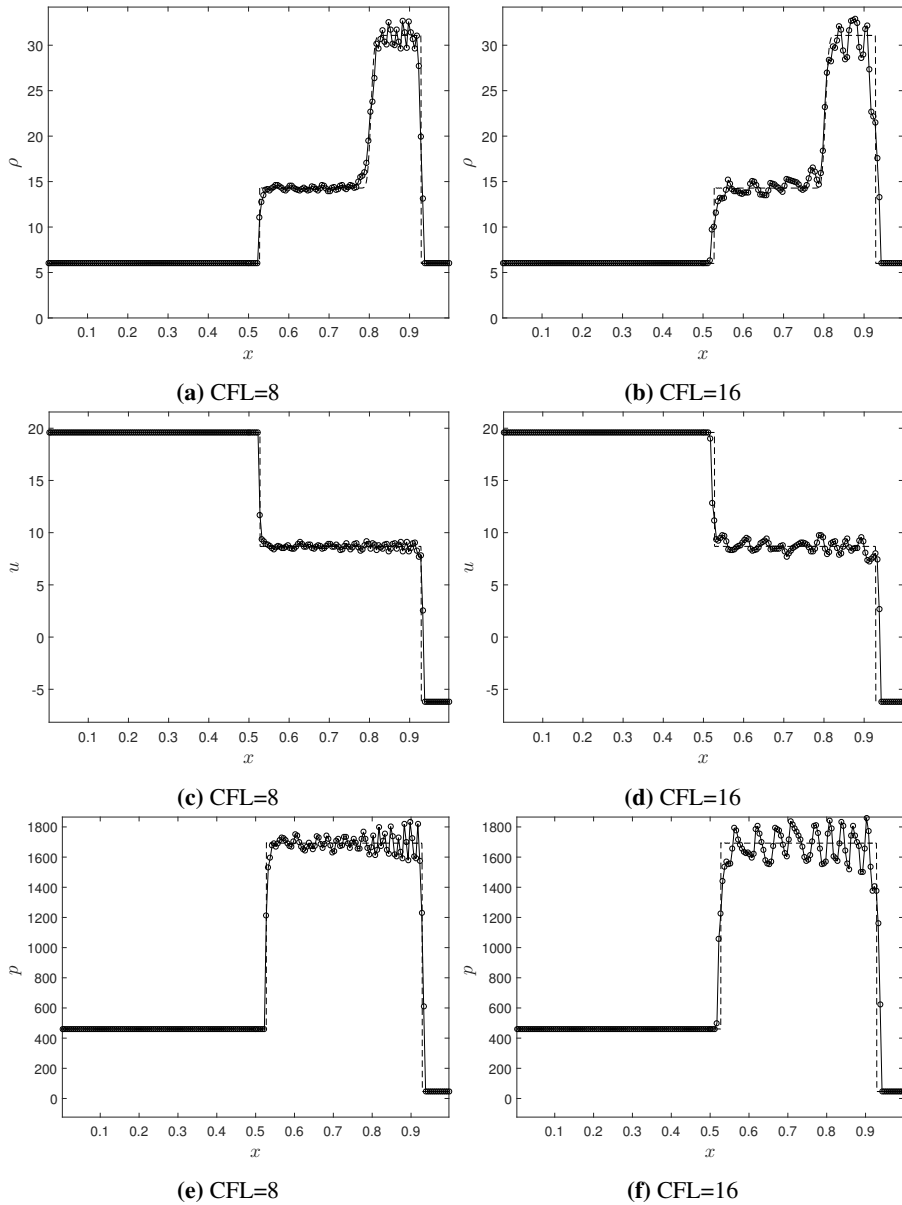
Figure 6.23: Numerical solutions of Toro's test 4 using LTS-Roe with $N = 200$.

(a) CFL=1

(b) CFL=4

(c) CFL=1

(d) CFL=4

(e) CFL=1

(f) CFL=4
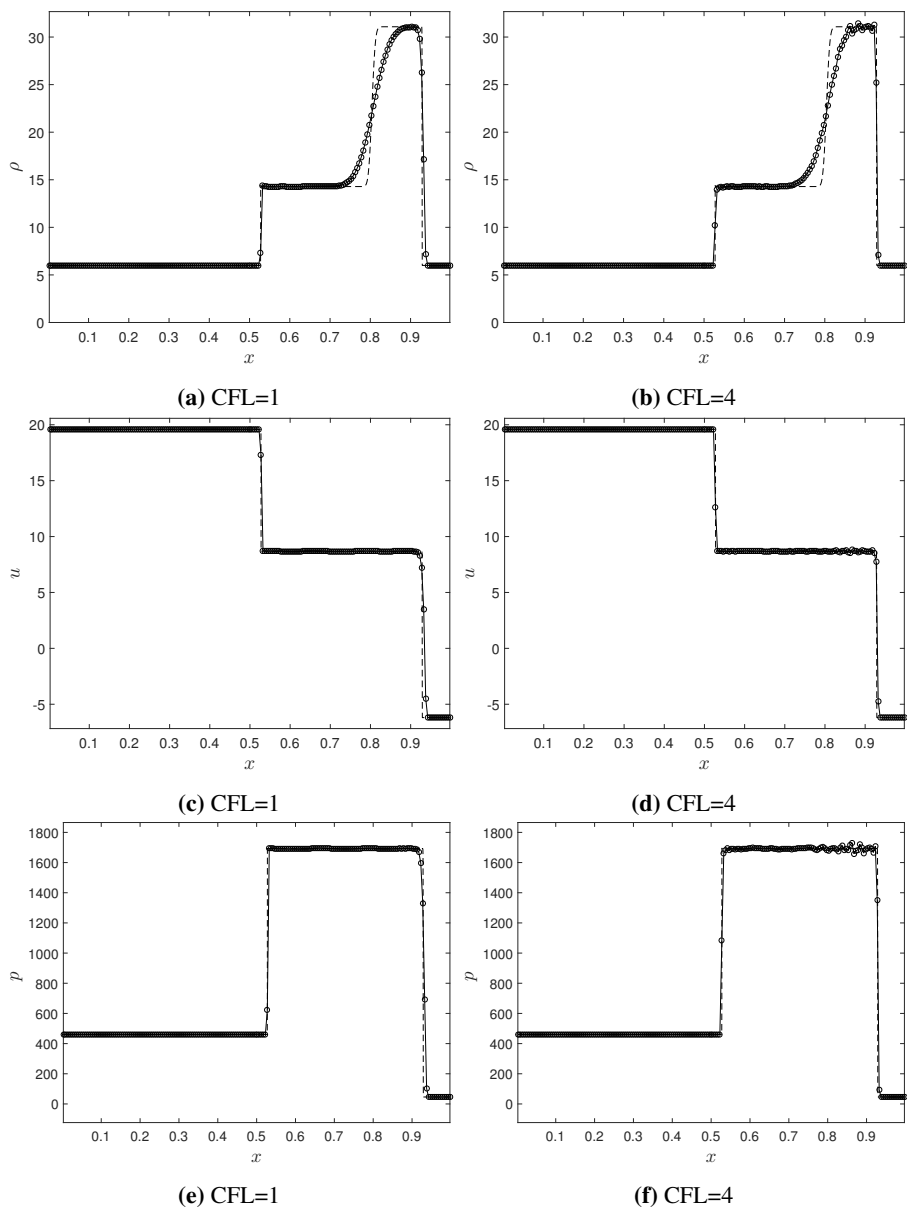
Figure 6.24: Numerical solutions of Toro's test 4 using LTS-HLLEϕ^* with $N = 200$.

(a) CFL=8

(b) CFL=16

(c) CFL=8

(d) CFL=16

(e) CFL=8

(f) CFL=16
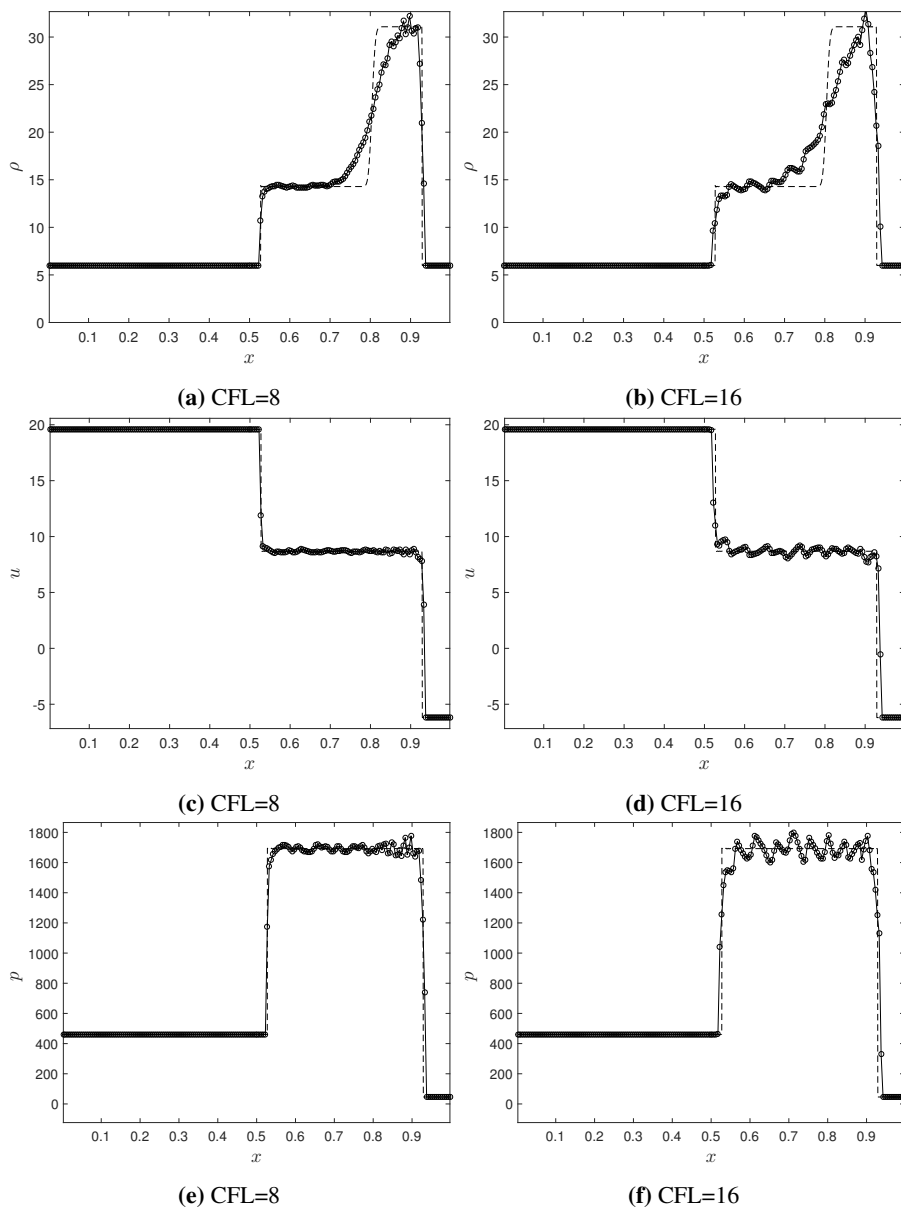
Figure 6.25: Numerical solutions of Toro's test 4 using LTS-HLLEϕ^* with $N = 200$.

(a) CFL=1

(b) CFL=4

(c) CFL=1
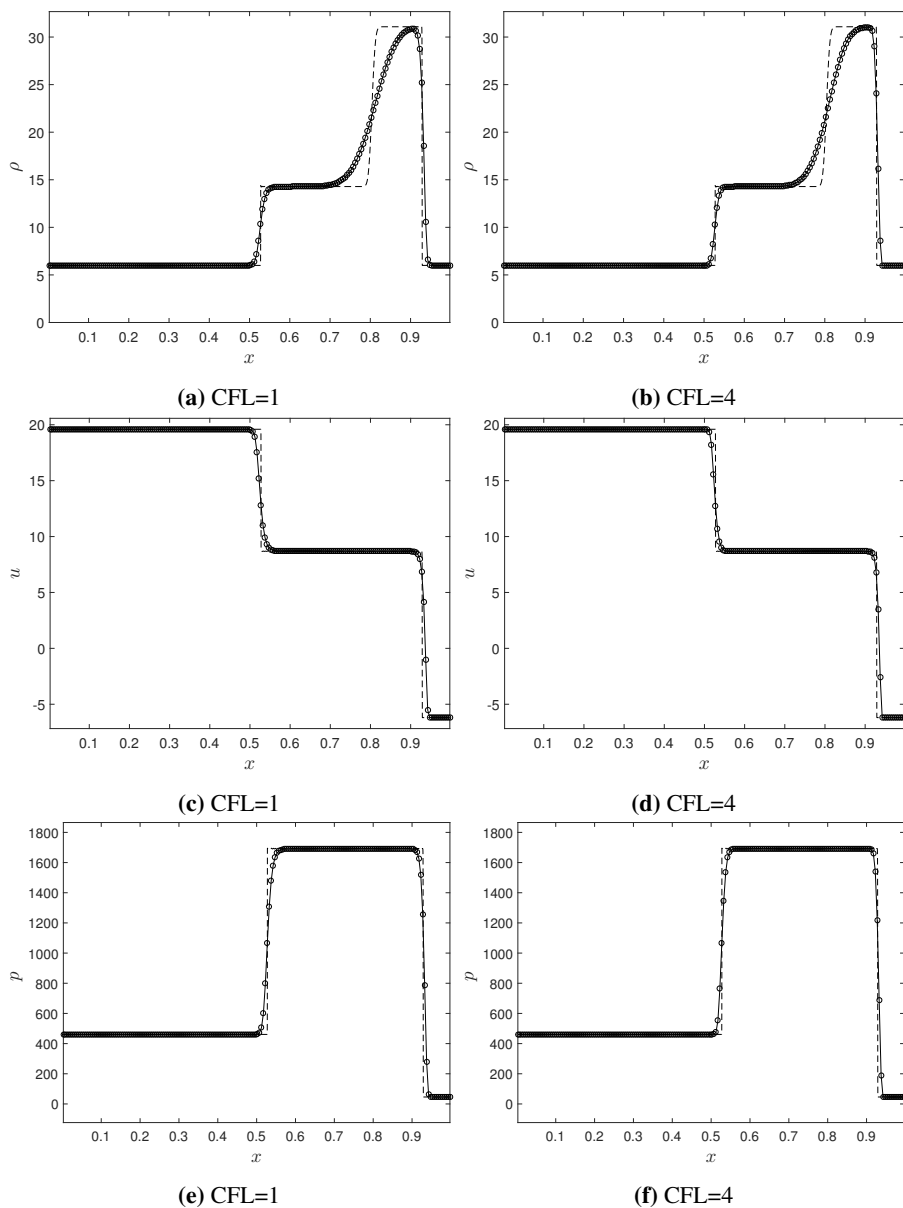
(d) CFL=4

(e) CFL=1

(f) CFL=4

Figure 6.26: Numerical solutions of Toro's test 4 using Solberg* with $N = 200$.
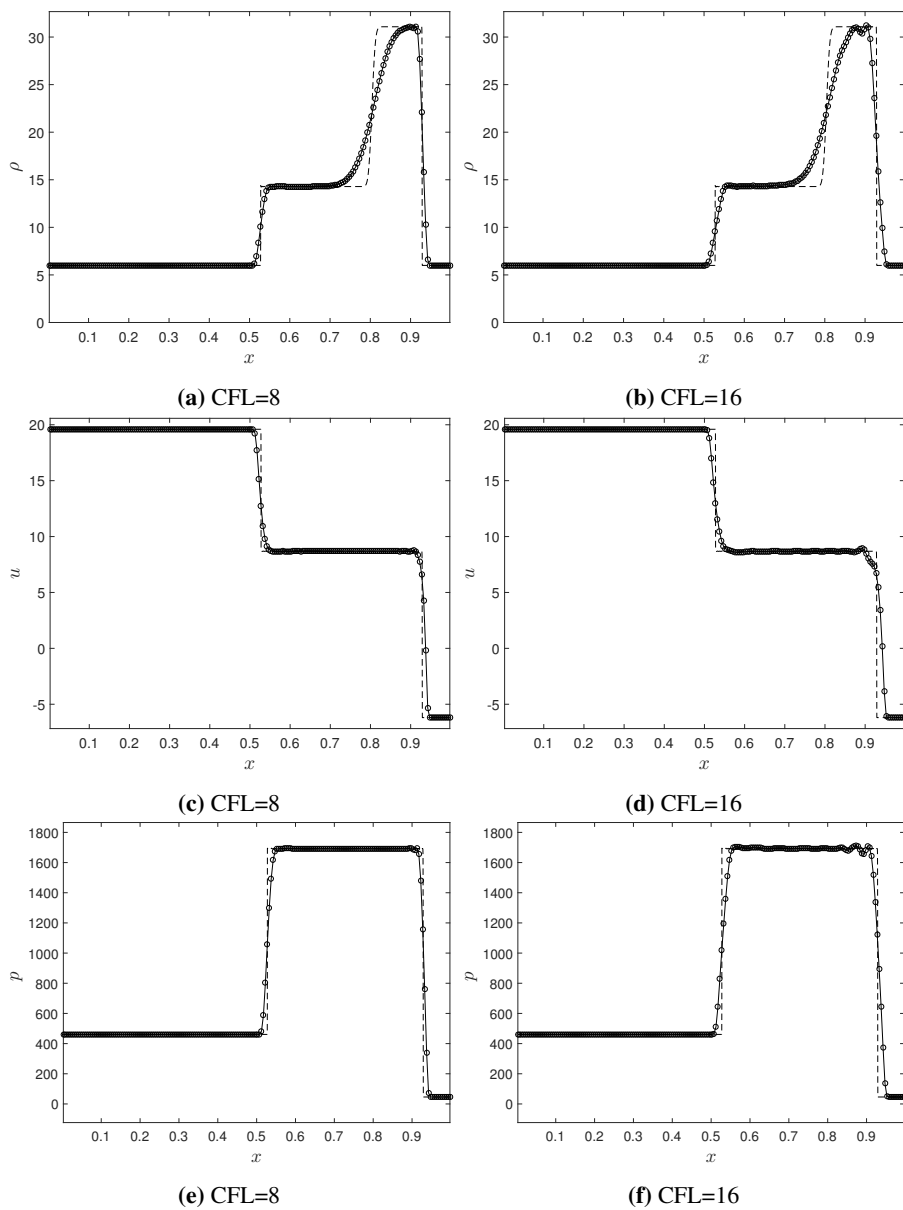
Figure 6.27: Numerical solutions of Toro's test 4 using Solberg* with $N = 200$.
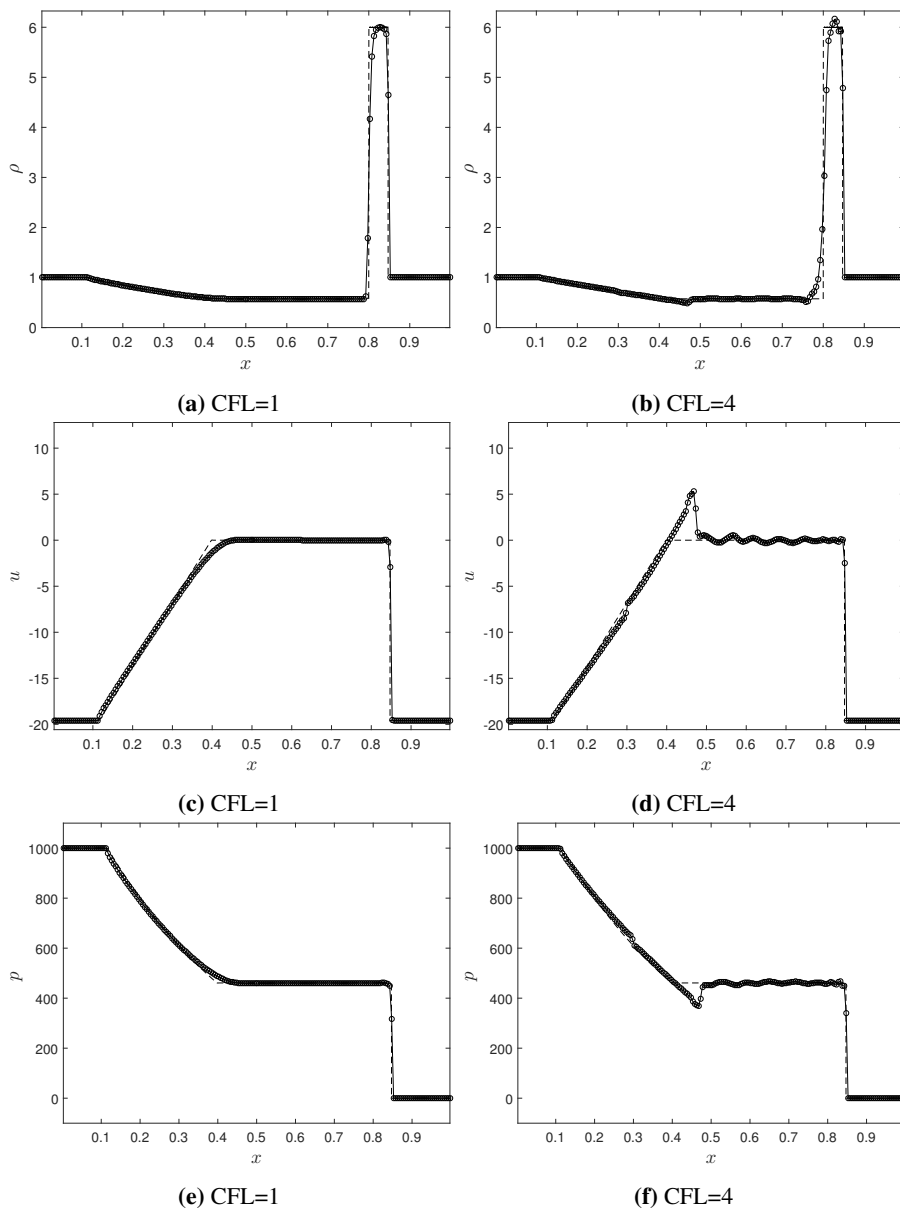
Figure 6.28: Numerical solutions of Toro's test 5 using LTS-Roe with $N = 200$.
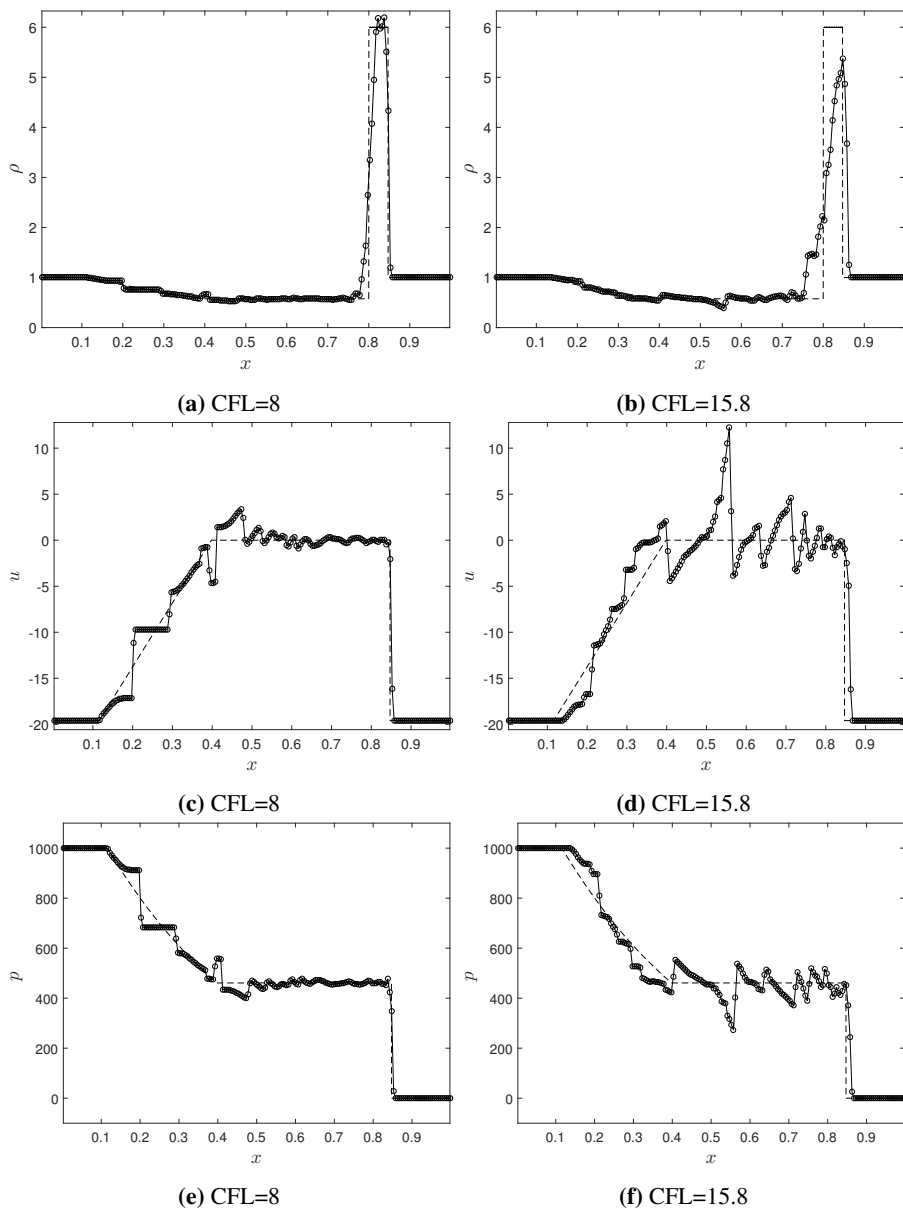
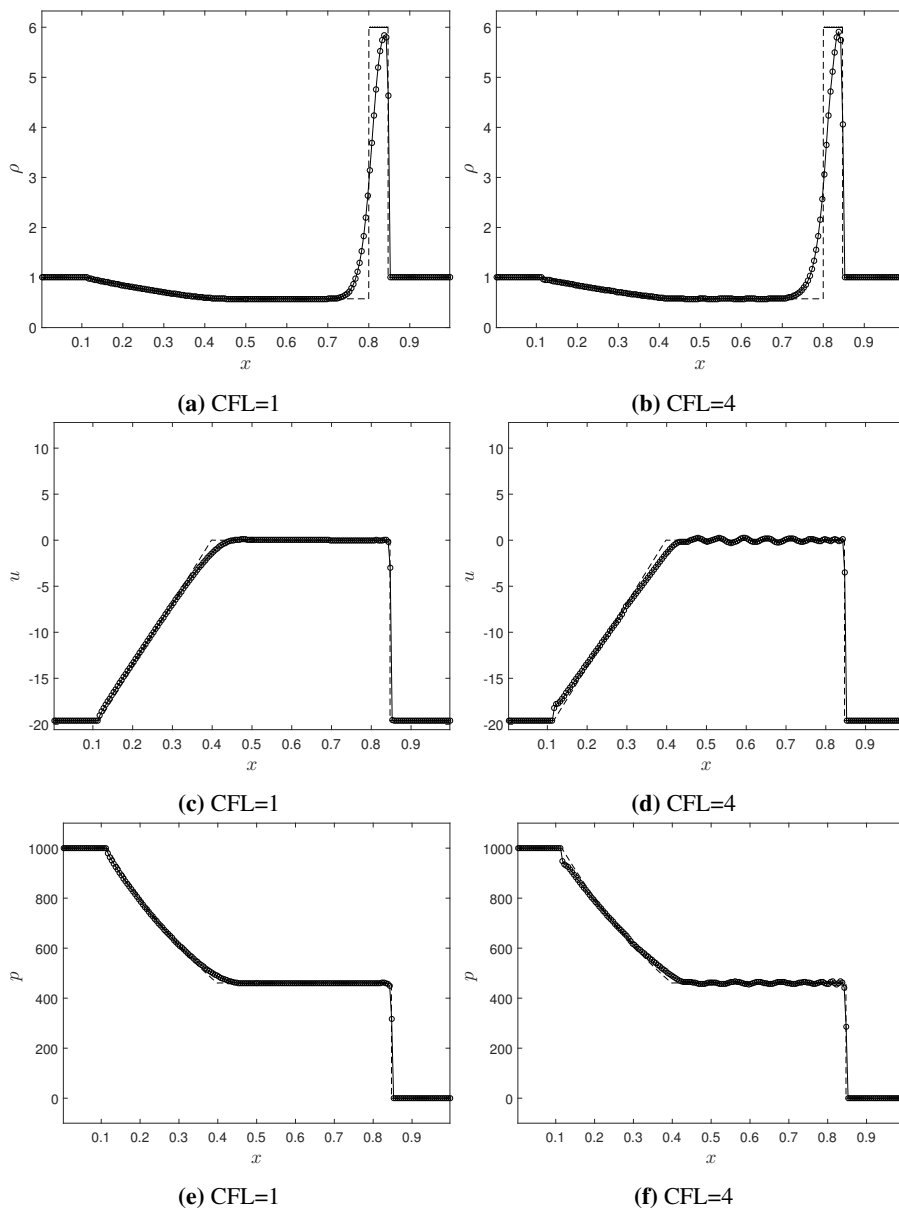**Figure 6.29:** Numerical solutions of Toro's test 5 using LTS-Roe with $N = 200$.

Figure 6.30: Numerical solutions of Toro's test 5 using LTS-HLLEϕ^* with $N = 200$.

Figure 6.31: Numerical solutions of Toro's test 5 using LTS-HLLEϕ^* with $N = 200$.

(a) CFL=1

(b) CFL=4

(c) CFL=1

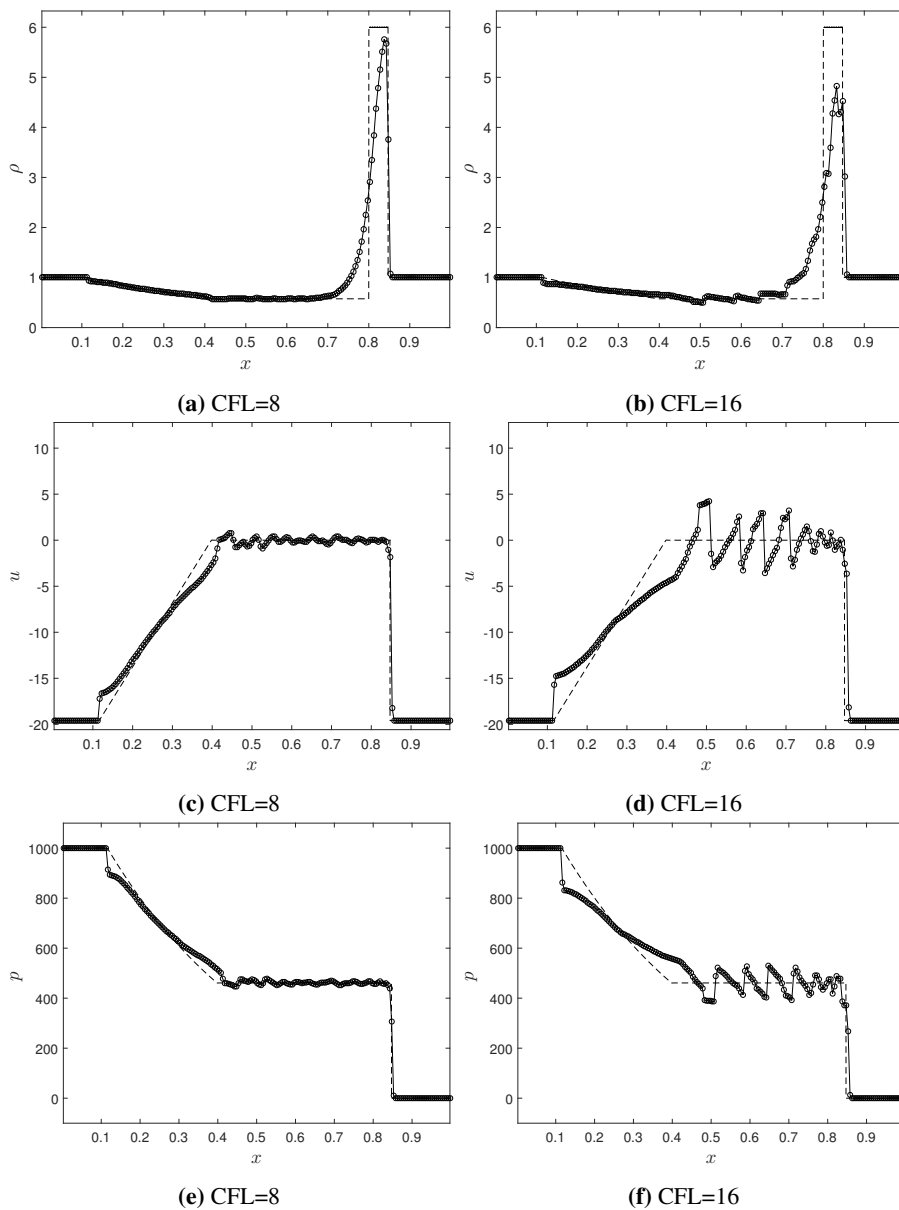**(d)** CFL=4

(e) CFL=1

(f) CFL=4
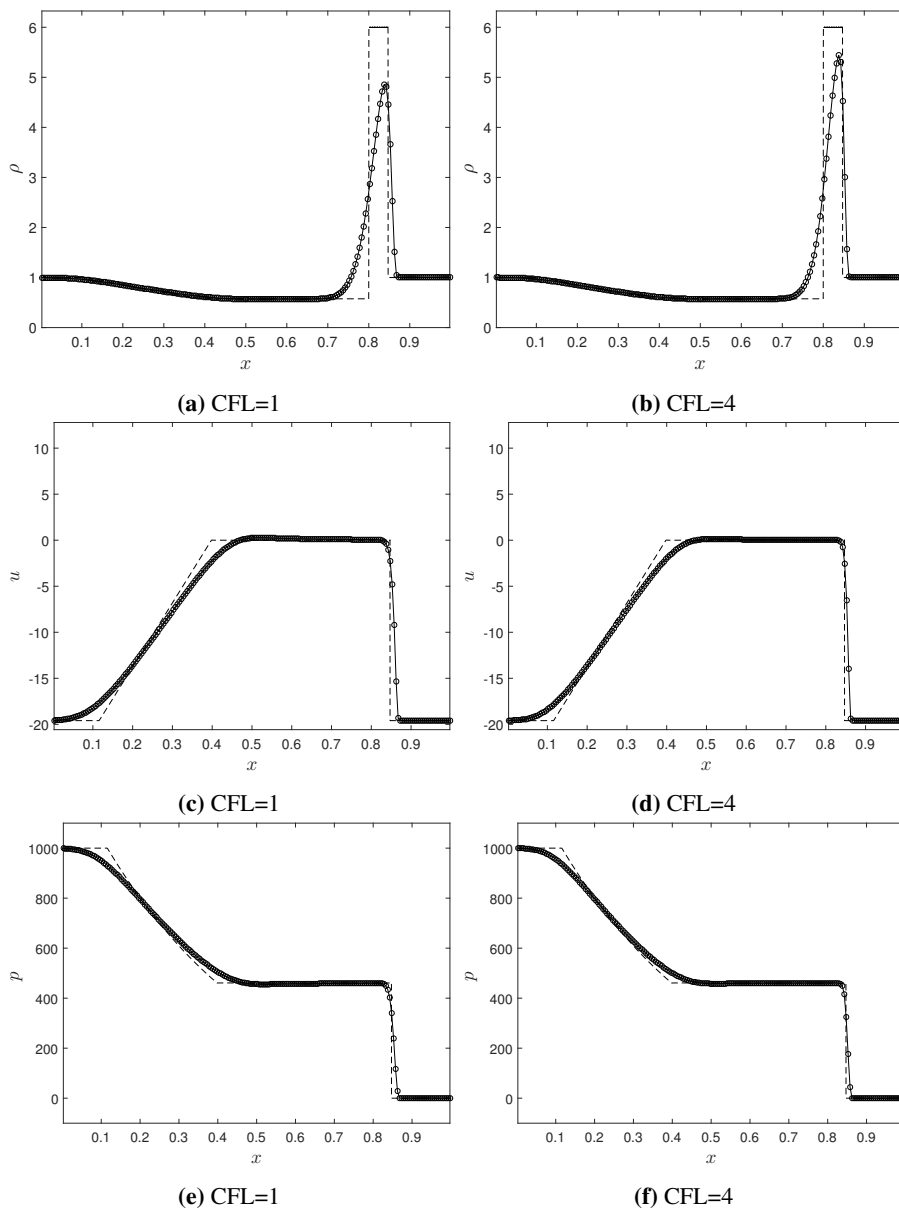
Figure 6.32: Numerical solutions of Toro's test 5 using Solberg* with $N = 200$.
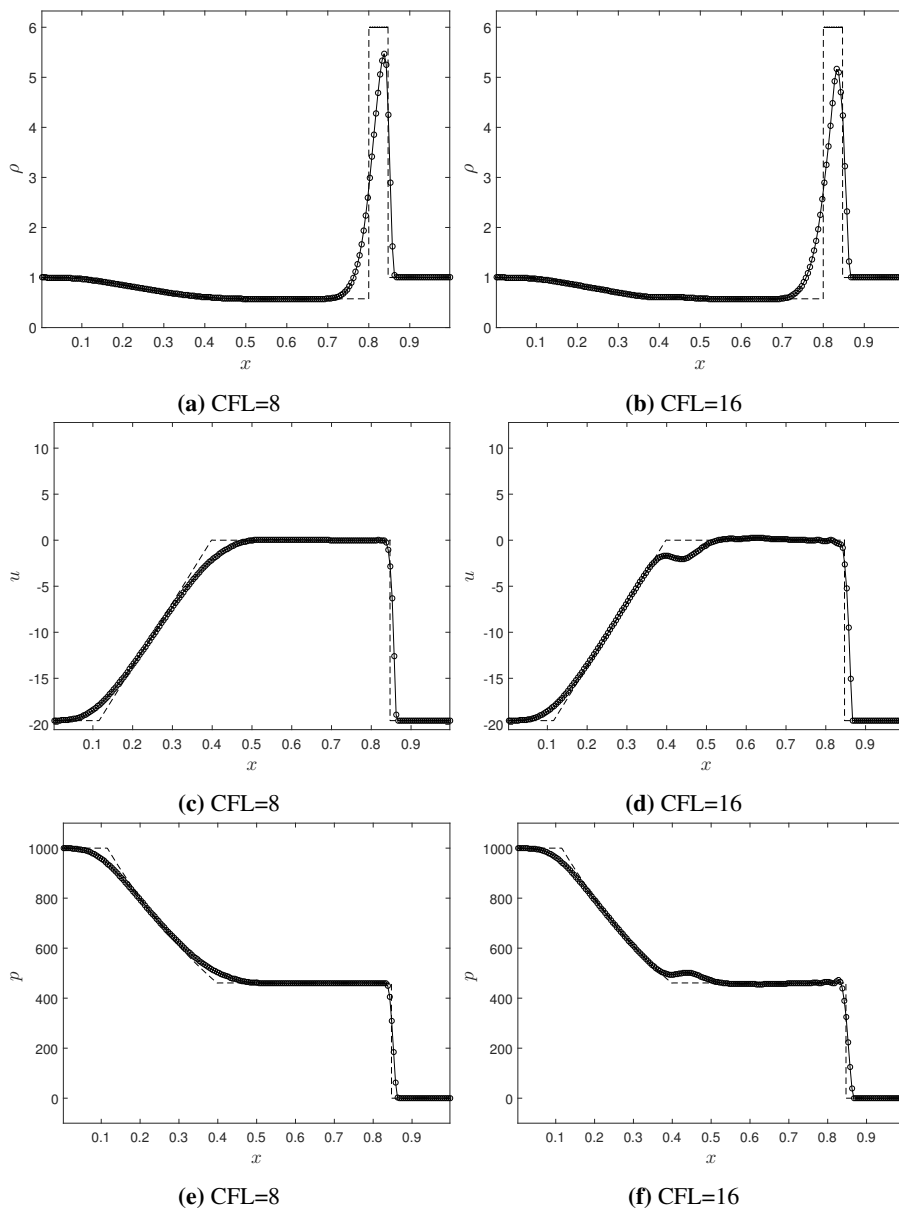
Figure 6.33: Numerical solutions of Toro's test 5 using Solberg* with $N = 200$.

(a) First order LTS-Roe

(b) Second order LTS-Roe

(c) First order LTS-HLLEϕ^*

(d) Second order LTS-HLLEϕ^*

(e) First order Solberg*

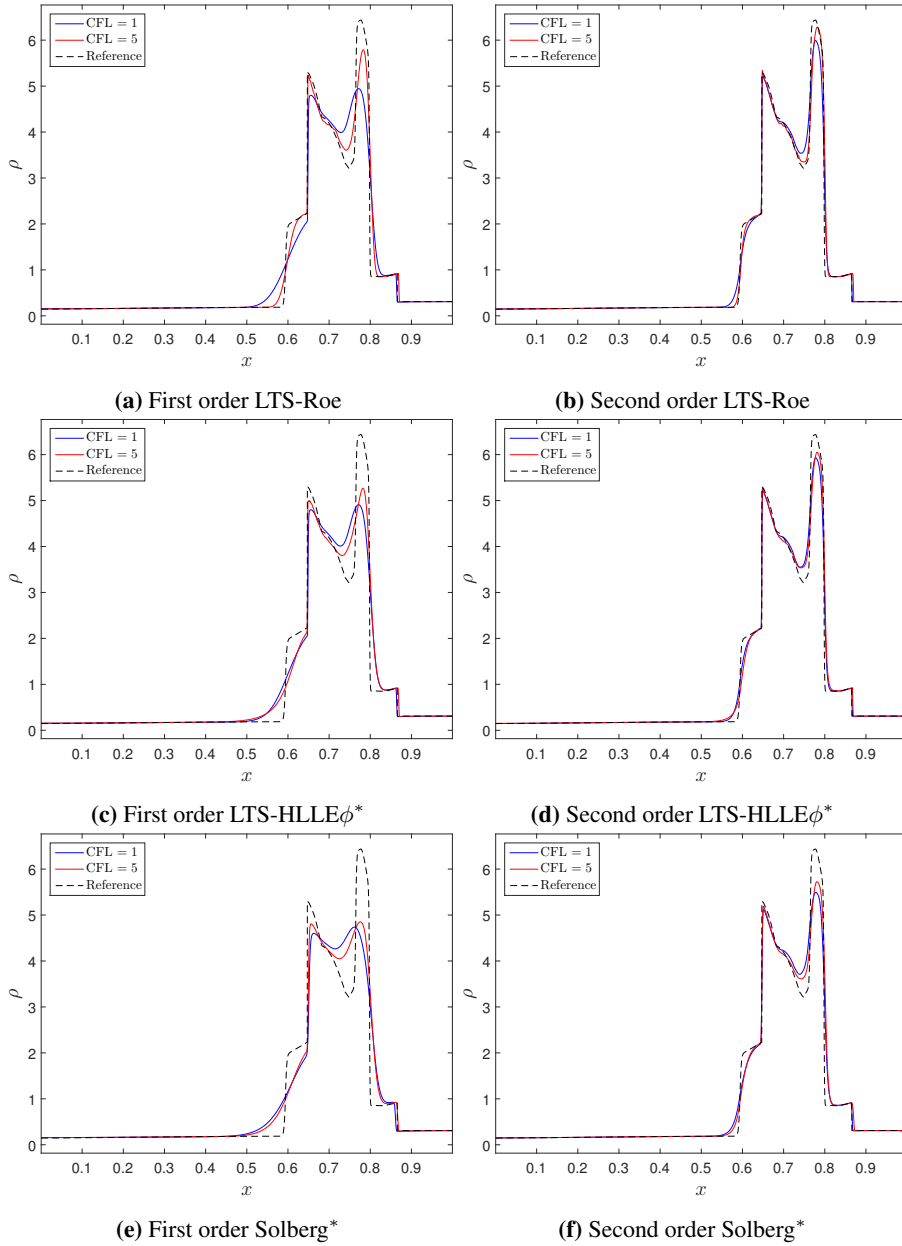**(f)** Second order Solberg*

Figure 6.34: Numerical solutions of density for the Woodward-Colella blast-wave problem, with $N = 1000$.

Chapter 7

Conclusion

In this thesis, we presented large time step methods for hyperbolic conservation laws. We studied different discretization schemes, and compared their robustness and numerical diffusion. The main results are given below.

7.1 Artificial flux function framework

The artificial flux function framework, presented in section 4.5, gives us a new way of describing LTS schemes. We showed how finding the artificial flux function of a 3-point scheme can yield a natural large time step extension of the scheme, through the LTS-Godunov method. In this framework we can easily construct new, sophisticated schemes.

7.2 The new LTS scheme

A new LTS scheme, denoted LTS-HLLϕ, was presented in chapter 5. By changing the three parameters of the scheme, we showed that the scheme is a generalization of the following LTS schemes: LTS-Roe, LTS-HLL, LTS-Lax-Friedrichs, LTS-Lax-Wendroff, the Solberg scheme and the Solbergϕ scheme. The flux-difference splitting coefficients of the LTS-HLLϕ scheme in (5.7), is the main original result from this thesis. From this result, we derived the flux-difference splitting coefficients for the Solbergϕ scheme. We also suggested a method for selecting the parameters of the Solbergϕ scheme.

7.3 Numerical simulations

Numerical simulations on the Burgers' equation demonstrated the limitations of many of the current LTS methods with regard to entropy violations and wave interaction treatment. If we can add the right amount of numerical diffusion in the LTS-HLLϕ scheme, it seems like the scheme has the potential to yield very accurate, entropy satisfying solutions for

different initial data. We also saw that we can use numerical diffusion in shocks, to absorb errors that appear due to wave interactions.

Numerical simulations on the Euler equations demonstrated that the LTS-Roe scheme give strong oscillations for systems of equations, for many different test cases. The problem is increasingly severe for high Courant numbers, and can lead to lack of positivity in low pressure regions of the domain. Although the LTS-HLLEϕ^* schemes yielded entropy satisfying solutions, it did little to reduce the oscillations. Only the Solberg* scheme yielded robust results for all Courant numbers, and the suggested procedure for selecting parameters gave a good trade off between accuracy and robustness in most of the presented test cases. However, it does not guaranty robustness, as Toro's test case 2 demonstrated. By adding additional diffusion, we were able to make the Solberg scheme more robust, although more inaccurate.

7.4   Future prospects

The artificial flux function framework opens up for endless rapid prototyping of new LTS schemes, as the flux-difference splitting coefficients and the numerical diffusion coefficient can be evaluated numerically. One suggestion, also mentioned by Solberg [23], is to choose higher order polynomials as artificial flux functions. An n-th order polynomial will satisfy the consistency conditions with $n-1$ free parameters. By carefully selecting these parameters, it might be possible to achieve very high order of accuracy, by canceling the higher order terms of the modified equation.

We still have no sufficient way of determining whether the LTS-HLLϕ scheme will be robust for a given Courant number and initial data. In order to determine this, it might be interesting to investigate if the scheme is positivity preserving for certain choices of parameters.

Bibliography

[1] S. L. Bore. High-resolution large time-step schemes for hyperbolic conservation laws. Master's thesis, NTNU, 2015.

[2] R. Courant, K. Friedrichs, and H. Lewy. On the partial difference equations of mathematical physics. *IBM journal*, 11(2):215–234, 1967.

[3] M. Dumbser, M. Castro, C. Parés, and E. F. Toro. Ader schemes on unstructured meshes for nonconservative hyperbolic systems: Applications to geophysical flows. *Computers & Fluids*, 38(9):1731–1748, 2009.

[4] B. Einfeldt. On Godunov-type methods for gas dynamics. *SIAM Journal on Numerical Analysis*, 25(2):294–318, 1988.

[5] S. K. Godunov. A difference method for numerical calculation of discontinuous solutions of the equations of hydrodynamics. *Matematicheskii Sbornik*, 89(3):271–306, 1959.

[6] A. Harten. High resolution schemes for hyperbolic conservation laws. *Journal of computational physics*, 49(3):357–393, 1983.

[7] A. Harten. On a large time-step high resolution scheme. *Mathematics of computation*, 46(174):379–399, 1986.

[8] A. Harten, P. D. Lax, and B. Van Leer. On upstream differencing and godunov-type schemes for hyperbolic conservation laws. *SIAM Review*, pages 35–61, 1983.

[9] A. Jameson and P. D. Lax. Conditions for the construction of multi-point total variation diminishing difference schemes. *Applied numerical mathematics*, 2(3-5):335–345, 1986.

[10] P. Lax and B. Wendroff. Systems of conservation laws. *Communications on Pure and Applied mathematics*, 13(2):217–237, 1960.

[11] R. J. LeVeque. Large time step shock-capturing techniques for scalar conservation laws. *SIAM Journal on Numerical Analysis*, 19(6):1091–1109, 1982.

[12] R. J. LeVeque. Convergence of a large time step generalization of Godunov's method for conservation laws. *Communications on pure and applied mathematics*, 37(4):463–477, 1984.

[13] R. J. LeVeque. A large time step generalization of godunov's method for systems of conservation laws. *SIAM journal on numerical analysis*, 22(6):1051–1073, 1985.

[14] R. J. LeVeque. Wave propagation algorithms for multidimensional hyperbolic systems. *Journal of Computational Physics*, 131(2):327–353, 1997.

[15] R. J. LeVeque. *Finite Volume Methods for Hyperbolic Problems*, volume 31. Cambridge university press, 2002.

[16] S. Lindqvist, P. Aursand, T. Flåtten, and A. A. Solberg. Large Time Step TVD Schemes for Hyperbolic Conservation Laws. *SIAM Journal on Numerical Analysis*, 54(5):2775–2798, 2016.

[17] R. Nygaard. Numerical Treatment of Source Terms in Hyperbolic Partial Differential Equations, 2016. Project work, NTNU.

[18] M. Prebeg. Numerical viscosity in Large Time Step HLL-type schemes. Preprint on webpage at http://folk.ntnu.no/marinpr/pre16.pdf, 2016.

[19] M. Prebeg, T. Flåtten, and B. Müller. Large time step HLL and HLLC schemes. Preprint on webpage at https://www.math.ntnu.no/conservation/2016/012, 2016.

[20] P. L. Roe. Approximate riemann solvers, parameter vectors, and difference schemes. *Journal of computational physics*, 43(2):357–372, 1981.

[21] R. B. Rood. Numerical advection algorithms and their role in atmospheric transport and chemistry models. *Reviews of geophysics*, 25(1):71–100, 1987.

[22] A. A. Solberg. Large Time Step (LTS) Methods for Fluid Flow Problems, 2015. Project work, NTNU.

[23] A. A. Solberg. Large time step explicit schemes for partial differential evolution equations. Master's thesis, NTNU, 2016.

[24] E. F. Toro. *Riemann Solvers and Numerical Methods for Fluid Dynamics: A Practical Introduction*. Springer Science & Business Media, 2009.

[25] E. F. Toro. *Riemann Solvers and Numerical Methods for Fluid Dynamics: A Practical Introduction*. Springer Science & Business Media, 2009.

[26] P. Woodward and P. Colella. The numerical simulation of two-dimensional fluid flow with strong shocks. *Journal of computational physics*, 54(1):115–173, 1984.

[27] H. M. Zhang. A theory of nonequilibrium traffic flow. *Transportation Research Part B: Methodological*, 32(7):485–498, 1998.